DEVELOPMENT OF THE CONE PRESSUREMETER

by

Nigel Robert Forbes Nutt

A thesis submitted for the Degree of
Doctor of Philosophy
at
The University of Oxford

St. Catherine's College

Hilary Term 1993

DEVELOPMENT OF THE CONE PRESSUREMETER

Nigel Robert Forbes Nutt
St. Catherine's College, University of Oxford

A thesis submitted for the Degree of Doctor of Philosophy
Hilary Term, 1993

SYNOPSIS

The cone pressuremeter is an *in situ* testing device comprising a pressuremeter mounted behind a cone penetrometer of the same diameter. Previously reported tests had indicated that the cone pressuremeter can provide measurements of soil strength, stiffness and *in situ* stress. The study presented in this thesis is aimed at developing methods of interpretation of the cone pressuremeter that can be applied with confidence to a variety of soil types.

Carbonate sands have been the cause of significant problems associated with the design of foundations for offshore structures. A programme of cone pressuremeter testing in a carbonate sand from the west coast of Ireland is presented. Tests were carried out in a calibration chamber where conditions of vertical and horizontal stress and relative density were controlled. The influence of these parameters on measured values of cone resistance and pressuremeter limit pressure is assessed. Similar tests were also carried out in a felspathic sand, and correlations have been presented for deriving horizontal stress and relative density that are applicable to most types of sand.

The influence of creep strains and of overconsolidation were other features of carbonate sand that have been assessed with the cone pressuremeter. A numerical model which accounts for the crushing characteristics of carbonate sand is presented, and is shown to improve significantly predictions of limit pressure measured in the calibration chamber.

Cone pressuremeter tests were carried out in soft clay at the Bothkennar test site in Scotland. An analysis based upon cavity expansion theory was shown to provide good estimates of undrained shear strength and stiffness compared with results from other *in situ* and laboratory tests. Estimates of the *in situ* horizontal stress were found to be unrealistically high.

Shear modulus in both sand and clay has been measured from unload-reload cycles carried out during pressuremeter expansion. The stress levels and strain amplitudes of these cycles have been shown to influence the shear modulus greatly. In sand, a procedure for relating these moduli to those at an extremely small reference strain is presented. In clay, shear moduli are shown to give a remarkably close agreement to others reported from Bothkennar, when due account of the strain amplitude is made.

Finally, a time/cost analysis between the cone pressuremeter, the cone penetrometer and the self-boring pressuremeter is presented. The cone pressuremeter is found to be a cost-effective device bearing in mind the amount and quality of information it can provide.

Acknowledgements

Among many things, the completion of this thesis has been a great personal challenge. The whole programme has only been possible with the support of many friends and groups within the University.

I would like to express my sincere thanks to Professor Guy Houlsby. As my supervisor, he has shown tremendous patience, guidance, and enthusiasm for my work. His door has always been open to me.

The funding for the experimental programme in Dogs Bay sand, provided by BP Research is gratefully acknowledged. I would also like to thank Southampton University and the Norwegian Geotechnical Institute for making available a quantity of Hokksund sand for further testing. Cone pressuremeter testing at Bothkennar was carried out by Fugro McClelland.

The technical assistance and "know-how" of Mr Bob Earl in the Soil Mechanics Laboratory was called upon on many occasions - many thanks to him. My gratitude also goes to all members of the Civil Engineering Group. I have thoroughly enjoyed working and socialising with this superb bunch of people.

Finally, thanks to my parents who have been behind me all the way. A very special thank you to my fiancée Megs, who not only put in hours of her time in the final stages of production, but has been a constant source of love and encouragement.

Contents

Nomenclature v

Chapter 1 Introduction

1.1 Background 1.1
1.2 Objectives 1.5
1.3 Outline 1.6
1.4 Interpretation of the cone penetration test 1.7
1.4.1 Soil classification 1.8
1.4.2 Clay 1.9
1.4.3 Sand 1.11
1.5 Interpretation of the pressuremeter test 1.14
1.5.1 Clay 1.14
1.5.2 Sand 1.15
1.6 Interpretation of the cone pressuremeter test 1.17
1.6.1 Clay 1.17
1.6.2 Sand 1.18
1.6.3 Summary 1.19

Chapter 2 Experimental apparatus and sample preparation

2.1 The cone pressuremeter 2.1
2.2 The Oxford sand calibration chamber 2.4
2.2.1 The chamber and pressurisation system 2.4
2.2.2 The driving rig 2.8
2.3 Instrumentation and data acquisition 2.9
2.3.1 Instrumentation 2.9
2.3.2 Data acquisition 2.12
2.3.3 Calibrations 2.12
2.4 Sample preparation 2.14
2.4.1 Techniques for the uniform placement of sand 2.14
2.4.2 Preparation of Hokksund sand 2.16
2.4.3 Preparation of Dogs Bay sand 2.17

Chapter 3 Tests in Hokksund sand

3.1 Introduction 3.1
3.2 A general procedure for cone pressuremeter testing 3.2
3.2.1 Test programme 3.2
3.2.2 Preparation of equipment for testing 3.4
3.2.3 Test procedure 3.5
3.2.4 Data reduction and corrections 3.7
3.3 Soil properties 3.11
3.3.1 Classification 3.11
3.3.2 Strength tests 3.14

3.3.3 Compressibility tests 3.15
3.4 Test results 3.17
3.4.1 Test series 3.17
3.4.2 Cone results 3.19
3.4.3 Pressuremeter results 3.22
3.4.4 Verification of cone and pressuremeter results 3.22

Chapter 4 Tests in Dogs Bay sand
4.1 Introduction 4.1
4.2 Mechanical properties of carbonate sand 4.2
4.2.1 Constituents 4.2
4.2.2 Classification 4.3
4.2.3 Voids ratio 4.4
4.2.4 Grain crushing 4.5
4.2.5 Calcium carbonate content 4.6
4.2.6 Friction angle 4.6
4.2.7 Deformation 4.7
4.3 Properties of Dogs Bay sand 4.8
4.3.1 Origins 4.8
4.3.2 Classification 4.10
4.3.3 Strength tests 4.12
4.3.4 Compressibility and crushing characterictics 4.14
4.4 Cone pressuremeter tests 4.17
4.4.1 Summary of results 4.17
4.4.2 Cone results 4.17
4.4.3 Pressuremeter results 4.23
4.5 Tests in overconsolidated sand 4.27
4.6 Time-dependent behaviour 4.31
4.6.1 Pressure holding tests 4.31
4.6.2 Strain holding tests 4.37
4.6.3 Variation of strain rate 4.39
4.7 Conclusions 4.42

Chapter 5 Interpretation of the cone pressuremeter tests in sands
5.1 Introduction 5.1
5.2 Analytical methods of CPM interpretation 5.2
5.2.1 Small strain elastic-plastic analysis 5.2
5.2.2 Large strain elastic-plastic analysis 5.4
5.2.3 Large strain critical state analysis 5.7
5.2.4 General comments 5.10
5.3 Normalising parameters 5.12
5.4 Correlations for the determination σ_h and D_r 5.14
5.5 Chamber size effects 5.19
5.6 Conclusions 5.23

Chapter 6 Tests in soft clay at Bothkennar

6.1 Introduction 6.1
6.2 The test site at Bothkennar 6.2
6.3 15cm² cone pressuremeter 6.5
6.3.1 Cone pressuremeter details 6.5
6.3.2 Test procedure 6.6
6.3.3 Corrections and calibrations 6.10
6.4 Test results 6.11
6.4.1 Pressuremeter testing 6.11
6.4.2 Cone penetration 6.13
6.5 Analysis 6.17
6.5.1 Undrained shear strength 6.17
6.5.2 Elastic shear modulus 6.21
6.5.3 *In situ* horizontal stress 6.22
6.6 Conclusions 6.24

Chapter 7 Shear modulus

7.1 Introduction 7.1
7.2 Measurement of shear modulus 7.4
7.2.1 10cm² cone pressuremeter 7.4
7.2.1 15cm² cone pressuremeter 7.6
7.3 Corrections to pressuremeter data 7.6
7.3.1 Compliance 7.6
7.3.2 Pressuremeter length correction 7.8
7.4 Stiffness measurements in sand 7.9
7.4.1 Summary of results 7.9
7.4.2 Comparison between arm and volume change strain measurements 7.9
7.4.3 Comparison between G measured by chord and least square methods 7.13
7.4.4 Influence of stress level 7.14
7.4.5 Influence of strain level 7.17
7.5 Stiffness measurements in clay 7.22
7.5.1 Summary of results 7.22
7.5.2 G_{ur} and G_{cc} 7.24
7.5.3 Comparisons with other field tests 7.25
7.5.4 Methods of interpretation 7.26
7.6 Conclusions 7.31

Chapter 8 Numerical analysis

8.1 Introduction 8.1
8.2 Cavity expansion by finite element analysis 8.1
8.3 Yield surfaces 8.5
8.3.1 von Misis yield surface (Model 12) 8.5
8.3.2 Matsuoka yield surface (Model 13) 8.7

8.4 Variable friction and dilation angles (Model 14) 8.9
8.5 Particle crushing (Model 15) 8.13
8.6 Conclusions 8.18

Chapter 9 Applications, summary and conclusions
9.1 General remarks 9.1
9.2 Practical applications 9.2
9.2.1 Time/cost analysis 9.2
9.2.2 Limitations 9.3
9.3 Summary of CPM testing in sand 9.4
9.3.1 Procedures 9.4
9.3.2 Strength and horizontal stress 9.6
9.3.3 Time-dependent behaviour 9.8
9.3.4 Stiffness 9.8
9.3.5 Particle crushing 9.9
9.4 Summary of CPM testing in clay 9.10
9.4.1 Procedures 9.10
9.4.2 Strength 9.11
9.4.3 Horizontal stress 9.11
9.4.4 Stiffness 9.11
9.5 Future research 9.12
9.6 Conclusions 9.13

References R.1

Bibliography R.13

Nomenclature

a area ratio of a cone penetrometer

A strain rate intercept

B constant strain rate

c_1, c_2, c_3, c_4 empirical constants

C_c coefficient of compressibility

C_s coefficient of expansion

d_c cone diameter

D stress intensity = $\frac{\psi}{\psi_l}$

D_c calibration chamber diameter

D_r relative density

D_r^e estimate of relative density from empirical relations

$\boldsymbol{D}_e$ elastic stiffness matrix

$\boldsymbol{D}_{ep}$ elastic-plastic stiffness matrix

D_{10} particle size at 10% passing

D_{50} particle size at 50% passing

D_{60} particle size at 60% passing

e voids ratio

e_{max} maximum voids ratio

e_{min} minimum voids ratio

f yield function

g plastic potential

G^a shear modulus from arm measurements

G_{cc} shear modulus determined from cavity contraction analysis

G_{ch} shear modulus determined from chord measurements in unload-reload loops

G_{ls} shear modulus from least square measurements

G_s secant shear modulus

G_{ur} shear modulus determined from unload-reload loops

G_{ur}^c calculated values of shear modulus

G_{ur}^{m} measured values of shear modulus

G^{v} shear modulus determined from volume change readings

G_0 maximum shear modulus

I_p plasticity index

I_r rigidity index

I_R dilatancy index

I_1, I_2, I_3 stress invariants

k shift from the origin in shear stress-normal stress space due to the plastic potential

K strain rate intercept

K_G modulus number

K_0 *in situ* stress ratio

K_1, K_2 constants for hyperbolic function

m slope of the $\log_e\dot{\varepsilon} : \log_e t$ plot

n $\dfrac{1-\sin\nu}{1+\sin\nu}$

n modulus exponent

N $\dfrac{1-\sin\phi}{1+\sin\phi}$

N_{cv} $\dfrac{1-\sin\phi_{cv}}{1+\sin\phi_{cv}}$

N_k cone factor

N_{kt} cone factor corrected for pore pressures

p' mean effective stress

p_a atmospheric pressure

p_c critical isotropic crushing pressure

p_x critical pressure at which crushing commences

q deviator stress = $(\sigma_1-\sigma_3)/2$

q_c cone resistance

q_c^{nc} cone resistance determined from normally consolidated tests

q_c^{oc} cone resistance determined from overconsolidated tests

q_t corrected cone resistance

Q Bolton's constant

R	radius
R_0	initial radius
s_u	undrained shear strength
S_d	slope of the unloading portion of the $\log\psi$: $\log\varepsilon$ plot
S_e	slope of the loading portion of the $\log\psi$: $\log\varepsilon$ plot
SG	specific gravity
t	time (minutes)
t_0	time from which a test commences
t_1	time at 1 minute
u	pore pressure
U	coefficient of uniformity
α	gradient of the strain rate-stress intensity plot
$\Delta\varepsilon$	strain amplitude
ε	strain
ε_c	cavity strain
ε_e	maximum cavity strain in a CPM test
$\underline{\varepsilon}^e$	vector of elastic strain increment
ε_{max}	maximum cavity strain
$\underline{\varepsilon}^p$	vector of plastic strain increment
ε_r	radial strain
ε_s	secant shear strain
ε_θ	hoop strain
$\dot{\varepsilon}$	strain rate
γ	shear strain
$\gamma_{d\max}$	maximum unit weight
$\gamma_{d\min}$	minimum unit weight
κ	slope of the isotropic expansion line
λ	slope of the isotropic compression line
ν	dilation angle
ξ	state parameter
σ_h	horizontal stress
σ_h'	horizontal effective stress

σ_h^{max} maximum horizontal stress applied during a cycle of overconsolidation

σ_{h0} *in situ* horizontal stress

σ_h^e estimate of horizontal stress from empirical relations

σ_r radial stress

σ_v vertical stress

σ_v' vertical effective stress

σ_v^{max} maximum vertical stress applied during a cycle of overconsolidation

σ_{v0} in situ vertical stress

σ_θ hoop stress

υ Poisson's ratio

ϕ friction angle

ϕ_{cv} constant volume friction angle

ϕ_p peak friction angle

ϕ_{ps} plane strain friction angle

ϕ_{resid} residual friction angle determined from direct shear tests

ϕ_{tc} triaxial compression friction angle

ψ cavity pressure

ψ_l limit pressure

ψ_l^{nc} limit pressure determined from normally consolidated tests

ψ_l^{oc} limit pressure determined from overconsolidated tests

ψ_l^{27} limit pressure determined in a calibration chamber with a chamber diameter to cone diameter ratio of 27

ψ_l^{∞} limit pressure in an infinitely bounded medium

ψ_m maximum cavity pressure prior to unloading

CHAPTER 1

INTRODUCTION

1.1 Background

The design of foundations for structures, whether offshore or onshore, requires a good understanding of the underlying ground conditions. Such information can be obtained either from laboratory testing, large scale structural monitoring or *in situ* testing. The last of these, *in situ* testing, has the distinct advantage over other approaches of being fast and relatively inexpensive. With recent developments in equipment and theoretical methods of interpretation, *in situ* testing has become a standard requirement of most site investigations.

Interpretation of the data that are produced from an *in situ* test can be made in one of two ways, as shown in Figure 1.1. Firstly, a direct, empirical approach can be adopted, where the results of tests are related directly to the design of structures, or the solution of standard geotechnical problems. An example of such an approach is the application of the Menard Pressuremeter, commonly used in France (Baguelin *et al.*, 1978). In this test, a standardised procedure is related directly to a set of design rules, and draws upon an extensive database of case histories from across the country. This method has limitations when applied to unusual or new soil conditions, or specific design problems where an understanding of the fundamental behaviour of the soil is required.

The second approach to interpretation of *in situ* tests involves the measurement of specific soil properties, which are then used in the design process. Interpretation can be based on a theory of soil behaviour, or set against a programme of calibration in a soil where the

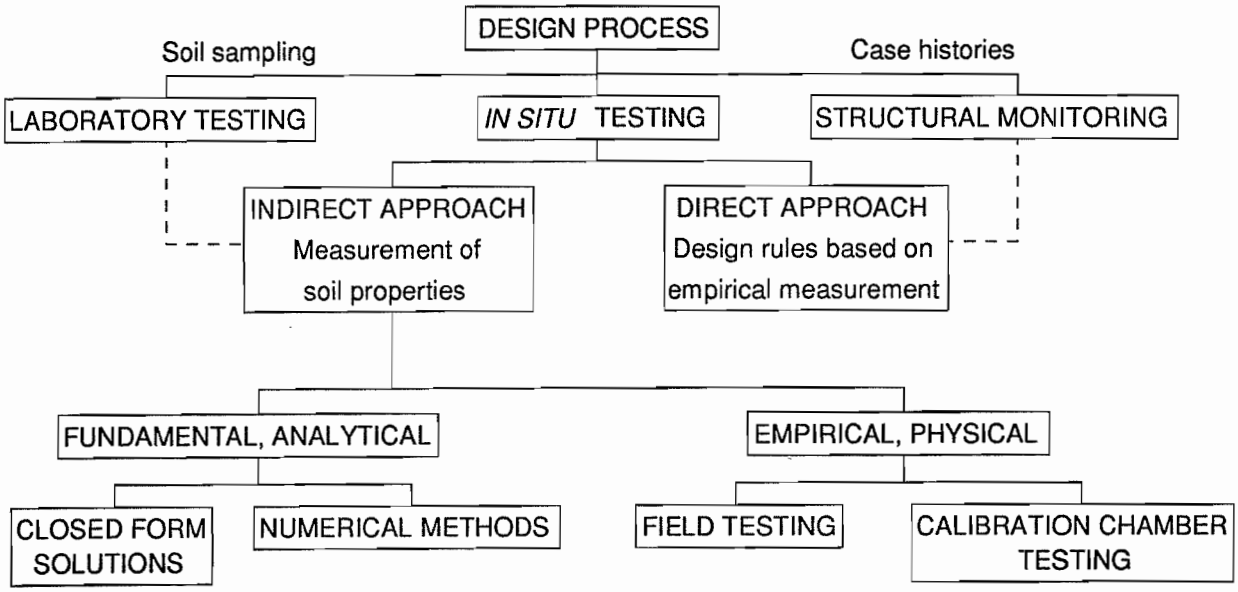


Figure 1.1 Interpretation of *in situ* tests

conditions are either controlled or measured independently. This philosophy is strongly favoured in the United Kingdom, and is of great advantage when applied to the development of new *in situ* devices. The research presented in this thesis has been based upon such an approach.

The results of a qualitative study carried out by Campanella and Robertson (1983) of the relative applicability of a wide range of *in situ* devices in measuring various soil parameters are presented in Table 1.1. The table is by no means exhaustive; rather it should be used to highlight two devices which appear to show much potential in measuring many aspects of soil behaviour, namely the piezo/friction cone penetrometer, and the self-boring pressuremeter.

The cone penetrometer (CPT) is now well established as a fast and economical tool of particular value in making detailed profiles of soil strata. While reliable measurements of strength in sands or clays can be made, the cone penetration test gives only a poor indication of soil stiffness. In contrast, the self-boring pressuremeter (SBPM) has been developed specifically for the measurement of soil properties at selected depths. It is well suited to the measurement of soil strength, stiffness and *in situ* horizontal stress, as long as disturbance is

	Soil type	Profile	Density	Friction angle	Undrained shear strength	Pore pressure	Stress history (OCR)	Moduli; Young's and shear	Compressibility	Consolidation	Permeability	Stress strain curve	Liquefaction resistance
Dynamic cone	C	A	B	C	C	-	C	-	-	-	-	-	C
Static cone:													
Mechanical	B	A	B	C	B	-	C	B	C	-	-	-	B
Elec. Friction	B	A	B	C	B	-	C	B	C	-	-	-	B
Elec. Piezo	A	A	B	B	B	A	A	B	B	A	B	B	A
Elec. Piezo/Friction	**A**	**A**	**A**	**B**	**B**	**A**	**A**	**B**	**B**	**A**	**B**	**B**	**A**
Accoustic probe	C	B	B	C	C	-	C	C	-	-	-	-	C
Dilatometer	B	A	B	C	B	-	B	B	C	-	-	C	B
Vane shear	B	C	-	-	A	-	B	-	-	-	-	-	-
Standard Penetration Test	B	B	B	C	C	-	-	-	C	-	-	-	A
Seismic CPT downhole	C	C	C	-	-	-	-	A	-	-	-	B	B
K_0 Blade	-	-	-	-	-	-	B	-	-	-	-	-	-
Resistivity probe	B	B	A	B	C	-	C	C	C	-	-	C	A
Borehole permeability	C	-	-	-	-	A	-	-	-	B	A	-	-
Hydraulic fracture	-	-	-	-	-	B	B	-	-	C	C	-	-
Screw Plate	C	C	B	C	B	-	B	A	B	C	C	B	B
Seismic downhole	C	C	C	-	-	-	-	A	-	-	-	B	B
Impact cone	C	B	C	C	C	-	C	C	C	-	-	-	C
Borehole shear	C	C	-	B	B	-	C	C	-	-	-	C	-
Menard pressuremeter	B	B	C	B	B	-	C	B	B	-	-	C	C
Self-boring pressuremeter	**B**	**B**	**A**	**A**	**A**	**A**	**A**	**A**	**A**	**A**	**B**	**A**	**A**
Self-boring devices:													
K_0 meter	-	-	-	-	-	-	A	-	-	-	-	-	-
Lateral penetrometer	C	C	B	B	B	-	B	B	C	-	-	-	-
Shear vane	B	C	-	-	A	-	B	-	-	-	-	-	-
Seismic crosshole	C	C	B	-	-	-	-	A	-	-	-	B	B
Nuclear tests	-	-	A	B	-	-	-	C	-	-	-	-	C
Plate load tests	C	C	B	B	C	-	B	A	B	C	C	B	B

A = High applicability
B = Moderate applicability
C = Low applicability

Table 1.1 Percieved applicability of *in situ* test methods (after Campanella and Robertson, 1983)

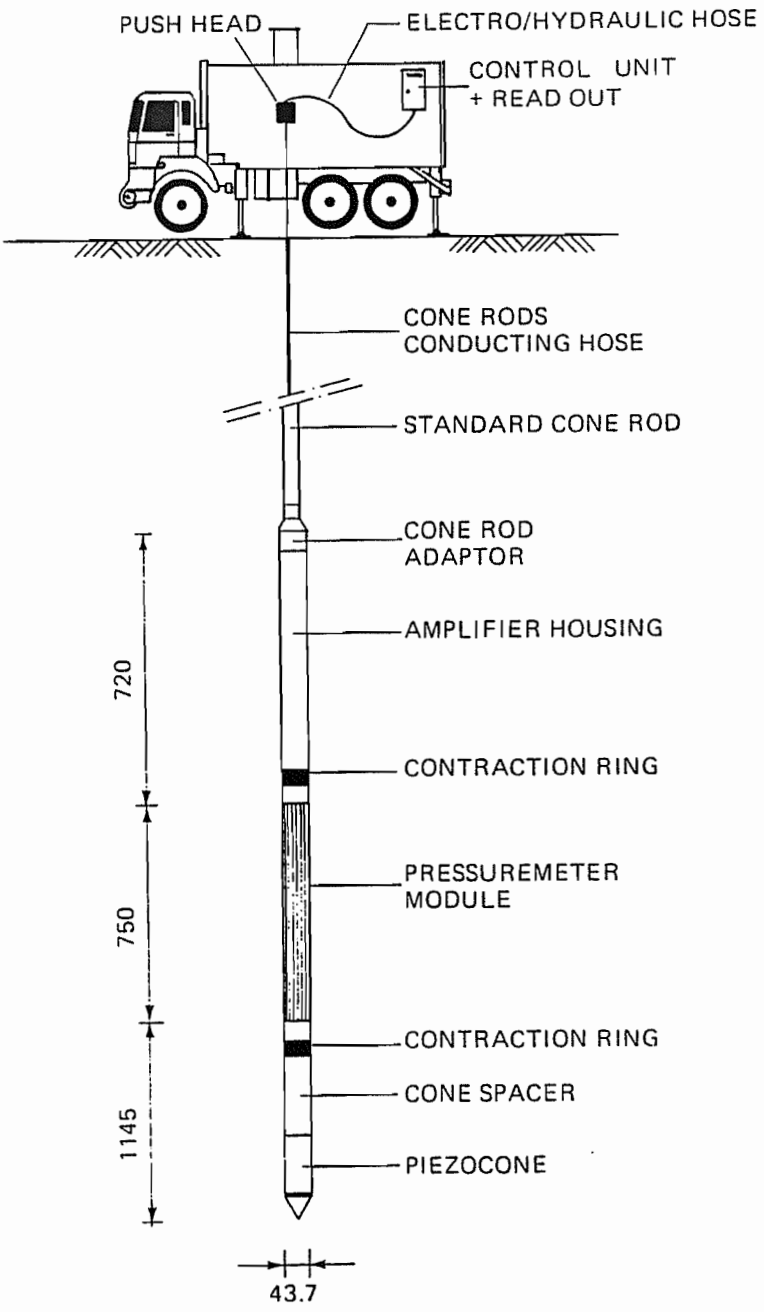


Figure 1.2 Schematic representation of the cone pressuremeter (not to scale)

minimised during installation of the device. The installation procedure, however, can be slow and requires an experienced operator if results are to be repeatable.

The cone pressuremeter (CPM) is a relatively new *in situ* device which was developed to combine the profiling effeciency of the CPT with the merits of the SBPM in measuring soil strength and stiffness. The device comprises a pressuremeter mounted behind a 60° cone

penetrometer of the same diameter, as shown in Figure 1.2. Details of the CPM are reported by Withers *et al.* (1986). While interpretation of the cone data is no different from the CPT, analysis procedures applied to the SBPM are not necessarily valid, since insertion of the CPM causes gross disturbance to a zone of soil adjacent to the pressuremeter.

If methods of interpretation of the cone pressuremeter test can be developed, so that the device can be used in most soil types, then significant savings in time (and hence money) can be made in future site investigations. For this reason, much recent work has been centered around the cone pressuremeter test, experimentally (Schnaid, 1990), numerically (Yu, 1990), and in the field (Houlsby and Withers, 1988; Withers *et al.*, 1989; Campanella *et al.*, 1990; Houlsby and Nutt, 1992).

1.2 Objectives

The aim of this thesis is to develop methods of interpretation of the cone pressuremeter test. Particular attention is paid to three objectives:

(1) to extend the database of cone pressuremeter tests to a variety of soil types,

(2) to measure fundamental soil properties with the cone pressuremeter; specifically strength, *in situ* stress and stiffness,

(3) to assess the application of cavity expansion theory to cone pressuremeter testing, and make improvements or present alternatives where necessary.

These objectives will be addressed firstly, through a programme of calibration chamber testing in a carbonate sand and a feldspathic sand, and secondly, through a set of field tests in soft clay at a well-documented research site.

Carbonate sand has been encountered in many offshore engineering problems, and strong emphasis will be placed on understanding and modelling the behaviour of this sand when subjected to cone pressuremeter insertion and inflation.

In the light of successful interpretation of the CPM test, a fourth objective is also addressed:

(4) to demonstrate the practical advantages of the cone pressuremeter as a site investigation tool.

A time/cost analysis will be presented to meet this objective, so that, combined with the first three objectives, it is hoped that the cone pressuremeter will gain widespread acceptance at a commercial level.

1.3 Outline

In the remainder of this chapter, a literature review is presented. The review is focused on methods of interpretation of the cone penetration test, the self-boring pressuremeter test, and the cone pressuremeter test.

In Chapter 2, a description is presented of the cone pressuremeter used in the experimental programme, and includes a summary of components and dimensions. Details of the calibration chamber are given. This includes the chamber, the driving rig and CPM pressurisation system, instrumentation and data acquisition. The techniques adopted for sample preparation are then discussed.

A procedure for CPM testing and data reduction in the calibration chamber is presented in Chapter 3. This is followed by a description of the properties of Hokksund feldspathic sand, and the results from a set of CPM tests carried out in this sand.

The mechanical properties of carbonate sand are reviewed in Chapter 4, and differences between the behaviour of carbonate sand and silica sand are highlighted. The properties of Dogs Bay sand have been determined, and are also reported. Results from CPM tests in this sand carried out in the calibration chamber are presented and discussed.

In Chapter 5, the behaviour of different sands tested in the calibration chamber is analysed. Cavity expansion theories are used to interpret the test results, and comments on the applicability of these theories are given. Empirical correlations are presented which can be applied to the interpretation of all sands tested.

A set of CPM field tests at Bothkennar is reported in Chapter 6. The tests are analysed and the results are compared with results reported from other *in situ* and laboratory tests.

The measurement of shear modulus in sand and clay is discussed in Chapter 7, and particular emphasis is placed on moduli measured from unload-reload loops.

In Chapter 8, a numerical analysis of the cone pressuremeter test is described. Finite element models are presented which have been used to improve predictions of limit pressure based on calibration chamber tests in sand.

Finally, a set of conclusions to the work presented is given in Chapter 9. The application of the cone pressuremeter is discussed in the light of a time/cost analysis. Recommendations are made for future research.

In addition to a list of references, a bibliography has been presented at the end of this thesis which contains, to the best knowledge of the author, an exhaustive list of references relating to full displacement pressuremeters.

1.4 Interpretation of the cone penetration test

The cone penetration test, which saw much of its early use in the Netherlands, was originally used as a means of determining the ultimate capacity of driven piles founded in sand (Barentsen, 1936). It was not until a friction sleeve was incorporated into the penetrometer, as described by Begemann (1953), that its potential as a profiling tool became obvious.

Attempts have been made to measure deformation parameters with the CPT (Mitchell and Gardener, 1975; Senneset *et al.*, 1982), however, these have resulted in only poor estimates of soil compressibility. This problem was summarised by Wroth (1988), who emphasised that relationships with moduli are secondary, because cone penetration is inherently a measure of soil strength. Indeed, the need for reliable measurements of stiffness has been an important reason for the development of the cone pressuremeter, and so in this review, attention is focused on the use of the CPT in soil classification, and for determining strength properties in clay and sand.

1.4.1 Soil classification

From the combination of the cone end resistance and friction measurements, charts have been developed which categorise most commonly encountered soil types, based loosely on grain size. Schmertmann (1975) and Searle (1979) used this method to classify sands by varying ranges of density, and clays by analogous ranges of strength. There are limitations to these charts, because they apply only to specific soil types, and do not take into account factors such as ageing, cementation, overconsolidation or fissuring.

With the increasing prominence of carbonate soils in foundation problems, particularly those related to the offshore industry, more specific correlations have been demanded. Beringen *et al.* (1982) have presented a broad classification system for carbonate sands and silts based on cone resistance and friction ratio, and this is reproduced in Figure 1.3. The comparitive lack of data available for carbonate soils, however, resulting in the broad classification groups shown in the figure, suggests that more fundamental approaches are required in classifying these soils.

Stronger emphasis is being placed on normalised parameters, leading to more rigorous interpretation of *in situ* tests (Wroth, 1984, 1988), and this has been reflected in recent developments in soil classification charts. Robertson (1990) has produced a system of

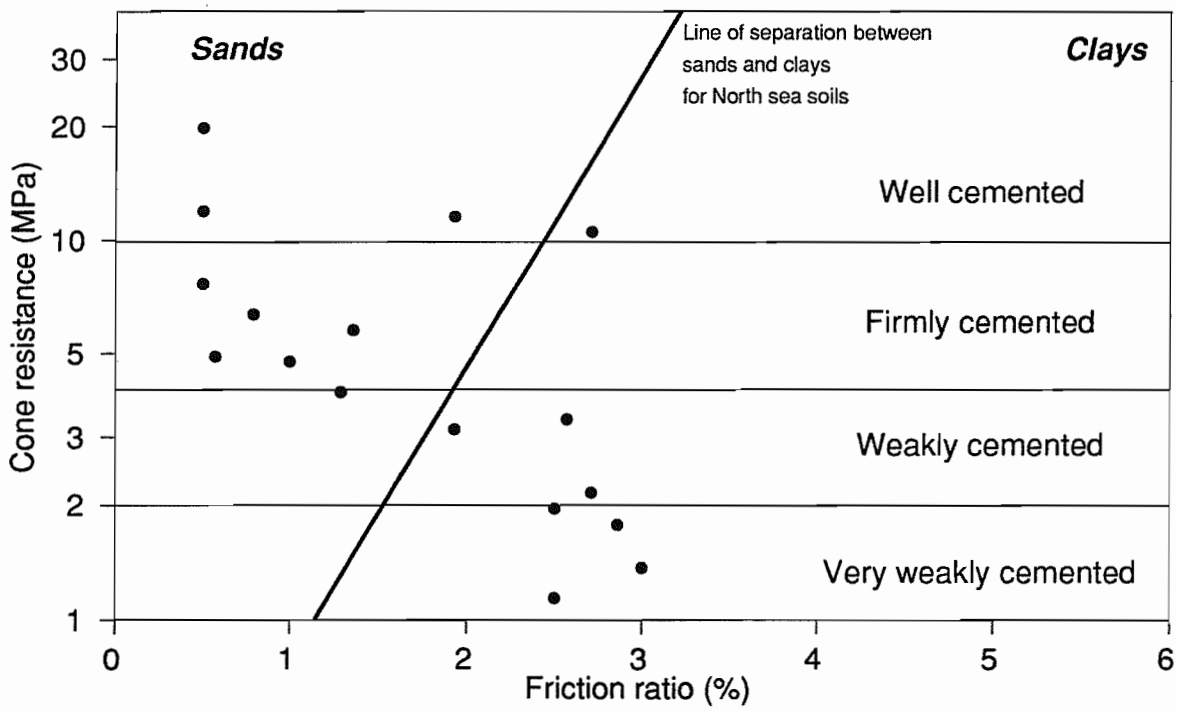


Figure 1.3 Interpretation of CPT tests in carbonate sands and silts from offshore Western Australia (after Beringen *et al.*, 1982)

classification, shown in Figure 1.4, based on normalised measurements of cone resistance, friction ratio and pore pressure. Factors such as changes in stress history, *in situ* stresses, sensitivity, stiffness, microfabric and voids ratio influence classification of the soil. Another more recent classification chart is presented by Jefferies and Davies (1991). With the increasing database of cone penetration test results throughout the world, this work allows much greater confidence to be placed in the CPT as a profiling tool.

1.4.2 Clay

The undrained shear strength of clay related to failure caused by cone penetration is given by the relationship

$$s_u = \frac{q_t - \sigma_{v0}}{N_{kt}} \qquad ...(1.1)$$

where q_t is the total cone resistance, σ_{v0} is the total overburden stress, and N_{kt} (or N_k if no piezometric measurements were taken) is an empirical cone factor related to q_t (Aas *et al.*, 1986). The cone factor is normally determined from direct measurements of s_u specific to the

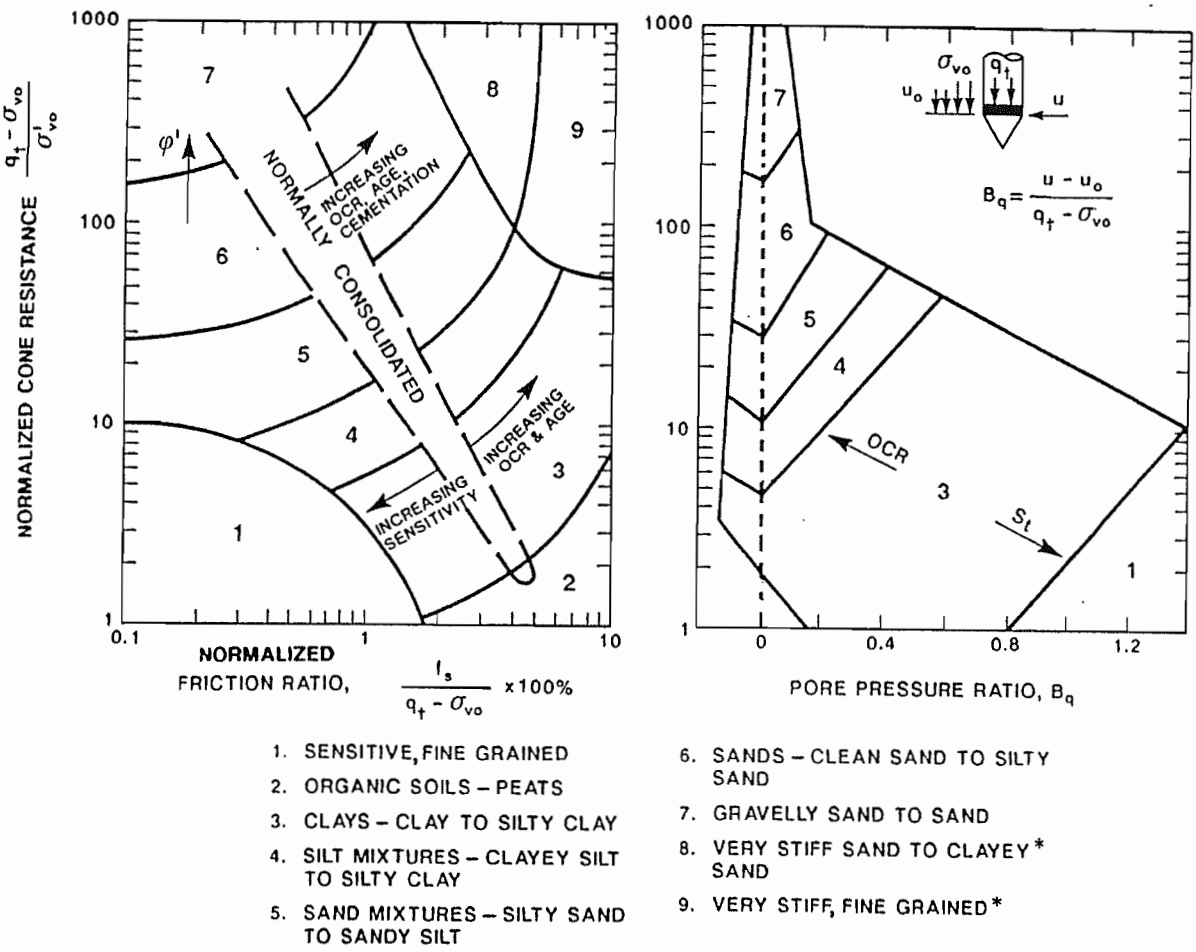


Figure 1.4 Soil classification chart, after Robertson (1990)

test site (Lunne *et al.*, 1976; Baligh *et al.*, 1980). Lacasse and Lunne (1982) report cone factors measured from field vane tests in two soft Norwegian clays, ranging from 12.5 to 19.5. From an extensive number of piezocone tests in nine types of clay, Aas *et al.* (1986) report that N_{kt} varies with the plasticity index, I_p. N_{kt} values ranged from 13±2 at I_p = 0, to 18±2 at I_p = 50%, which is applicable to young and aged clays. The importance of defining a reference strength for establishing such a correlation, for example the undrained triaxial compression strength or the field vane strength, was also emphasised.

Marsland and Quarterman (1982) present results where N_{kt} is back analysed from plate loading tests and embankment failures. They found that features of soil fabric can significantly influence the results of cone penetration tests. In soft clays, the particle

arrangements at the micro scale can have an important effect on stress strain relationships and sensitivity. In stiff clays, discontinuities and other macro fabric features can reduce the mass strength to a fraction of the intact strength of the clay between discontinuities.

A more fundamental approach was adopted by Houlsby and Wroth (1982), who used the lower bound theorem of plasticity to determine s_u. Their analysis, however, is only appropriate for indentation by penetrometers near the surface of a soil. The most rational analysis of the deep penetration problem is the Strain Path Method proposed by Baligh (1986). In an infinite soil mass, the penetration process can be modelled by a steady flow of soil past a stationary penetrometer. The velocities of the soil elements are estimated from the flow field of an ideal fluid.

Teh (1987) presented a finite element analysis of cone penetration based on the Strain Path Method, in which an equation relating N_{kt} to soil parameters and cone roughness was proposed. For typical soil cases, N_{kt} factors range from 9 to 17. The procedure requires estimates of stiffness, strength and *in situ* stress (as well as cone roughness). A further conclusion reported by Teh (1987) was that far behind the cone tip, the stress distribution using the Strain Path Method is similar to the stress distribution predicted from the expansion and subsequent contraction of a cylindrical cavity from zero initial radius. This finding has implications on the interpretation of the cone pressuremeter test, and will be discussed again further in the chapter.

1.4.3 Sand

Bearing capacity theory, for determining the penetration resistance of a deep cone in sand, depends upon an assumed shape and location of the plastic zone in the form of slip planes (Mitchell and Keaveny, 1986). Meyerhof (1961) assumed a shear failure that extended back to the shaft of the cone. Bearing capacity factors were developed for wedges in plane strain which could be modified for the axisymmetric case of a cone penetrometer. Durgonoglu and

Mitchell (1975) assumed a failure surface that exended to the free surface of the soil. Their method, and that of Meyerhof (1961), however, assumed a rigid-plastic stress-strain soil behaviour, which involves incorrect assumptions about the boundary conditions of the problem. This is because slip line solutions are not able to take into account the elastic deformation of the soil.

Vesic (1972, 1975) demonstrated that the cone penetration resistance of sands can be predicted from cavity expansion theory. The principal parameters affecting the ultimate cavity pressure were shown to be *in situ* stress, strength and compressibility, and the rigidity index of the soil. When applied to data from a large number of sands reported by Mitchell and Keaveny (1986), reasonably good predictions of friction angle were made, based on triaxial compression tests.

Recently, Collins *et al.* (1992) have concentrated on obtaining a large strain cavity expansion solution for cone penetration. They have recognised that material parameters such as friction and dilation angles are not constant and are dependent on the deformation history of the material element. Using the concepts of a state parameter and the test results reported by Been and Jeffries (1985), Collins *et al.* (1992) developed a set of governing equations which were solved numerically. The distribution of stresses and voids ratio in the plastic regime were obtained, as well as the variation of limit cavity wall pressure with different initial void ratios and hydrostatic pressures. Their results suggest a close relationship between limit pressure and state parameter.

Determining sand strength by empirical correlations is now a well documented approach (Schmertmann, 1975; Baldi *et al.*, 1986; Lunne, 1991). Jamiolkowski *et al.* (1985) report a logarithmic relationship between relative density, D_r and cone resistance, q_c normalised by *in situ* vertical stress. The correlation was shown to fit well the measurements of q_c from calibration chamber tests in six sands. It is applicable, however, only to normally

consolidated, uncemented, unaged sands in which quartz minerals are predominant. When applied to carbonate sands, such a correlation can potentially lead to too conservative an estimate of D_r, due to their highly compressible and crushable nature. Almeida *et al.* (1991) showed that at similar relative densities, q_c measurements from calibration chamber tests in Quiou sand (a shell based carbonate sand) were up to half the measured values in Ticino silica sand. At high densities and high mean effective stresses, this behaviour is best explained by the presence of crushing. At lower mean effective stresses, however, Houlsby and Nutt (1992) reported that relative density is still a suitable normalising parameter for tests in Dogs Bay carbonate sand.

An empirical approach by Been and Jefferies (1985) depends upon a "state parameter", defined as the change in void ratio due to shear under mean effective stress from the initial state to the "steady state line" on a plot of void ratio versus mean effective stress. Based on a relationship between cone resistance and state parameter for several sands, a relationship between cone resistance and friction ratio was obtained. The function, however, does require knowledge of the *in situ* horizontal stress.

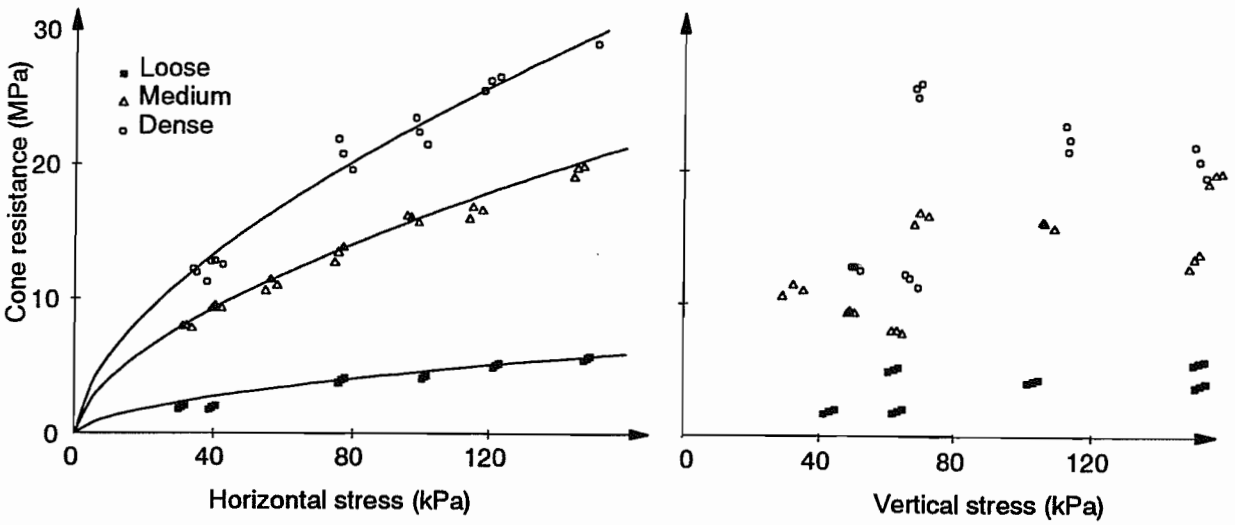


Figure 1.5 The influence of *in situ* stresses on cone resistance (after Houlsby and Hitchman, 1988)

From a series of calibration chamber tests in a uniformly graded silica sand, Houlsby and Hitchman (1988) reported that cone resistance in sand depends primarily on the horizontal stress and the angle of friction, but is relatively unaffected by the vertical stress, as shown in Figure 1.5. An empirical power law relationship was shown to fit the data remarkably well.

1.5 Interpretation of the pressuremeter test

Most pressuremeter analyses are based on cavity expansion theory. With the application of a cavity pressure, ψ, stresses and strains are experienced by a soil element as illustrated in Figure 1.6. If the pressuremeter is long, then conditions of plane strain prevail, and strains in the vertical direction are zero. Furthermore, if axial symmetry is assumed, then all stresses and strains can be related solely to their radial distance from the centre of expansion, and the analysis is one-dimensional. Such assumptions are necessary if closed form solutions to the cavity expansion problem are to be obtained.

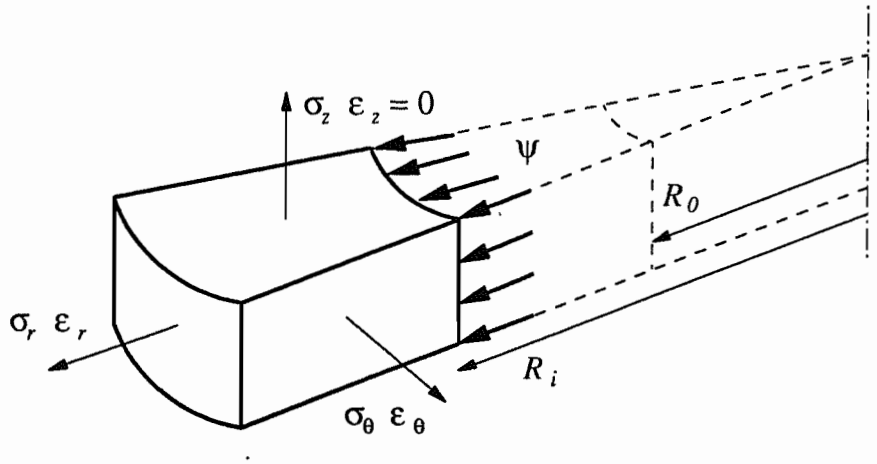


Figure 1.6 Stresses and strains experienced by an element of soil during cavity expansion

1.5.1 Clay

Gibson and Anderson (1961) presented a closed form solution to obtain the limit pressure of an expanding cylindrical cavity in an elastic-perfectly plastic Tresca soil. The expansion commences from a finite initial radius, and by assuming no plastic volume change but large

strains in the plastic regime, the solution has remained valid for clay behaviour, although is unrealistic for sand behaviour. Their analysis was reinterpreted by Palmer (1972) who abandoned the assumption that soil behaves in a perfectly plastic manner. Palmer went on to present a graphical method by which the stress-strain relation could be found as well as the elastic shear modulus of the soil. The expansion of cylindrical cavities in undrained conditions and small strains was also addressed by Baguelin *et al.* (1972) for pressuremeter tests. Carter *et al.* (1979) used numerical techniques to obtain the solution to a problem considering the soil to be a saturated two-phase material with pore pressure changes both during and after cylindrical cavity expansion. The analysis required an effective stress-strain law that could be written in incremental or rate form.

These closed form solutions assume both isotropic material behaviour and small strains throughout the elastic region. These limitations were abandoned by Sagaseta (1984) assuming elastic-perfectly plastic soil behaviour with a von Mises yield criterion. Large strain analysis was used throughout the elastic and plastic regimes with the assumption of material incompressibility in the plastic regime. The large strain validity of this solution is particularly relevant to cone pressuremeter interpretation, because any complexities in the stress distribution around the pressuremeter at the start of inflation are erased due to a sufficiently large expansion, and replaced by a simpler pattern.

1.5.2 Sand

Hughes *et al.* (1977) extended the work of Gibson and Anderson (1961) by accounting for volume change using a constant angle of dilation throughout the expansion. In their analysis, the elastic strains were neglected in the plastic regime and the flow rule used to quantify the effect of dilatancy was the stress-dilatancy theory of Rowe (1962). The analysis is capable of determining the shear strength parameters and the angles of friction and dilation of the sand requiring only the measured pressure-expansion curve of a SBPM test and the critical state friction angle, ϕ_{cv}. Because ϕ_{cv} is independent of initial sand density, it is easily

determined from laboratory tests. Small strain solutions were also presented by Wroth and Windle (1975).

The use of the pressuremeter unloading curve was reported by Houlsby *et al.* (1986) who extended the analysis of Hughes *et al.* (1977) for cavity contraction. Assuming the sand to be isotropic, linear elastic with a Mohr-Coulomb failure criterion, the use of a fixed dilation and friction angle is maintained, and the elastic strains in the plastic regime are neglected. The analysis was applied to field tests in an overconsolidated sand, at a site where ϕ_{cv} had not been measured in the laboratory. Using, therefore, both the loading analysis and the new unloading analysis, it was possible to bypass the need for determining ϕ_{cv}. The advantage of using the unloading curve is that it is less sensitive to initial disturbance, however, in their reported tests, fewer data were recorded on unloading than loading and the results were found to exhibit scatter due to non-homogeneity of the site.

Carter *et al.* (1986) presented closed form solutions for the expansion of cylindrical and spherical cavities in an ideal, cohesive frictional material allowing for elastic deformations in the plastic regime. Their solution for the entire pressure-expansion curve was obtained by imposing the restriction of small strains. When that restriction was relaxed, only the solution for the limit condition at infinitely large deformation was obtainable in closed form, and numerical techniques were needed to derive the full pressure-expansion curve. Their small strain analysis was applied to the interpretation of self-boring pressuremeters, and their large strain limit pressure solution was suggested as a means to providing a reasonable estimate for the normal stress acting on a pile shaft after installation.

The problem of obtaining a large strain closed form solution in a dilatant soil was solved by Yu and Houlsby (1991). Using an elastic-perfectly plastic soil model with a non-associated flow rule and Mohr-Coulomb failure criterion, an explicit solution for the pressure expansion relationship was presented, with no restriction placed on the magnitude of deformation. This

solution does result in slightly different limit pressure estimates from that of Carter *et al.* (1986). The primary limitation to this solution is that, as with other researchers, constant angles of friction and dilation are assumed.

1.6 Interpretation of the cone pressuremeter test

1.6.1 Clay

Houlsby and Withers (1988) extended the analysis of Gibson and Anderson (1961) to incorporate cavity contraction, assuming small strains in the elastic regime and large strains in the plastic regime. Cavity contraction solutions have the distinct advantage over expansion solutions in that they are less sensitive to initial disturbance of the soil.

For the cylindrical, plane strain analysis in an incompressible, linear elastic-perfectly plastic Tresca material, the expansion occurs at a constant limit pressure of

$$\psi_l = \sigma_{h0} + s_u(1+\log_e I_r) \qquad ...(1.2)$$

where $I_r = G/s_u$ is the rigidity index, and σ_{h0} is the initial *in situ* horizontal stress. After an initial unloading at a stiffness of $2G$ to a pressure of $\psi_l - 2s_u$, the unloading curve is given by

$$\psi = \psi_l - 2s_u \left[1 + \log_e\left(\frac{\sinh(\varepsilon_{max}-\varepsilon)}{\sinh(1/I_r)}\right)\right] \qquad ...(1.3)$$

This leads to the simple geometric construction shown in Figure 1.7 for the determination of s_u, G and σ_{h0}. Houlsby and Withers (1988) found that estimates of s_u and G were reliable when compared with the results from other *in situ* and laboratory tests at a stiff clay site at Madingley, near Cambridge. Estimates of σ_{h0}, however, were unrealistically high.

The effects of varying the length to diameter ratio of the cone pressuremeter on the measurement of clay properties was assessed numerically by Yu (1990). Further factors

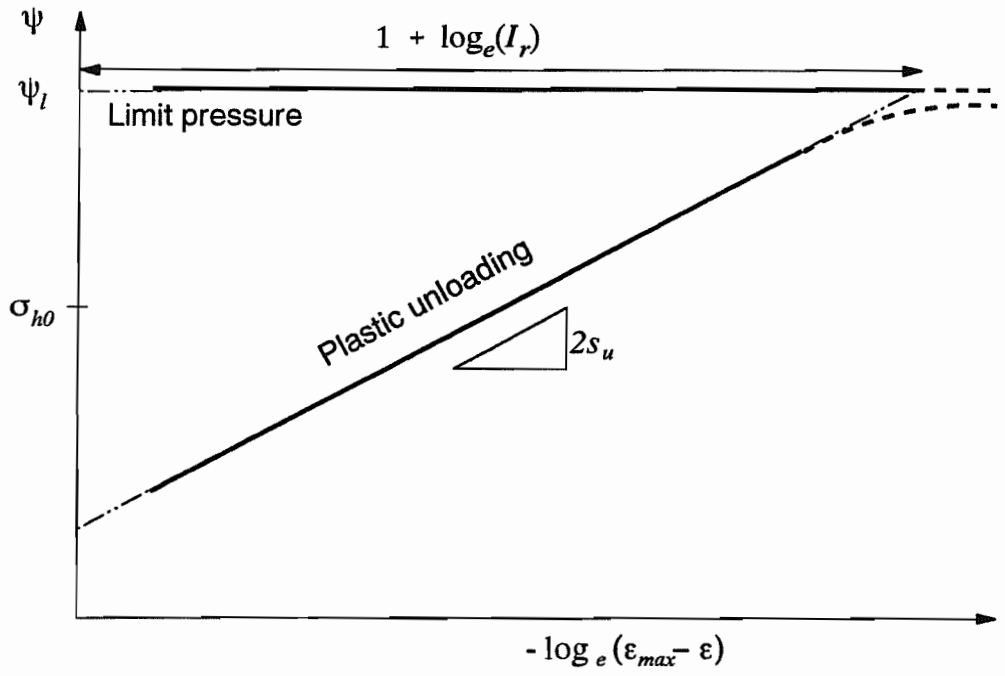


Figure 1.7 Graphical representation of the analytical solution for a cone pressuremeter test in clay (after Houlsby and Withers, 1988)

affecting the results of CPM tests in clay were discussed by Campanella *et al.* (1990).

1.6.2 Sand

The stress distribution that exists on the boundary of a cone as it is pushed into sand is discussed by Hughes and Robertson (1985), and has important consequences on interpretation of the pressuremeter inflation. It is suggested that very high stresses are developed when the cone tip passes an element in sand, followed by a substantial decrease of stresses when the sand element comes into contact with the sleeve. Hughes and Robertson attribute this to the presence of an arch of high mean effective stress generated at some radius from the instrument, and this explanation is supported by measured cone resistances significantly higher than measured friction stresses along the sleeve of the cone. Both the radial and effective stresses will vary with radius in a complex manner.

From the theoretical explanation of cone penetration in clay (Baligh, 1986), Withers *et al.* (1989) postulated that a zone of intense deformation exists adjacent to a cone penetrating sand

as well; a zone characterised by high shear strains and high shear strain rates. This, combined with the description of Hughes and Robertson (1985) of the complex pattern of stresses set up in the soil, suggests that the initial part of the pressure expansion curve is unlikely to be suitable for analysis using cavity expansion theory. At sufficiently large expansions, however, it is possible that such complexities would be erased and replaced by a simpler pattern of stresses. In Figure 1.8, the stages in a cone pressuremeter test are presented, as described by Withers *et al.* (1989). With point A initially on the centreline prior to insertion, the figure is used to illustrate the formation of a plastic zone (including an intense shear band) after CPM insertion, after pressuremeter inflation, and after pressuremeter contraction. The stress paths followed by points at increasing radii from the centreline are traced through this process. A cavity expansion solution, applying the Hughes *et al.* (1977) analysis for the self-boring pressuremeter, was used to estimate strength and stiffness properties of sand, based on field tests at two sites. The method was found to be unreliable in the estimation of strength properties.

1.6.3 Summary

The primary difference between cone pressuremeter tests and self-boring pressuremeter tests is that, in the former, pressuremeter expansion takes place in soil that has already been disturbed by insertion of the device. From results reported by Teh (1987) and Hughes and Robertson (1985) for clay and sand behaviour respectively, the distribution of stresses around the pressuremeter prior to expansion is similar to that due to an initial cavity expansion followed by a smaller cavity contraction. In analyses for the cone pressuremeter, it is important, therefore, that large strains in the plastic zone are incorporated into the calculation of limit pressure to erase the effects of this stress distribution. In sands, such a calculation is made more complicated by the fact that the shearing resistance and volumetric change characteristics vary at these large strains. Closed form solutions which incorporate this feature of soil behaviour do not, at present, exist.

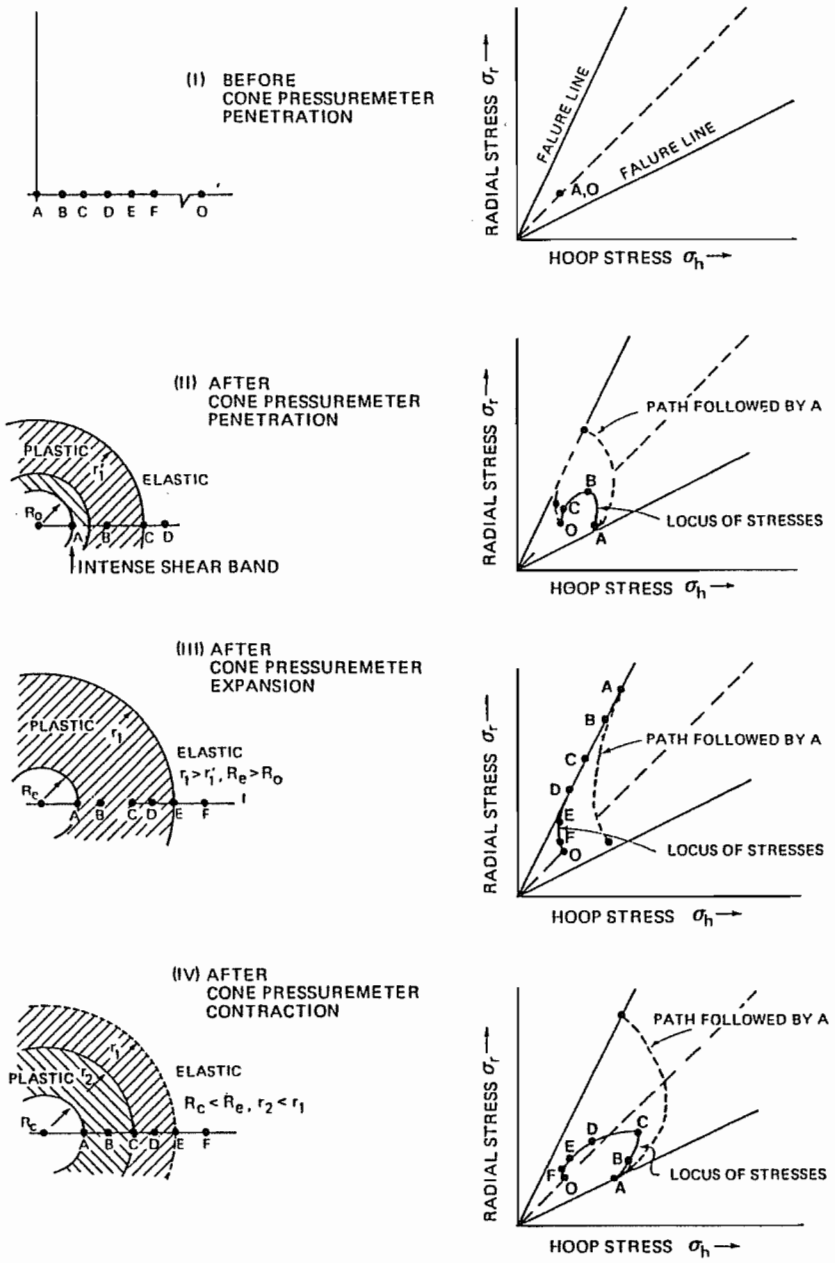


Figure 1.8 Elastic-plastic boundaries and stress paths during a cone pressuremeter test (after Withers *et al.*, 1989)

CHAPTER 2

EXPERIMENTAL APPARATUS AND SAMPLE PREPARATION

2.1 The cone pressuremeter

All tests carried out in the sand calibration chamber that have been reported in this thesis used a purpose-built 10cm^2 cone pressuremeter. The device was built by Cambridge In Situ to the specification set out by Fugro McClelland and Oxford University in 1987. A smaller 5cm^2 cone pressuremeter was also built and used in the testing reported by Schnaid (1990).

Similar in design to the 15cm^2 device used in the field tests reported in Chapter 6, the 10cm^2 CPM comprised a pressuremeter probe mounted behind a cone penetrometer of the same dimensions. Dimensions and essential features of the device are presented in Figure 2.1.

During insertion, measurements of cone resistance q_c were recorded using a load cell located immediately behind the cone tip. Since all tests were carried out in dry sand (the rationale for this procedure is discussed in section 2.4), there was no generation of excess pore pressures, and hence the corrected cone resistance q_t was always equal to the measured cone resistance q_c.

The pressuremeter module was inflated by silicon oil. A latex rubber membrane was clamped at the ends of the pressuremeter by two tapered clamping rings, which were locked into

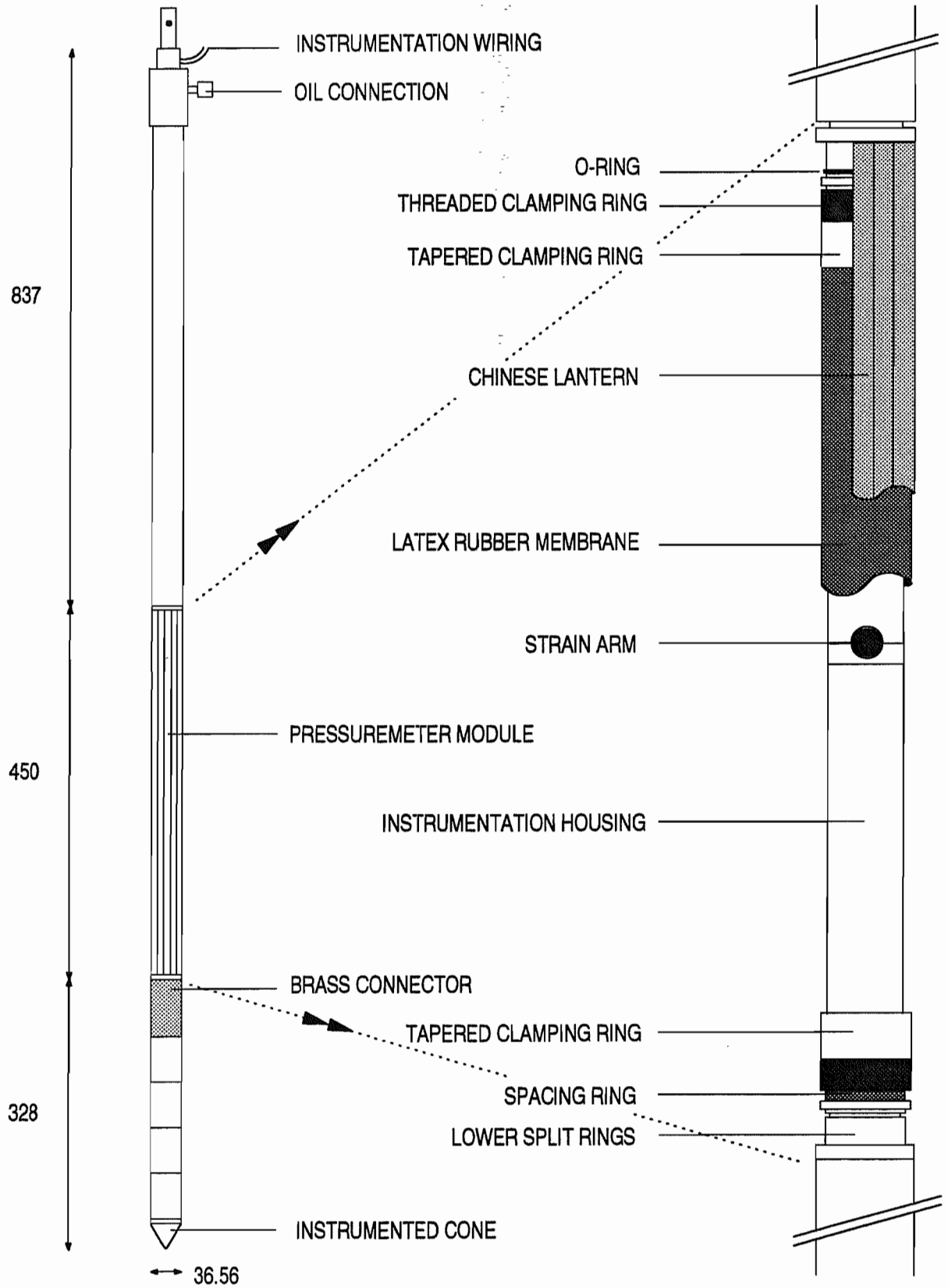


Figure 2.1 Dimensions and components of the 10cm² cone pressuremeter

position by two threaded rings. Central expansion of the membrane was measured by three strain gauged arms located at equal spacing of 120° around the circumference of the shaft, as shown in the photograph of Figure 2.2. The arms were calibrated using a micrometer that had been fitted to a brass ring for clamping onto the pressuremeter body.

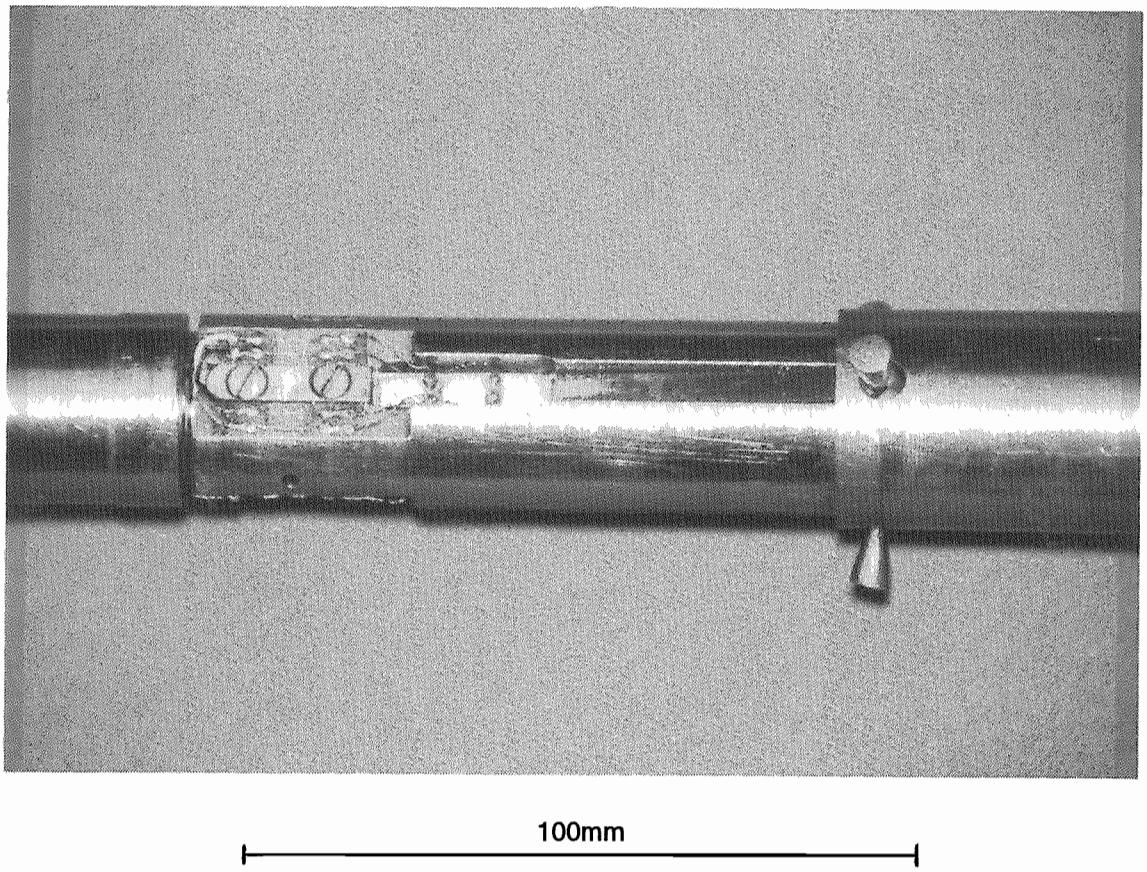


Figure 2.2 Central strain measuring system of the pressuremeter

The process of replacing the latex rubber membrane after calibration involved the following: An oversized length of cylindrical latex rubber was cut and folded back over each end of a thin, open-ended tube of larger diameter than the pressuremeter. Applying a slight vacuum to the tube sucked back the rubber enough to allow it to be slid over the pressuremeter. On release of the vacuum, the rubber retracted to the size of the pressuremeter. The ends were trimmed to size and the clamping rings fastened. Protection of this membrane from abrasion and tearing during insertion was provided by a "Chinese lantern" type outer sheath. The Chinese lantern comprised a cylindrical sheath of stainless steel strips to which was fixed on

the inside another rubber membrane. Because the Chinese lantern could not withstand compression, spacers were inserted before it was fastened to the pressuremeter thus allowing it to be drawn by its lower end on installation.

2.2 The Oxford Sand Calibration Chamber

2.2.1 The chamber and sand pressurisation system

To investigate the behaviour of the cone pressuremeter in sand, a controlled environment was created in a laboratory calibration chamber where conditions of sand density and *in situ* stresses were measured directly. The sand calibration chamber at Oxford was designed by Schnaid (1990) who performed cone pressuremeter tests in a uniformly graded, coarse grained silica sand. The need existed, therefore, to create a sand sample with dimensions suitably large so that boundary effects were kept to a minimum, but within the confines of an area of the laboratory where both head room and floor space were limited. As a result, the chamber dimensions were fixed to produce a sand sample approximately 1m diameter and 1.5m height, corresponding to a volume of around $1.2m^3$.

These dimensions are of the same order of magnitude as samples created by other researchers for validation of similar *in situ* devices. A comprehensive list of calibration chambers is given by Ghionna and Jamiolkowski (1991). Some of the larger chambers in this list include: The University of Florida, USA, 1.2m diameter, 1.2m height; Monash University, Australia, 1.2m diameter and 1.8m height; ISMES, Italy, 1.2m diameter and 1.8m height; The University of Tokyo, Japan, 0.9m diameter and 1.1m height; and the largest at Cornell University, USA, 2.1m diameter and 2.9m height.

Details of the Oxford calibration chamber are presented in Figure 2.3, including the essential dimensions which determine the sample size. The chamber is also shown in a photograph in Figure 2.4. Vertical stresses were applied to the sample through a shotblast rubber membrane

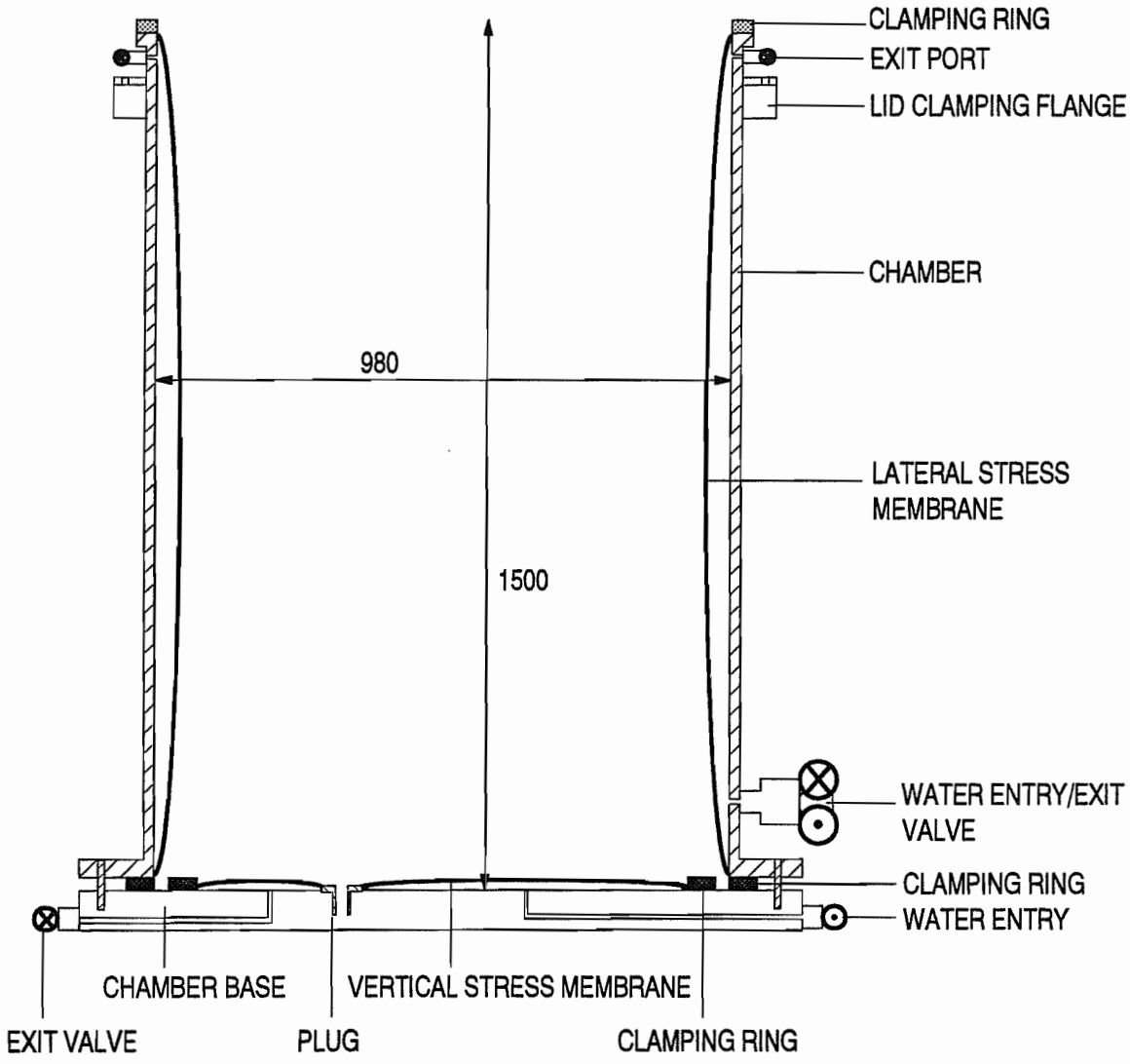


Figure 2.3 Components of the Oxford calibration chamber

attached to the base plate of the chamber. Entry and exit ports connected to the base plate allowed water to fill the membrane and provide the required stresses. The membrane was connected to the base plate by means of a steel annulus (or clamping ring). A plug, clamping the membrane off centre in the base plate, provided a means by which a sand specimen could be emptied from the chamber.

Attached to the base plate through a bolted flange was the cylindrical chamber itself. A cylindrical shotblast rubber membrane was clamped to the top and bottom of the chamber by steel clamping rings and provided the lateral confining stress to a sand sample. A valve at the

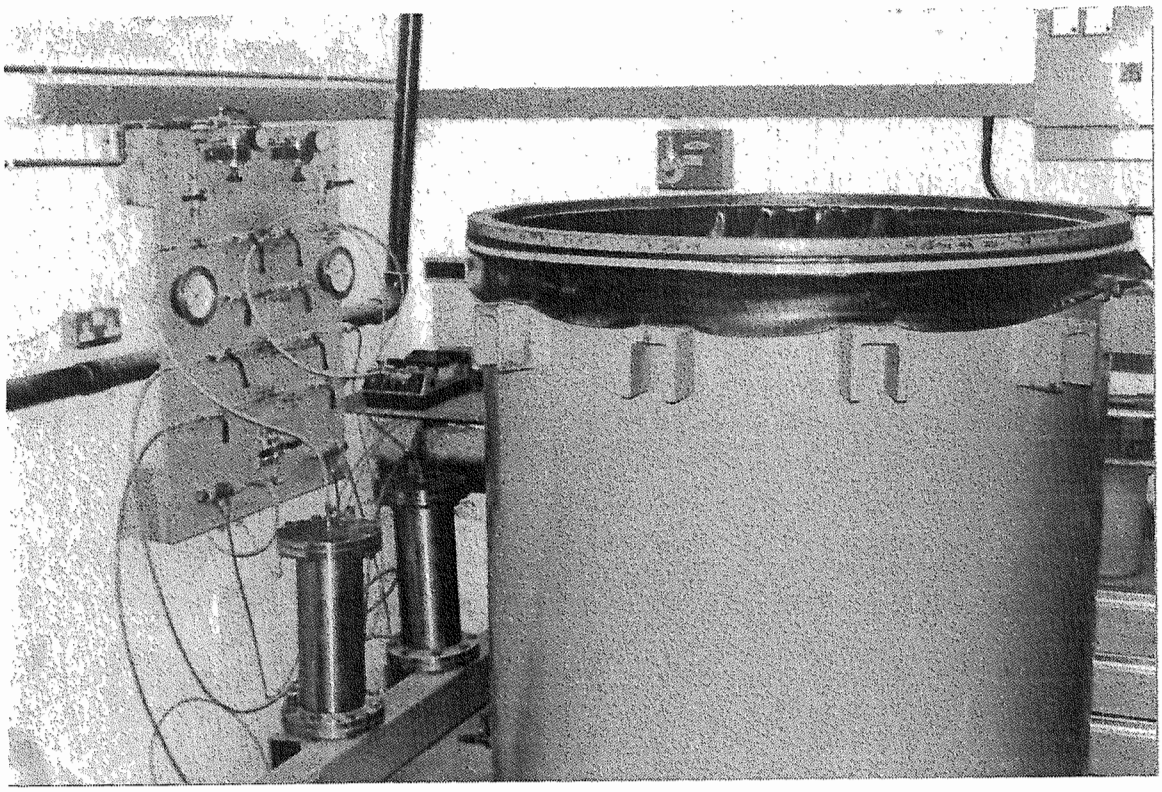


Figure 2.4 The calibration chamber and pressurisation panel

bottom of the chamber allowed the entry of water behind the membrane, and any air enclosed during filling was released through two diagonally opposite exit ports at the top.

Although securely clamped at the top and base of the chamber, it was these connections which limited the maximum stresses that could be applied to a sample. One of the tests reported in Chapter 4 required maximum confining stresses on both base and side membranes of 250kPa. The test was successfully completed. However, it was noted at the time that a lifting of the top clamping ring was beginning to occur, allowing a small amount of water seepage.

The top boundary was provided by a rigid top plate bolted to flanges on the chamber. Rigidity of the plate was ensured by tapered vertical webs welded at regular radial intervals. A hole in the centre of the plate allowed insertion of the *in situ* device being tested.

The testing programme reported in this thesis required the independent control of both the vertical and horizontal stresses. The rubber membranes attached to the base and inside wall of the chamber as previously described, were provided with water pressure through two independent air/water interfaces, which were in turn connected to a compressed air supply, represented schematically in half view in Figure 2.5. In order to control these stresses, a pressure regulating valve and gauge was attached to each interface. Pressures thus determined were recorded accurately at the air/water interface by a two channel Druck Digital Pressure Indicator (DPI). The whole pressurisation system was panel mounted.

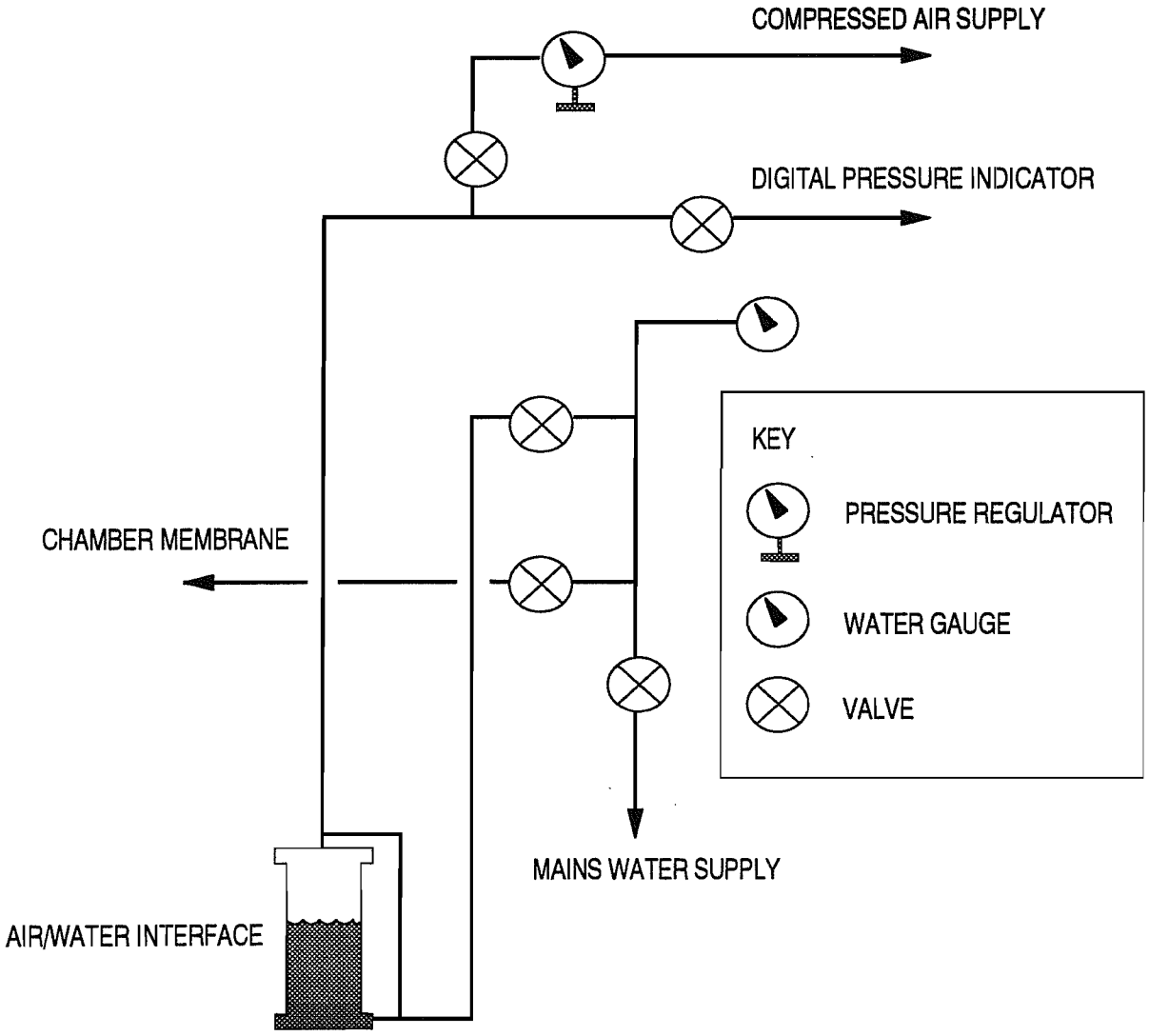


Figure 2.5 Schematic representation of the pressurisation panel (identical systems for applying lateral and vertical stresses)

2.2.2 The driving rig

A driving rig capable of providing sufficient thrust (up to 100kN) for insertion of a range of *in situ* devices, was attached to the rigid top plate of the calibration chamber by four pins. A large clay calibration chamber reported by Smith (1990) also made use of this driving rig for insertion of a Marchetti Dilatometer, and hence throughout the course of the research programme, the rig was often detached from the top plate. The rig and its components are shown in Figure 2.6. It comprised a large steel frame, a driving head, ball screw, DC motor and the pressuremeter pressurisation system.

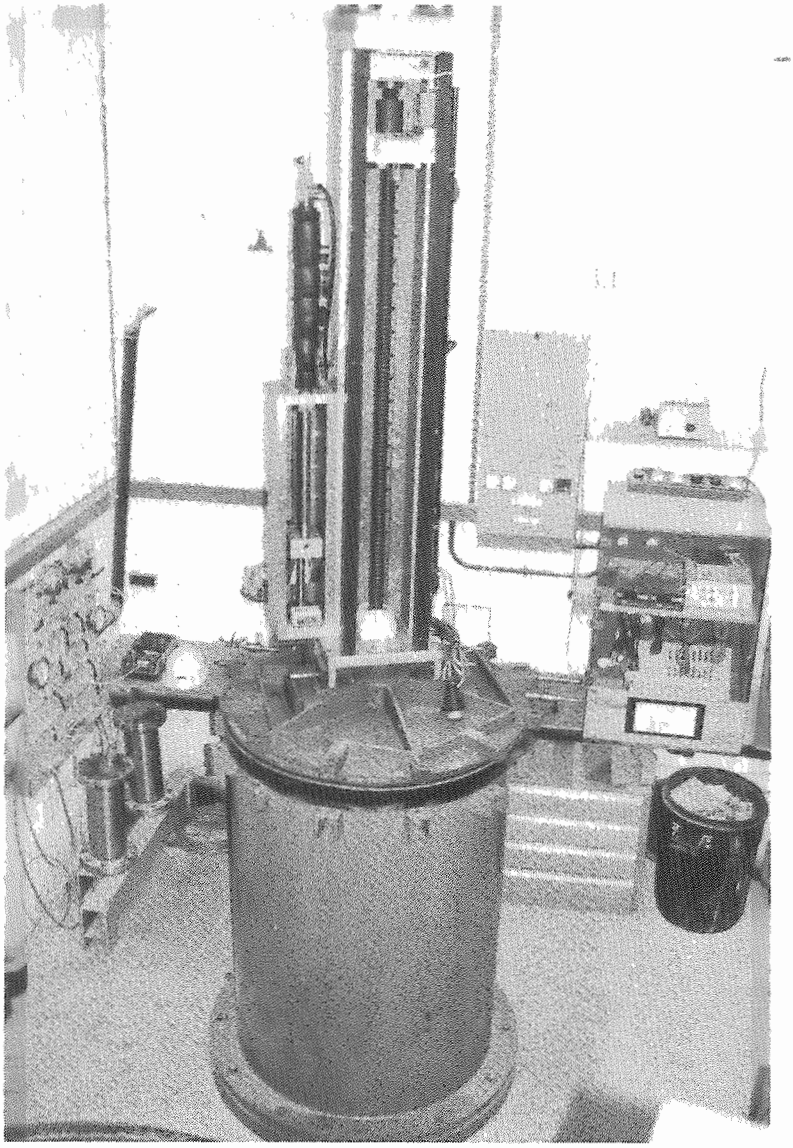


Figure 2.6 The driving rig and pressuremeter inflation system

The 3kW DC motor was mechanically connected by a chain to the 48.8mm diameter ball screw. The gear ratio on the motor was fixed to provide a constant rate of rotation to the ball screw which in turn provided a constant rate of linear travel to the driving head of 20mm/s ±5mm/s. The driving head, to which precision linear bearings were fixed, travelled along twin steel tracks mounted to the frame. The tracks ensured that no rotation of the driving head occurred as it ran along the ball screw. A simple threaded connector piece allowed attachment of the cone pressuremeter to the driving rig.

The 10cm^2 cone pressuremeter was inflated by silicon oil; an inert oil which did not cause deterioration of the latex rubber membrane of the cone pressuremeter. A small 31.9mm diameter ball screw operated by a McClennan DC tacho motor drove a stainless steel piston through a cylinder which was mounted on the frame of the pressurisation system, also shown in Figure 2.6. Displacement of the oil in the cylinder by the piston forced the inflation of the pressuremeter through a rubber pressure hose. Variation of speed and direction of turn of the ball screw was provided by a DC servo motor control box, thus allowing both inflation and deflation of the pressuremeter at monitored strain rates. Strain rates of up to 1.5% radial displacement per minute were possible. The capacity of the pressurisation system was 10MPa.

2.3 Instrumentation and Data Acquisition

2.3.1 Instrumentation

Instrumentation was set up to monitor both the performance of the cone pressuremeter during insertion and inflation, and to measure the conditions under which the sand sample was tested, and is summarised in Figure 2.7.

Cavity strain in the 10cm^2 cone pressuremeter was measured in two ways. Firstly, three strain gauged arms located at the mid-height of the pressuremeter were used to record changes in voltage as the membrane expanded or contracted. Secondly, strain was calculated from

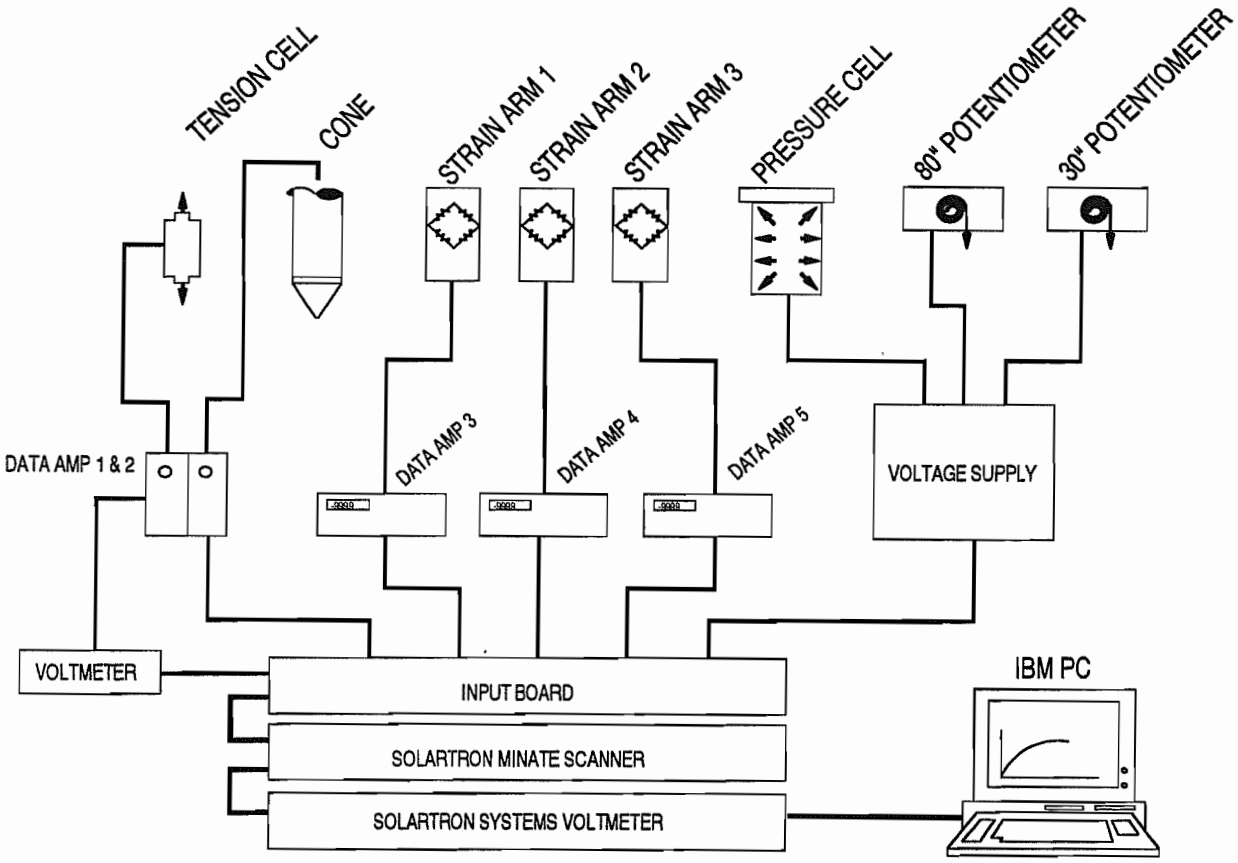


Figure 2.7 Configuration of instrumentation and data acquisition

measurements taken of the volume of oil pumped into the pressuremeter and the assumption that the membrane expanded and contracted at all times as a right cylinder.

The three strain arms at the centre of the membrane were located at 120° spacing. Each arm comprised a full "Wheatstone" bridge of four interlinked strain gauges as schematically illustrated in Figure 2.8. The arms were powered by a 5V DC supply, and three RDP E302.1 DC voltage amplifiers received the arms' output signals. They were capable of reading displacements of up to 9mm which was about 43% logarithmic cavity strain.

Strain measurements of the pressuremeter by volume readings were calculated from the amount of travel of the piston in the pressurisation system. This was measured by a Calvin position transducer, type PT101-30 with a tensioned cable attached to the driving head on the small ball screw, powered by a 5V DC supply. It had an accuracy of 0.1% over the full range.

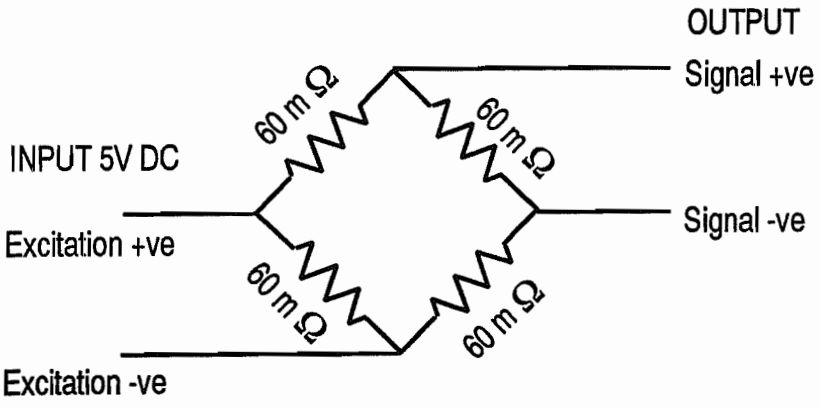


Figure 2.8 Full bridge arrangement for cone pressuremeter strain arms

A load cell located immediately behind the cone was powered by a 10V DC supply and the output signal returned to an amplifier. Both the load cell and the strain arms were built into the cone pressuremeter by Cambridge In Situ.

Inflation in the pressuremeter was measured by a Maywood P102 pressure transducer powered by a 10V DC supply. The capacity of the transducer was 7MPa, and it had an accuracy of 0.5% full scale capacity.

During the installation process, cone penetration was recorded through another Calvin position transducer type PT101-80A attached from the top of the rig's frame to the driving head. It had an accuracy of 0.1% full scale output and was powered by a 5V DC supply.

The applied vertical and horizontal stresses were measured for each test. A Druck Digital Pressure Indicator attached to each of the pressure lines was capable of reading pressures up to 700kPa to an accuracy of 0.1%. Sand unit weight was calculated by dividing the sample weight by its volume. Sample weight was measured by lifting the entire chamber on a Maywood T1040 Tension Cell with a capacity of 35kN and an accuracy of 0.1% full scale. The tension cell was powered by a 5V DC supply and the output signal was amplified by a Flyde FE-255-DA data amplifier.

2.3.2 Data Acquisition

During cone pressuremeter insertion, readings of cone resistance and travel of the driving head required two input channels. During pressuremeter inflation, readings on three strain arms, inflation pressure and oil volume change required five input channels. The output signals from all instrumentation were connected to a channel board as presented in Figure 2.7 which were then read by a Schlumberger Minate 7010 16 channel Analogue Scanner. Attached to the scanner was a Schlumberger Solartron 7060 Systems Voltmeter. Communication between the voltmeter and an IBM PC-XT computer was achieved by the IEEE 488 Programming Interface (also known as the GPIB - General Purpose Interface Bus). A set of programs written in Hercules BASIC by Schnaid (1990) and modified for the test programme in this thesis transferred the signals received from the voltmeter to hard disk, and also enabled test progress to be plotted on the screen.

2.3.3 Calibrations

The calibration of instrumentation was checked throughout the schedule of testing at regular intervals. All testing was carried out within the linear response of the calibration obtained from each instrument. Additionally, the instruments that were used to monitor pressuremeter inflation were checked for zero drift. This also gave a check on the resolution of the data that were recorded. Figure 2.9 shows a typical zero drift plot of the three strain arms over a period of about 30 minutes. While the magnitude of zero drift for each strain arm can be seen to be less than 0.5mV, the arms are also shown to be measuring voltages to the nearest ±0.05mV. In Table 2.1 the most recent calibration details of the instrumentation are summarised. The correlation coefficient, R^2 is shown to give an indication of the linearity of the calibrations. Maximum drift is presented as a percentage of the full range of the instrument over a period of 30 minutes. The calibrations remained reasonably constant, except in cases where the instrumentation or power supplies/amplifiers were actually changed.

Table 2.1 Calibration details of instrumentation

Instrument	Calibration /Volt	Capacity	R^2	Ave. drift %/30 min	Calibrated against
Arm 1	-6.051mm	9mm	0.9975	0.027	Micrometer
Arm 2	-7.147mm	9mm	0.9998	0.016	Micrometer
Arm 3	4.523mm	9mm	0.9999	0.010	Micrometer
P102	-10170kPa	7MPa	0.9998	0.044	DPI
PT101-30	16.06cm	750mm	1.0000	0.002	steel rule
PT101-80	41.01cm	2m	1.0000	-	steel rule
T1040	3.921kN	35kN	1.0000	-	Denison Press
Cone	3.868kN	32kN	0.9998	-	50kN load cell

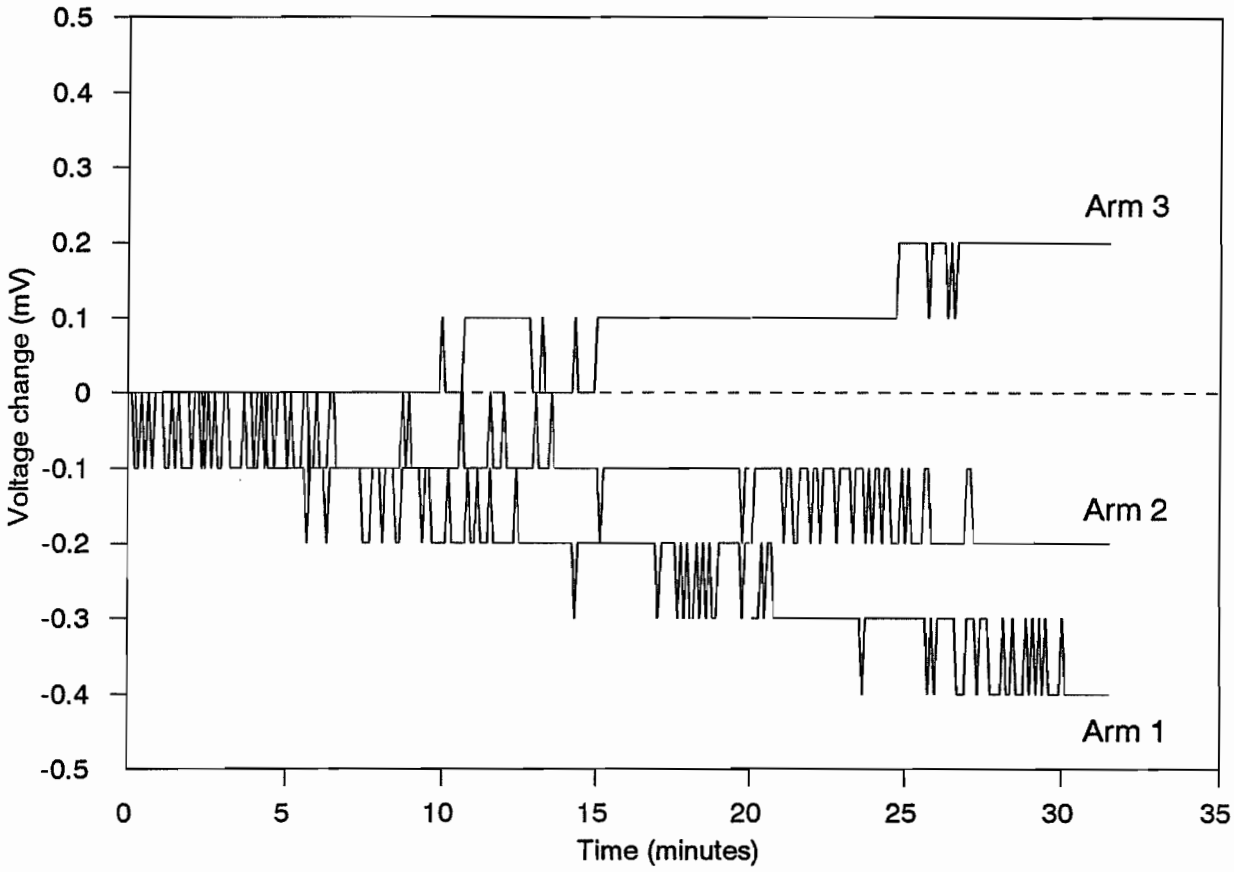


Figure 2.9 Zero drift of the cone pressuremeter strain arms

2.4 Sample preparation

2.4.1 Techniques for the uniform placement of sand

Calibration chamber testing in sand requires the placement of samples of uniform density. The most common approach used to obtain a required degree of homogeneity in a dry sample is that of pluviation, commonly referred to as sand "raining", although other techniques using vibration in layers are sometimes employed.

Pluviation is not a new technique, and has been used by many researchers (Kolbuszewski and Jones, 1961; Walker and Whitaker, 1967; Bieganousky and Marcusson, 1976), although there are a number of methods of pluviation. Bieganousky and Marcusson (1976) reported the use of a rotating rainer and a single hose rainer and made comparisons with results obtained from a circular perforated plate rainer. The concept of a travelling sand spreader was reported by Lo Presti (1990) where sand was poured from a hopper through a longitudinal slit in a moving plate. A similar principle was also reported for a rotating sand spreader. In this case, the calibration chamber was rotated at a constant rate while sand was poured from a hopper through a fixed plate with a single segment-shaped opening.

The most popular pluviation technique is where the sand is rained continuously over the whole area of the sample (Last, 1982; Belotti *et al.*, 1982; Rad and Tumay, 1987). Control of the intensity of pouring and the drop of height of the sand enables relatively uniform samples to be obtained with relative densities ranging from 20% to 90%. The kinetic energy of a single soil particle is directly related to the height of drop and to the mass of the particle. Beyond a critical drop height, however, further increase in height ceases to augment the kinetic energy of the grain if pluviation is carried out at atmospheric pressure. This has been experimentally verified by Vaid and Negussey (1984). The implication of this finding is that sample density can be controlled solely by varying the intensity of sand flow, as long as a minimum height of drop is maintained. This minimum drop height, based on the work of

several researchers (Miura and Toki, 1982; Vaid and Negussey, 1984; Rad and Tumay, 1987) is estimated for most sands to be 500mm.

Cole (1967) has validated the homogeneity of sand samples created by pluviation by radiographic examination of samples prepared in the Simple Shear Apparatus. Such a technique is extremely difficult to employ in a large steel calibration chamber, and a simpler but also quite effective method for verifying sample homogeneity is by placement of small containers in the calibration chamber prior to pluviation. Careful recovery and weighing of these containers after pluviation can give a good indication of the uniformity of the sample. This technique has been employed by Kolbuszewski (1948), Houlsby and Hitchman (1988), Crippa *et al.* (1990) and Al-douri *et al.* (1990).

At this stage, however, the limitations of sand placement by pluviation must be examined. Firstly, as reported by Ghionna and Jamiolkowski (1991), pluviation results in freshly reconstituted sand samples, which although they may be of uniform density throughout, do not reflect many of the factors affecting sand behaviour in the field. Natural soil deposits often exhibit a highly developed structure, built up in geological time by such phenomena as drained creep, early diagenesis and cementation (Mitchell and Solymar, 1984; Barton and Palmer, 1989).

Secondly, much of the research to date in calibration chambers has been on uniform, clean, predominately silica sands. While repeatability and uniformity of samples created by pluviation are evident in these soils, it should be noted that many engineering problems are linked to more crushable and compressible soils, and soils with a large silt or fines content (Evans, 1987; Almeida *et al.*, 1991). The applicability of pluviation to such soils, therefore, needs to be assessed on an individual basis.

2.4.2 Preparation of Hokksund sand

The preparation of sand samples in the Oxford calibration chamber was carried out by continuous raining deposition. A large hopper, capable of holding the complete amount of sand necessary for sample preparation was placed above the chamber. Required densities (within a range) were achieved by using a combination of perforated plates and diffusor sieves placed under the hopper. Schnaid (1990) used this technique to produce samples of Leighton Buzzard sand corresponding to loose, medium and dense. The terms loose, medium and dense are approximate terms used for convenience in sample description. While the pluviation process is repeatable, some amount of variation within a large testing programme is inevitable. Hence, each term refers to a range of densities into which fall most of the prepared samples.

The first series of tests reported in this thesis have been performed in Hokksund sand, the properties of which are discussed in Chapter 3. Loose samples were obtained using a perforated plate attached to the base of the hopper with holes of 20mm diameter on a 80mm triangular grid. Dense samples were obtained using a perforated plate with 6mm diameter holes on a 80mm triangular grid, under which was placed a diffusor sieve with an aperture size of 2.3mm, located 150mm from the base of the hopper. The minimum drop height of sand as discussed in section 2.4.1 of 500mm was observed.

Variation of density was checked using thin walled containers. The containers, of between 90mm and 110mm diameter, were placed in the chamber at different locations, mostly at the mid-height of the sample. After pluviation, the containers were carefully removed, levelled and weighed and the densities of the sand were calculated. Variations in unit weight of up to $\pm 0.4 kN/m^3$ were observed, and since this was within the scatter of the results presented in Chapter 3, the sample preparation technique was considered suitable. An additional check to the uniformity of the sample was provided by the profile obtained from each cone penetration test.

The sand to be tested was rained into a rigid, steel forming cylinder of 0.94m diameter, which had been placed in the chamber (of internal diameter 0.98m), and was lined with a thin neoprene rubber bag covering the sides of the forming cylinder and the base of the chamber. Once sample pluviation had ceased, the hopper was removed, and the neoprene bag was gathered, sealed and attached to a light vacuum of about -12kPa. This vacuum was sufficient to hold the shape of the sample intact, while the forming cylinder was then withdrawn. A slight backpressure, which had been applied to the lateral membrane of the cylinder was then removed, and the membrane was filled with water. This process produced a sample with reasonably vertical sides supported by water pressure and suitable for testing.

2.4.3 Preparation of Dogs Bay sand

The carbonate sand used in the testing programme was from Dogs Bay on the west coast of the Republic of Ireland. The properties of the sand are reported in Chapter 4. Particle size, shape and mineral composition were different to silica sands, and these features brought to question its suitability for sample preparation by pluviation. Evans (1987) and Almeida *et al.* (1991) both report the use of carbonate sands in calibration chambers, where pluviation was used with only a limited degree of success. Loose samples were created in the Oxford calibration chamber in the same manner as for the Hokksund sand, as discussed in section 2.4.2. The success of this technique was checked using small sampling containers. A study by Al-douri *et al.* (1990) assessed the applicability of pluviation in a calibration chamber for carbonate sand from the North West shelf of Australia. They found that a minimum drop height of about 450mm existed, beyond which sample density did not increase (with constant intensity of flow). The variation of density across the chamber found in their study using small containers has been replotted in Figure 2.10, with the results for loose Dogs Bay sand from this study added for comparison. In the figure, the container unit weights have been normalised by γ_{dmin}, the minimum unit weight. It is clear that both sets of results yield a similar degree of uniformity, and thus some confidence can be placed in the sample

preparation procedure for Dogs Bay sand.

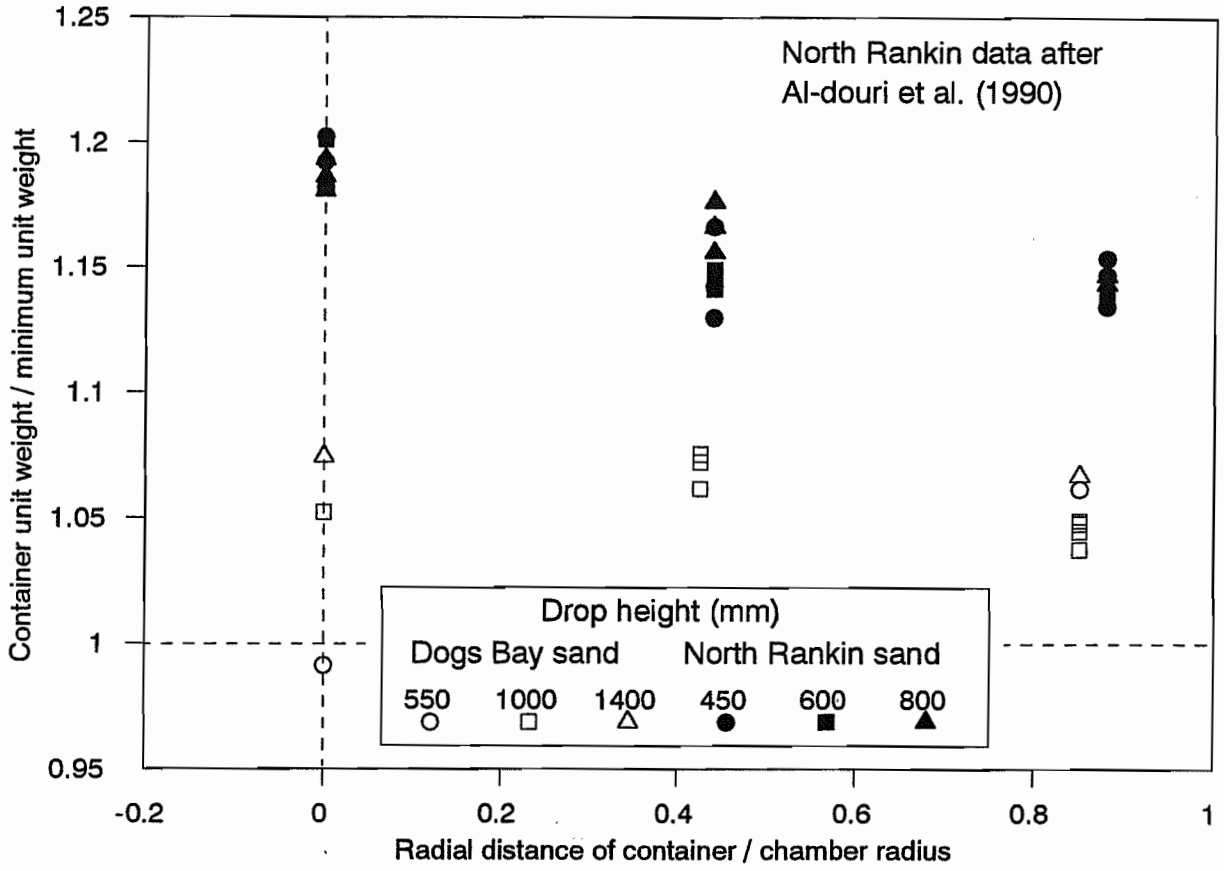


Figure 2.10 Density variation of pluvially deposited samples of carbonate sand in calibration chambers

It was found, however, that dense samples of Dogs Bay sand could not be created by the method of pluviation. Using the perforated plate with 6mm holes at 80mm spacings, it was found that the angular and platy nature of the sand caused it to block the holes. Instead, the plate with 20mm holes was tried, with the holes opened only sufficiently to start a continuous flow of sand (around 7mm or 8mm). This resulted in a sand only slightly denser than the loose samples (around 35% relative density). To determine the most suitable technique for creating samples of a denser state (at least 50% relative density) a study in a smaller calibration chamber (as used by Evans, 1987) was carried out. The most successful technique was found by vibrating the sand in layers of no more than 200mm thickness using a mechanical vibrating rod attached to a compressed air supply. For the preparation of samples in the large chamber, two such rods, 30mm diameter and fixed 300mm apart were used. Due

to the mechanical vibration of the sand some particle crushing may occur during this process. While this was unavoidable, particle size degradation was closely monitored throughout the test series. A discussion on the uniformity of samples produced using this method is presented in Chapter 4.

The procedure of applying a vacuum to the sample to remove the forming cylinder was repeated for the Dogs Bay sand.

CHAPTER 3

TESTS IN HOKKSUND SAND

3.1 Introduction

Calibration chambers provide the means by which the results of *in situ* tests, such as the cone pressuremeter test, can be correlated with both soil properties and *in situ* stresses. In this chapter, the results of a series of cone pressuremeter tests carried out in Hokksund sand are presented. The applied stresses have been varied, with sand samples being prepared in two different density ranges.

The rationale for the test programme is discussed and emphasis is placed on assessing the influence of *in situ* stress level, stress ratio and stress history (i.e application of an overconsolidation cycle) on the results obtained with the cone pressuremeter. Next, an outline of the procedure adopted for CPM testing in the calibration chamber is presented. This applies to both the preparation of equipment and the techniques involved in the basic test procedure. In order to convert the data obtained from a CPM test into results that can be correlated with the soil and *in situ* stress parameters, certain calibrations and corrections need to be applied, and these are also discussed.

An investigation into the fundamental properties of Hokksund sand follows, which draws together both a literature study and the results obtained from a series of laboratory tests. Classification tests, strength tests and compressibility tests have been carried out on the Hokksund sand, and are reported in this chapter.

Finally, the remainder of the chapter deals with the results obtained from the testing programme. The cone and the pressuremeter tests are dealt with separately, and the influence of the variable parameters on the test results is discussed.

3.2 A general procedure for cone pressuremeter testing

3.2.1 Test programme

A range of stress states has been used to assess independently the influence of stress level and stress ratio on the results obtained from the CPMT. The choice of stress states follows (deliberately) the states used in previous studies at Oxford (Schnaid, 1990; Houlsby and Hitchman, 1988) although some additional states have been added for the tests in carbonate sand. These states are shown in Figure 3.1 and quantified in Table 3.1.

Table 3.1 Nominal stress states

State	σ_v' (kPa)	σ_h' (kPa)	p' (kPa)	q (MPa)	K
A	60	30	40	30	0.5
B	150	75	100	75	0.5
C	40	40	40	0	1.0
D	100	100	100	0	1.0
E	24	48	40	-24	2.0
F	60	120	100	-60	2.0
G	150	150	150	0	1.0
H	250	250	250	0	1.0
J	50	25	33	25	0.5

Three primary stress ratios have been used of K = 0.5, 1.0 and 2.0. In field situations, high K values are normally associated with a cycle of overconsolidation, however, in this test programme, the stress ratios were required to isolate the influence of horizontal and vertical

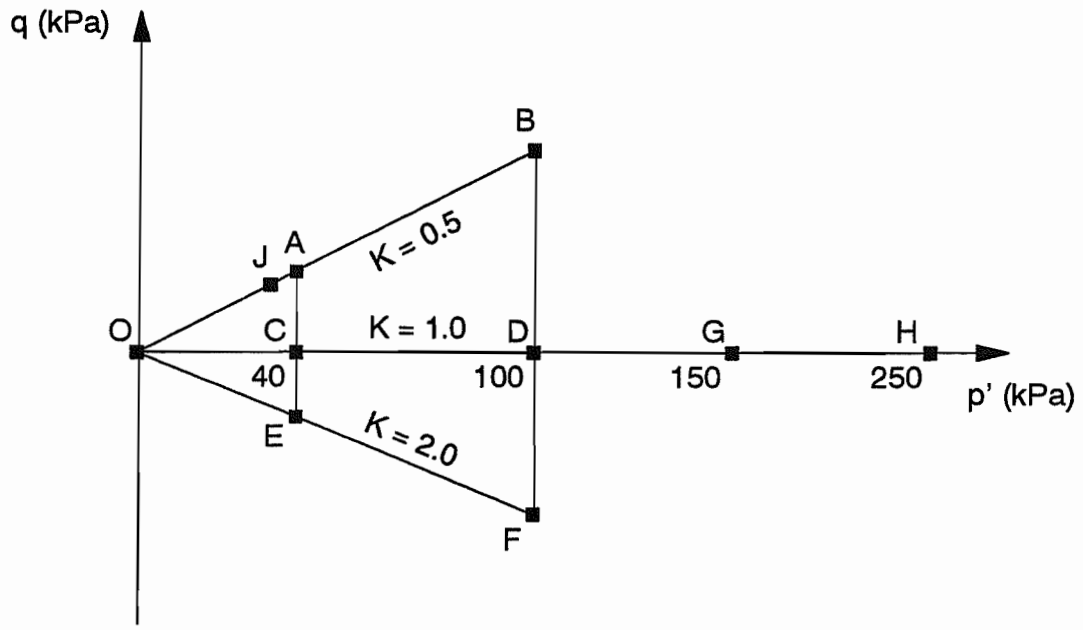


Figure 3.1 Nominal stress states for calibration chamber testing

stresses. The K values within the range used cover most conditions which represent the coefficient of earth pressure at rest, K_o, measured in natural sand deposits. Sand samples were prepared according to the procedures presented in Chapter 2. Prior to cone pressuremeter insertion, the applied chamber vertical and horizontal stresses were increased incrementally from roughly an "at rest" state to the state required for the particular test, with the ratio between the vertical and the horizontal stress being kept constant. Once all significant creep strains in the sample had been allowed to decay (evident by the stability of the water level at the air-water interfaces), the cone pressuremeter was inserted into the sample and a test was begun. Overconsolidated samples were achieved by incrementally reducing the chamber stresses (after decay of significant creep strains) from the higher to the lower stress state.

Most engineering problems associated with sand require the determination of drained parameters because of the rapid (usually immediate) dissipation of pore water, due to the high permeability of the sand. Previous studies with the cone penetrometer by Baldi *et al.* (1986) and Villet and Mitchell (1981) have shown that there is virtually no influence on test results

due to sand saturation when compared to tests in dry sand, and it is with this feature of sand behaviour in mind that the calibration chamber tests were carried out in dry sand, allowing ease of sample preparation.

Shear strength in drained conditions in sands depends upon the angle of friction, ϕ mobilised between sand particles. Friction angle in turn is dependent upon both the relative density, D_r and the mean effective stress level, p' (Bolton, 1986). Hence, in addition to the application of three different stress ratios as discussed, various stress levels corresponding to 40, 100, 150 and 250kPa mean effective stress have been used. Additionally, two ranges of relative density have been studied, corresponding to loose samples (15% to 25%) and dense samples (80% to 95%). Soil compressibility also influences the observed angle of friction in a sand (Baligh, 1976), although in hard grained sands such as Leighton Buzzard (Schnaid, 1990) and Hokksund sand, the influence of compressibility is small compared to the influence of stress level and relative density.

3.2.2 Preparation of equipment for testing

The following two sections outline the procedures that were used for cone pressuremeter testing in the calibration chamber.

With the cone pressuremeter attached to the head of the driving rig, a pressure membrane inflation in air was carried out. This inflation served two purposes. Firstly, as a standard procedure for pressuremeters (Windle, 1976; Baguelin *et al.*, 1978; Mair and Wood, 1987), an air calibration was necessary so that the stiffness of the pressuremeter membrane and Chinese lantern could be corrected for. The second function of an air inflation was to provide a check on the integrity of both the Chinese lantern and the instrumentation, by inflating the pressuremeter to the same strain magnitude that would be applied in the soil. The air inflation also provided an opportunity for cleaning out with a light brush any sand grains that may have become lodged in the grooves of the Chinese lantern from a previous test.

During any inflation, whether in soil or air, the presence of pockets of air trapped inside the pressuremeter or the oil inflation system can be the cause of inaccuracies in pressure measurement. Upon increase of pressure, such pockets compress until they are forced into solution. In order to minimise the influence of any entrapped air, a vacuum was applied to the oil inflation system and connected CPM for a period of around 20 to 30 seconds.

3.2.3 Test procedure

Once the chamber stresses had been applied, the sample was ready for testing. The CPM was inserted at a constant rate of 20mm/sec until the centre of the membrane was at mid-height of the chamber. At this point, a vacuum was applied to the pressure inflation system as described above after which pressuremeter inflation was begun.

Unless specified otherwise, all future references to cavity strains are made using measurements taken from the cone pressuremeter strain arms. Starting at 12%, 21% and 31% cavity strains, pressure holding tests followed by unload-reload loops were carried out. Pressure holding tests were controlled manually, with the strain rate and time increment being monitored continually. When the strain rate had reduced sufficiently, usually to around 0.03% per minute, the time was recorded and an unload-reload cycle commenced. This is represented in Figure 3.2 where a plot of strain rate against strain has been superimposed on a corresponding pressure-strain plot. Pressure holding tests allowed creep strains built up during inflation to decay, thus providing less hysteresis to the unload-reload loops which were used to estimate shear modulus. The size of an unload-reload loop was dictated by a preselected strain magnitude, $\Delta\varepsilon$ usually of 0.3% strain from the start of unloading, although in a group of tests in the Hokksund sand, the strain magnitude of the loops was deliberately varied. Unload-reload loops measured the elastic response of the soil and hence it was important that unloading was not so great as to cause reverse plasticity. Withers *et al.* (1989) recommended that the pressure magnitude of a loop, $\Delta\psi$ should not be greater than $0.4\psi_{max}$, where ψ_{max}

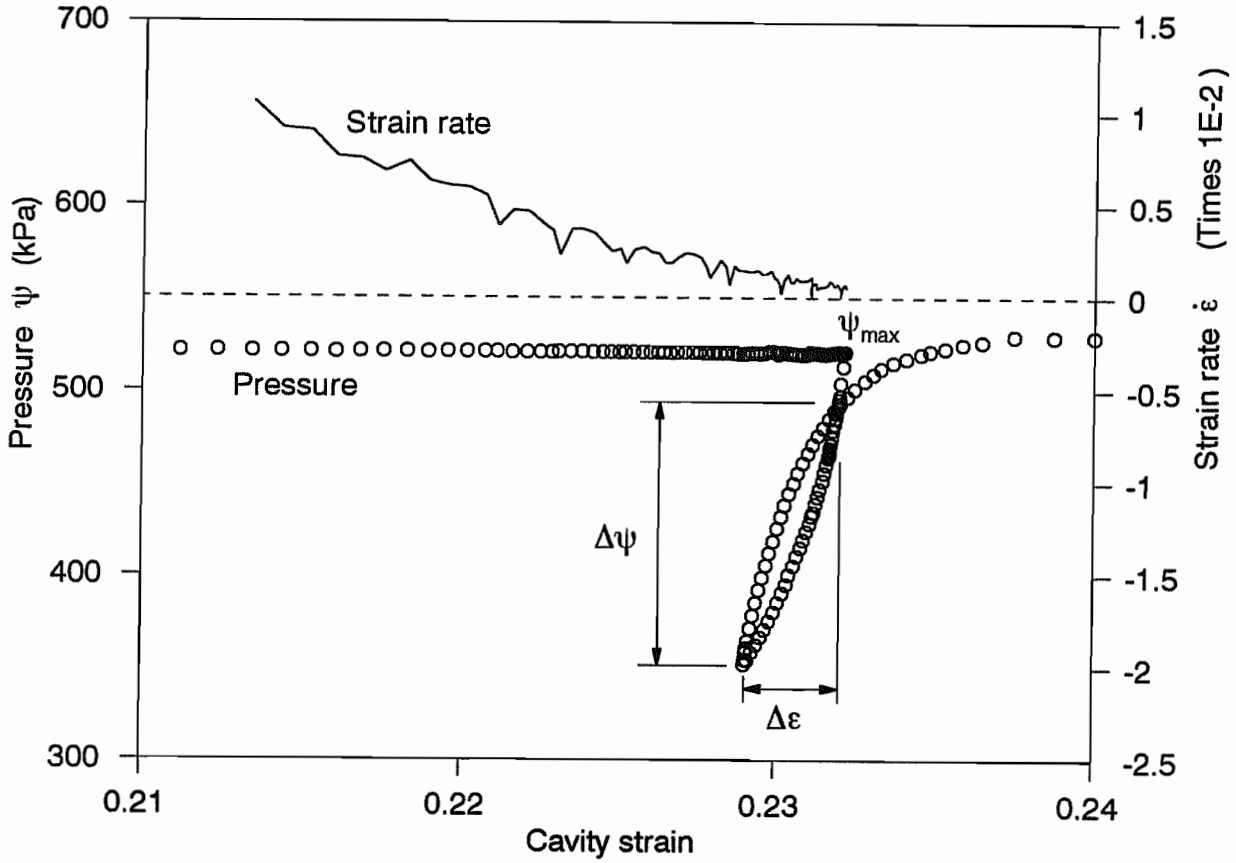


Figure 3.2 Test procedure for performing a pressure holding test followed by an unload-reload loop

is the maximum past inflation pressure. These limits, $\Delta\varepsilon$ and $\Delta\psi$ are shown in Figure 3.2 and were adopted in all tests reported in this thesis. In most tests, $\Delta\varepsilon$ was reached before $\Delta\psi$.

Full inflation of the pressuremeter was taken up to around 40% cavity strain at which point inflation was stopped and the applied pressure was allowed to relax for around 3 minutes. This is known as a strain holding test, and will be discussed further in Chapter 4. The pressuremeter was then deflated back to zero strain.

On completion of a pressuremeter test, the applied chamber stresses were released before the CPM was withdrawn from the soil. The $10cm^2$ cone pressuremeter was designed as a laboratory device for penetrating soil samples in one direction only. Without releasing the chamber stresses first, sufficient friction existed between the soil and the instrument to cause a permanent wrinkle in the Chinese lantern on extraction. These stresses were released

through exit ports in the chamber, and a measurement was made of the volume of water contained in each membrane. This was to provide a check on the diameter of the sample during a test where the sample volume was calculated as the difference between the total chamber volume and the volume of water from the membranes.

After extraction of the CPM, the driving rig was removed and the calibration chamber was weighed.

3.2.4 Data reduction and corrections

Reduction of the cone data obtained from insertion of the CPM was a relatively straight-forward process. The cone resistance corresponding to a particular pressuremeter test was taken as the value measured at mid-height of the chamber.

Before interpretations of the results of pressuremeter tests were made, however, raw test data were reduced to a form that best indicated the true response of the soil. Firstly, a correction was made to the air calibration curve due to the height difference between the CPM during an inflation in air and an inflation in the sample. Pressuremeter curves were reduced using a set of Fortran programs written by Prof. G.T. Houlsby. They are summarised as follows:

Program VTOENG Conversion of raw data in voltages to engineering units using the input of relevant calibration factors. Cavity strains based on the arm measurements and the volumetric measurements are output.

Program CALUNL Determines the offset on unloading generated from the input parameters which best fit the air calibration loading curve.

Program SUBCAL Subtraction of the best-fit air calibration curve from the pressuremeter test curve.

Program MODCAL Computation of the elastic shear moduli based on pressuremeter unload-reload loops. Moduli are calculated using chord and least square approximations for both arm and volumetric strain measurements.

With the independent measurement of three strain arms, it was possible to compute the hoop strain according to the definition

$$\varepsilon=\log_e\left(\frac{R}{R_0}\right) \qquad ...(3.1)$$

where R_o and R are the initial and inflated radii of the CPM respectively. This was done either by averaging the three measurements or fitting a circle through them. The latter approach accepts that the centre of the generated circle may shift slightly from the true centre of the pressuremeter, and is probably more realistic, especially since the design of the Chinese lantern is such that a spot welded join running the length of the lantern was probably somewhat stiffer than in other directions. The loading portion of a typical pressuremeter curve is shown in Figure 3.3.

The individual strain arms are plotted against the value of strain calculated by fitting a circle through the three readings. For comparison, the strain calculated by averaging the values is plotted as a bolder line, and shows that virtually no difference exists between the two methods. It can also be seen from the figure that the maximum possible strain measurement is recorded in arm one at about 39% strain. This feature has a consequence for selection of the limit pressure in a test, which will be discussed further in the next section.

It was found by Schnaid (1990) that a three parameter hyperbola of the form

$$\psi=K_1\varepsilon\left(\frac{\psi_f+K_2\varepsilon}{\psi_f+K_1\varepsilon}\right) \qquad ...(3.2)$$

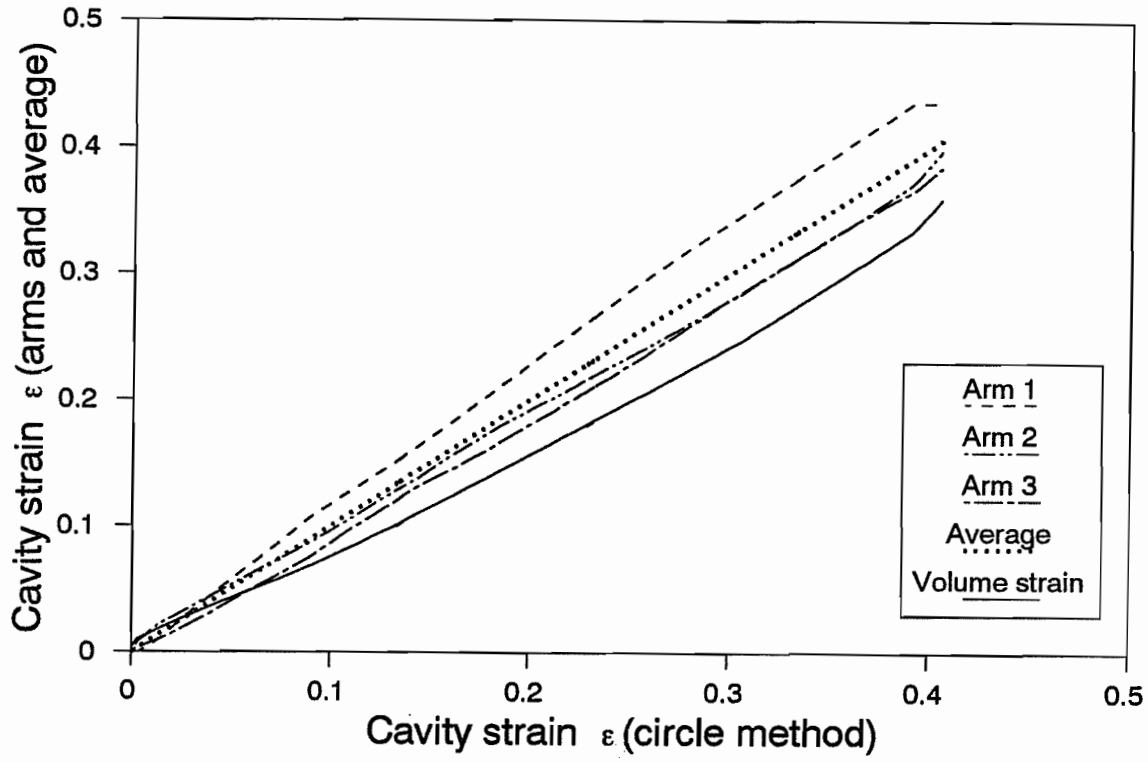


Figure 3.3 A comparison between volumetric and arm measurements of strain and strain computed from the circle method

provided a good fit to the air calibration data, where the parameters K_1, K_2, ψ_f are as shown in Figure 3.4, and ε is the pressuremeter cavity strain. A commercial program, STATGRAPHICS was used to estimate the three parameters based on the above non-linear regression analysis.

The true calibration curve for Test HS08 and the best fit curve generated by program CALUNL is shown in Figure 3.5. Despite the slight under-estimate of the membrane stiffness at the beginning of inflation and end of deflation, the modelled curve provides a good fit to the data. The correlation coefficient, R^2, quantifies the degree of fit, and for all the air calibrations used in this thesis, curves with R^2 greater than 0.97 were obtained.

The corrected pressuremeter curve was used to obtain information on the limit pressure, unload-reload shear moduli and rate behaviour from the pressure holding and stress relaxation tests.

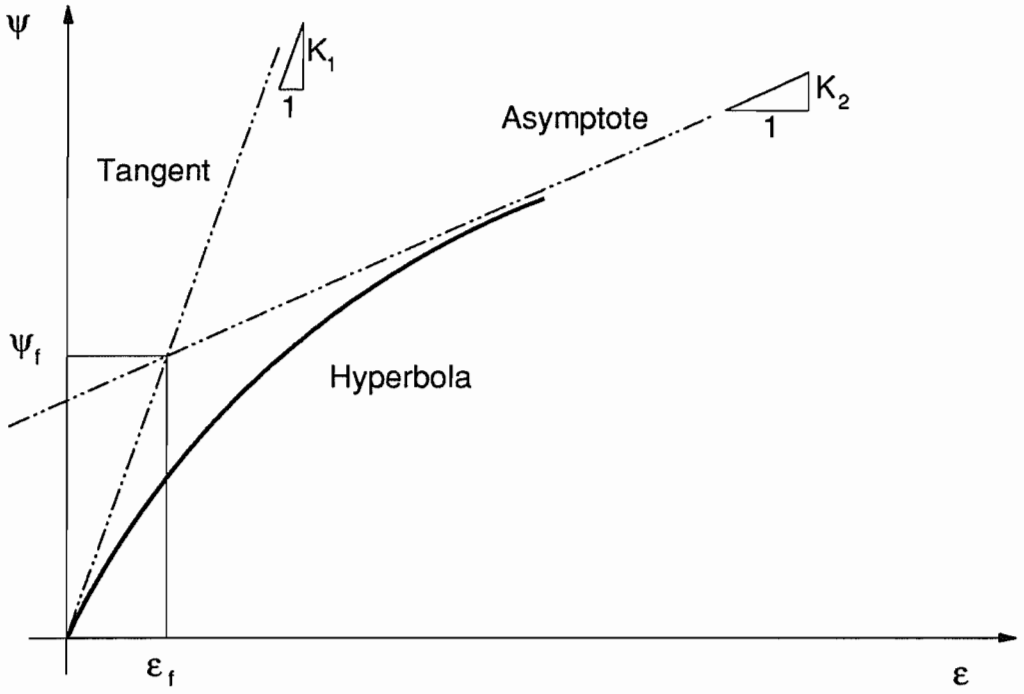


Figure 3.4 Three parameter hyperbola used as a fit to the air calibration data

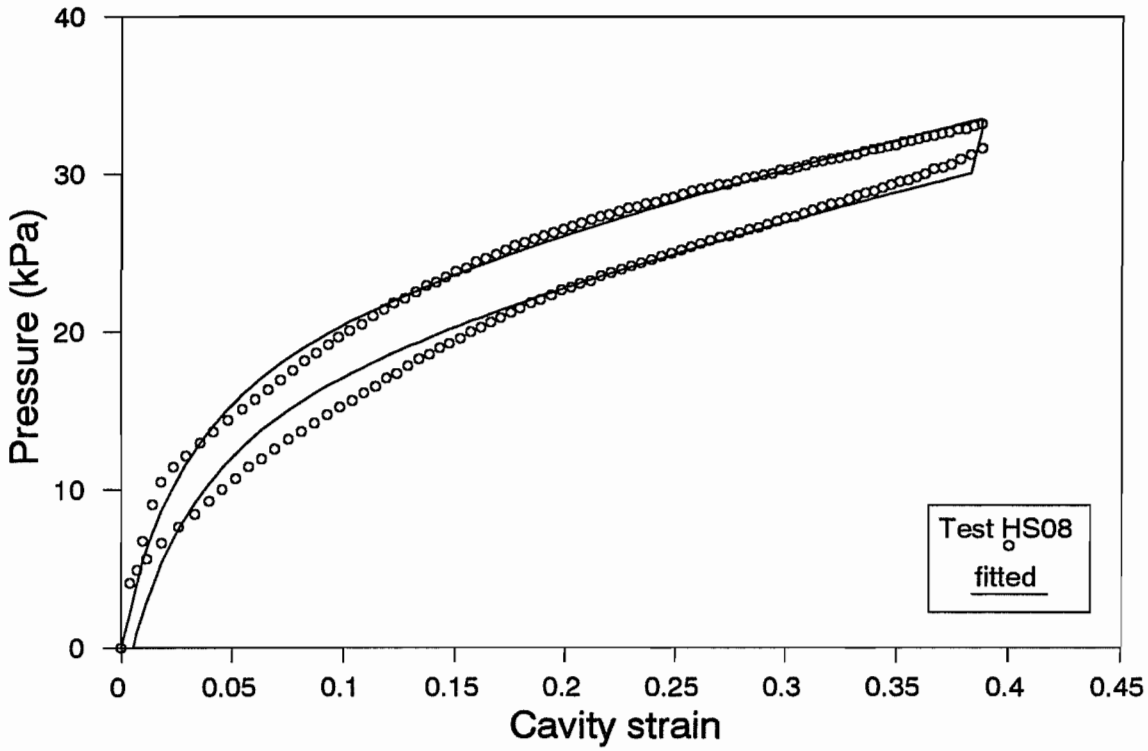


Figure 3.5 Typical measured and fitted pressuremeter inflation in air

Limit pressure is theoretically defined as the asymptotic pressure obtained by expanding a cavity to an infinite radius. For the sake of convenience in laboratory tests where the instrument capacity limits the maximum allowable strain, the term "limit pressure" has been

applied loosely to refer to the maximum inflation pressure achieved during a test up to a cavity strain of 38%. In most of the sand results reported in this chapter and by Schnaid (1990), the limit pressure was, in fact, reasonably well defined. In the tests in carbonate sand reported in Chapter 4, inflation pressures were often observed to be increasing slightly at large cavity strains.

A further correction applied to the pressuremeter data was that of system compliance. The effects of system compliance are significant in the measurement of shear moduli, and thus will be discussed fully in Chapter 7.

3.3 Soil Properties

A quantity of Hokksund sand was loaned to Oxford University by the Norwegian Geotechnical Institute (NGI) and Southampton University for tests carried out in this thesis, and was considered suitable for two reasons. Firstly, it was well documented, with much work being reported by NGI, (Last, 1979; Kildalen *et al.*, 1982; Parkin and Lunne, 1982), ISMES in Italy (Jamiolkowski *et al.*, 1985) and Southampton University (Last *et al.*, 1987). Secondly, it was a feldspathic sand in contrast to the carbonate sand from Dogs Bay used in the main test series and the Leighton Buzzard silica sand used by Schnaid (1990) in the same chamber. Hence, it was an ideal choice to assist in expanding the database of cone pressuremeter tests in different materials.

3.3.1 Classification

Hokksund sand is an angular, fluvio-glacial deposit found in the Drammen river valley near Oslo. The mineralogical component of the sand was studied by Kildalen *et al.* (1982) by X-Ray diffraction and the sand was found to comprise 45% feldspar, 35% quartz, 10% mica (primarily biotite), 5% amphibole and 5% unidentified. Hence it is a feldspathic sand with a significant silicate component. Feldspar is a softer mineral than quartz; 6 on the Möh's scale of hardness compared to 7, and hence Hokksund sand could be expected to exhibit somewhat

higher friction angles (Bolton, 1986). The influence of mica due to both the softness (4 on Möh's scale) and the single cleavage plane is difficult to assess, and Last (1982) postulated that a reduced elastic modulus and induced anisotropy at high stress levels could be expected.

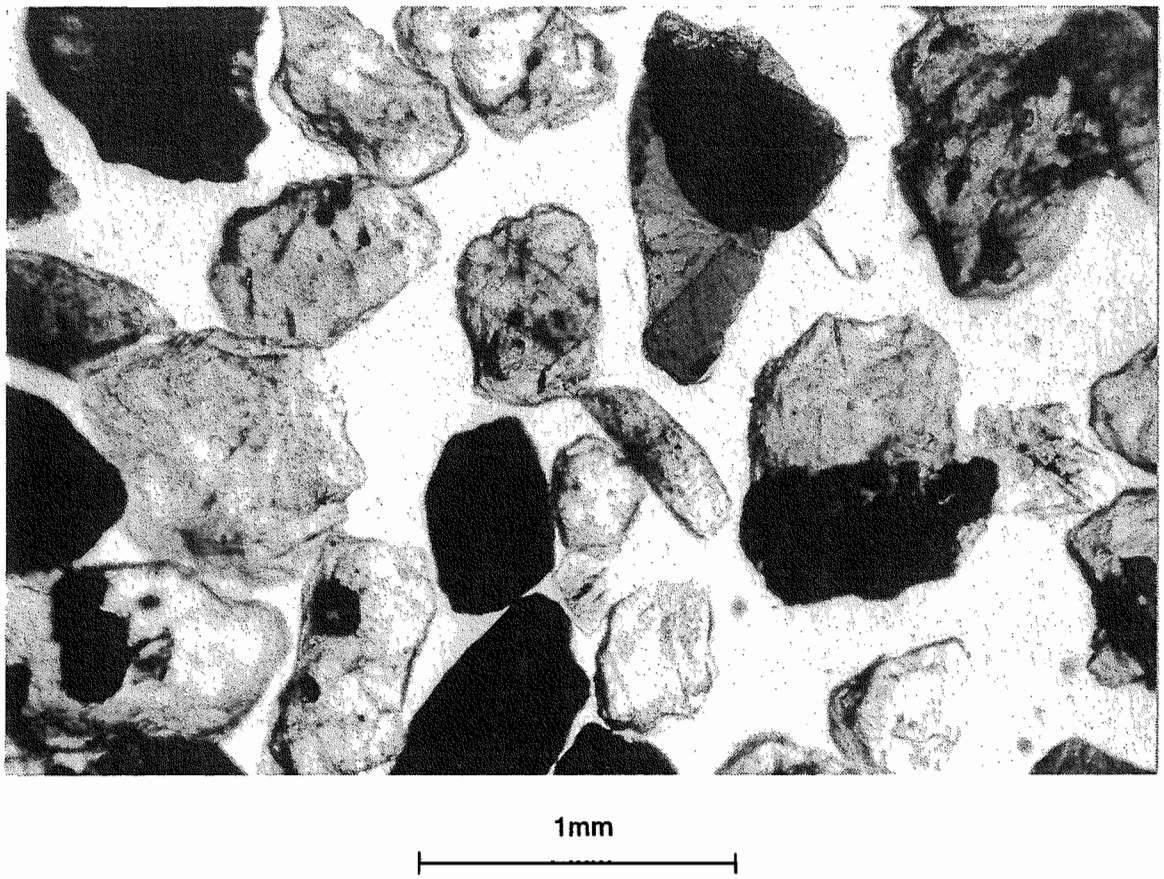


Figure 3.6 Micrograph of Hokksund sand

A micrograph of Hokksund sand is shown in Figure 3.6. Most of the sand components can be identified, and the particles are generally sub-angular in shape. Hokksund sand is a uniformly graded, medium grained sand containing negligible fines, as shown in the grading curve of Figure 3.7. D_{50} was found to be 0.43mm, D_{10} was 0.22mm, and the Coefficient of Uniformity, U was found to be 2.18.

Sand behaviour is often related to a density index, commonly referred to as relative density, analogous to the liquidity index of a clay. The calculation of relative density relies upon a knowledge of the maximum and minimum weights, γ_{dmax} and γ_{dmin} of the sand through the

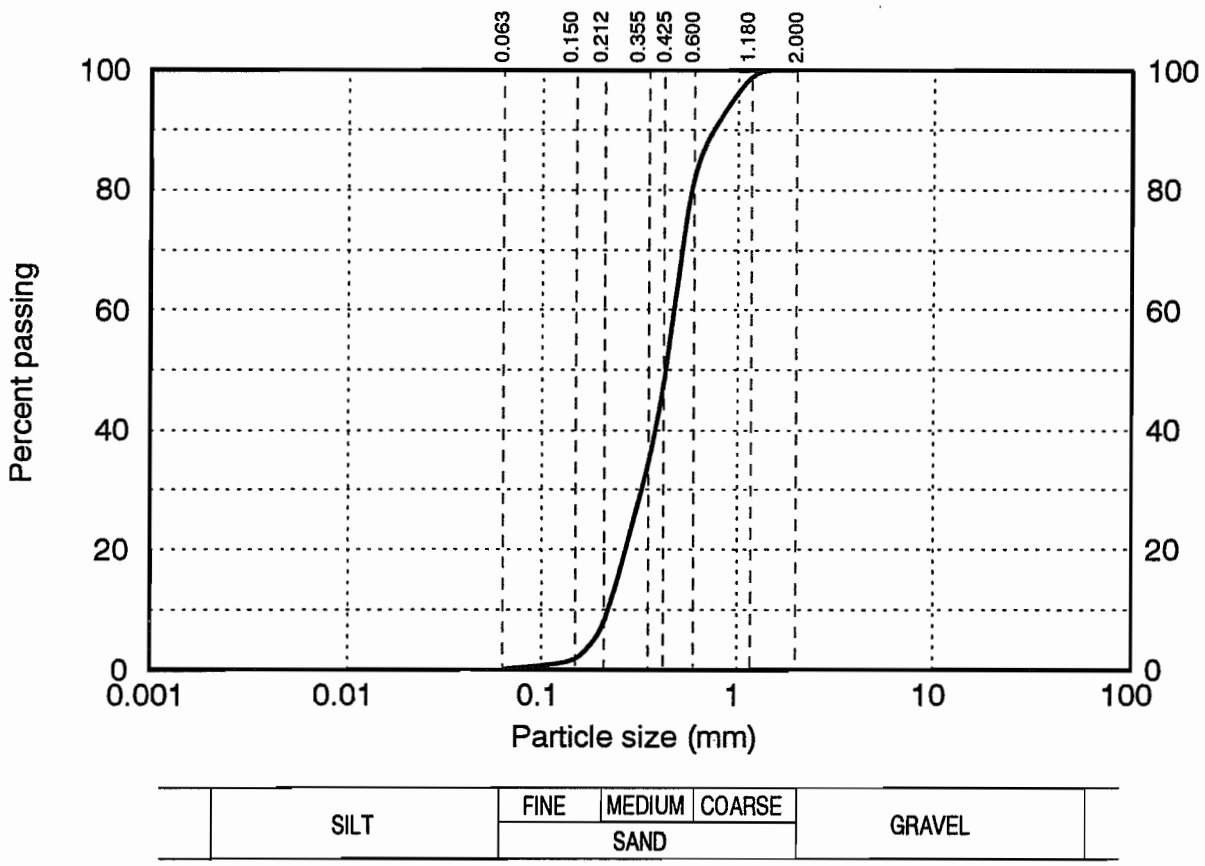


Figure 3.7 Grading curve for Hokksund sand

expression

$$D_r = \frac{e_{max} - e}{e_{max} - e_{min}} \qquad ...(3.3)$$

where e_{max} and e_{min} are the maximum and minimum voids ratios respectively. Voids ratio is related to density by

$$e = \left(\frac{\gamma_w}{\gamma_d} SG \right) - 1 \qquad ...(3.4)$$

where γ_w = the unit weight of water taken as 9.8 kN/m^3, and SG = specific gravity of the soil.

While standard methods for measuring γ_{dmax} and γ_{dmin} exist, they do not necessarily produce

absolute maximum or minimum values. Minimum unit weight for Hokksund sand was found using the method of Kolbuszewski (1948) of rapidly inverting a cylinder containing a known weight of sand and measuring the equivalent volume of water that it occupied. It was found to be 14.12 kN/m^3. The specific gravity of the sand grains was 2.70.

The methods available for the determination of the maximum unit weight can be grouped into the following:

(i) vibrating methods (including tapping); ASTM D4283, BS1377

(ii) pluviation methods; Crippa *et al.* (1990)

(iii) tamping methods; Last (1982)

A study by Crippa *et al.* (1990) compared the maximum unit weight as determined by pluviation using a Miura and Toki (1982) sand spreader with the vibration method of ASTM 4253. It was found that the former resulted in negligible particle crushing, less segregation of particle sizes, more accurate density measurement and better repeatability than the latter method. Since samples in this thesis have been prepared by pluviation, a maximum unit weight of 17.26 kN/m^3 has been used based on the findings of Crippa *et al.* (1990).

3.3.2 Strength tests

Kildalen *et al.* (1982) presented an extensive series of triaxial tests on Hokksund sand in order to define its laboratory characteristics for comparison with CPT tests in the NGI Calibration Chamber. In order to increase the available data on the strength parameters of Hokksund sand, a series of direct shear tests has been completed in the 60mm x 60mm Casagrande Shear Box. Loose samples were prepared by rapidly pouring the sand through a funnel and dense samples were prepared by pluviation. The results of the tests are shown in Figures 3.8(a) and 3.8(b) and are summarised in Table 3.2.

Table 3.2 Direct shear tests on Hokksund sand

	Test	σ_v (kPa)	$\sigma_{h\text{-}peak}$ (kPa)	D_r (%)	ϕ_{peak} degrees	ϕ_{resid} degrees	ν degrees
Loose	1	40.0	30.7	16.4	37.5	31.6	2.8
	2	100.0	62.2	20.9	33.4	32.0	-
	3	150.0	98.1	30.4	33.2	32.0	-
	4	200.0	129.5	25.9	32.9	32.1	-
Dense	5	40.0	37.5	73.4	43.1	32.0	15.6
	6	100.0	81.5	75.3	39.2	32.6	11.1
	7	150.0	128.3	75.5	40.5	32.5	15.2
	8	200.0	169.7	71.7	40.3	32.9	14.8

The results follow closely a similar set of tests reported by Last (1982). The constant volume friction angle, ϕ_{cv} has been determined after making an energy correction according to Taylor (1948), and found to be 32.4°. The dilation angles have been determined using the straight line portion of the volume change curves.

3.3.3 Compressibility tests

Oedometer tests were carried out on the sand up to normal stresses of 4 MPa as shown in Figure 3.9. Based on these results, the compression index, C_c was found to be 0.185. The expansion index, C_s was 0.00292. In normal compression, in which the principal stresses increase proportionally, the oedometric compression line should have the same slope as that for isotropic compression so that $C_c = \lambda \log_e 10 \approx 2.3\lambda$ (Wroth and Houlsby, 1985), where λ is the slope of the isotropic compression line in $V : \log_e p'$ space. In one-dimensional swelling, the stresses do not decrease proportionally so that $C_c \leq 2.3\kappa$ is the only relationship

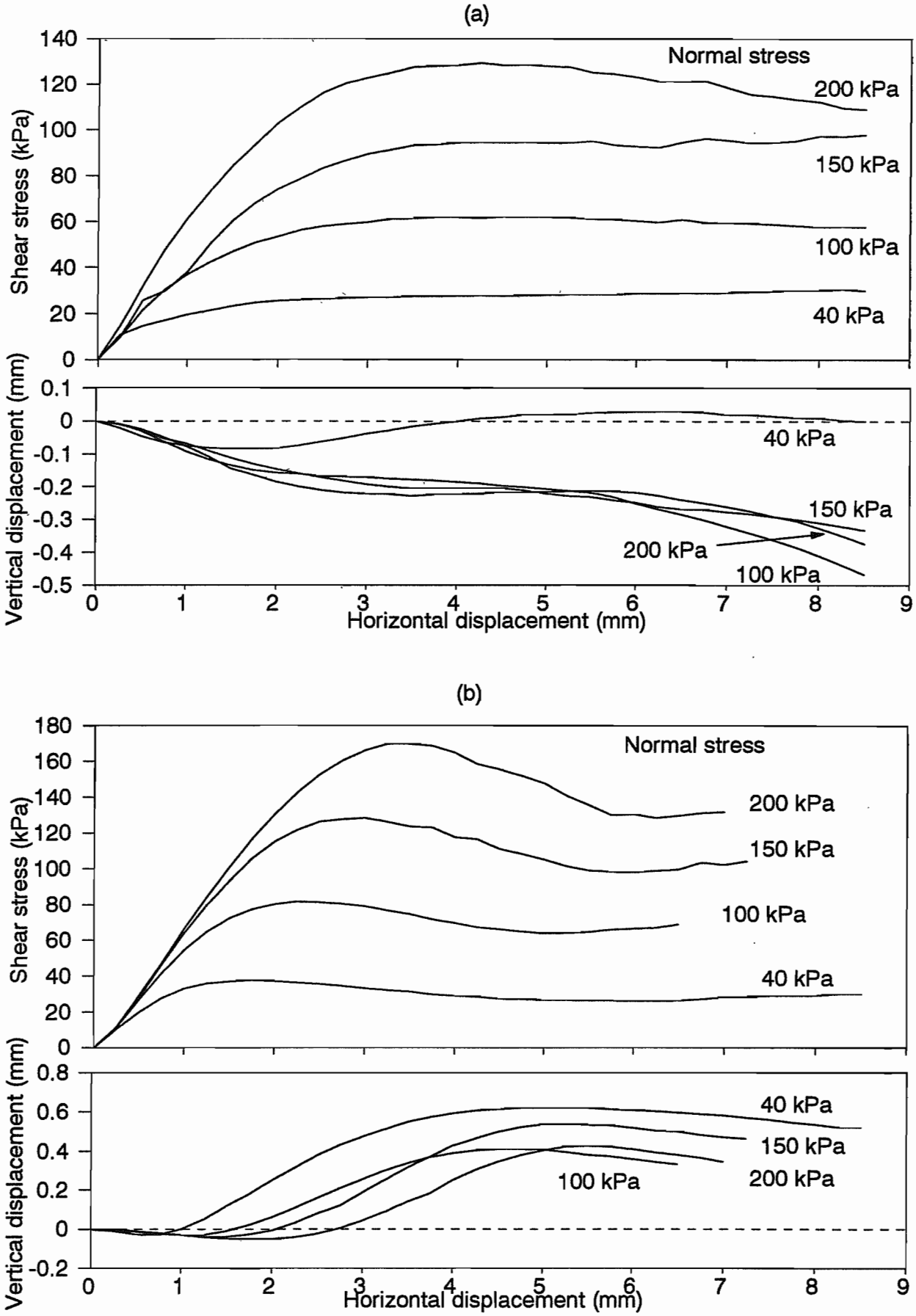


Figure 3.8 Results of shearbox tests on Hokksund sand (a) loose, (b) dense

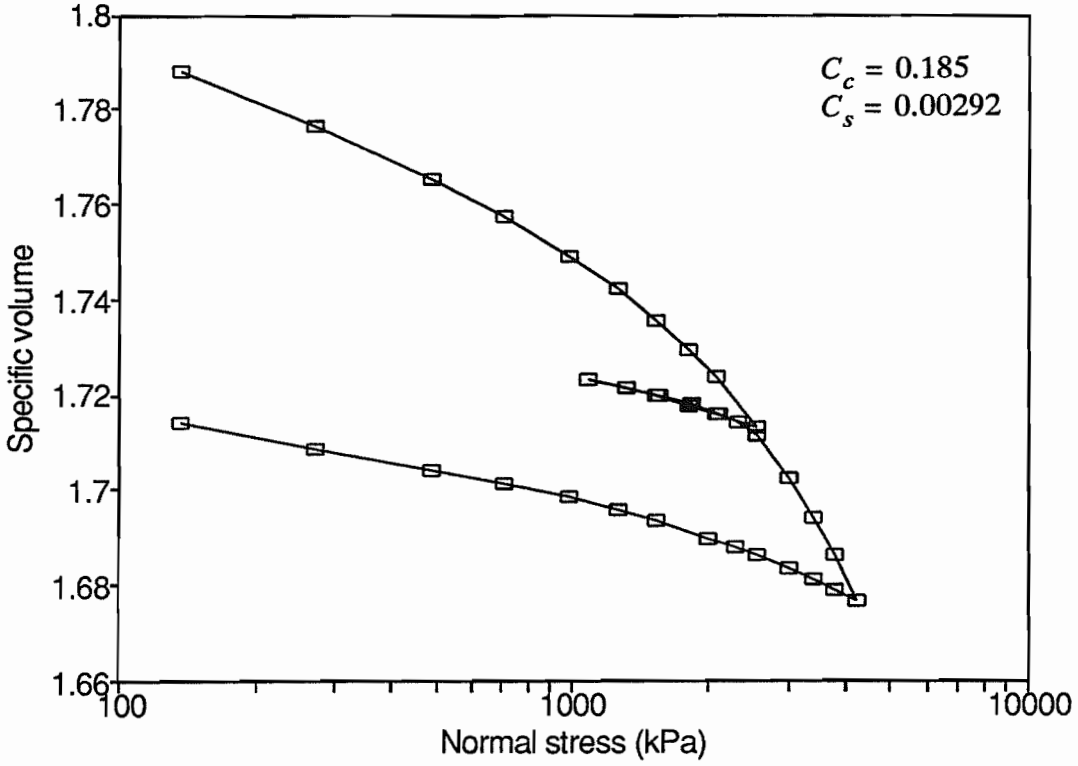


Figure 3.9 Oedometer test in Hokksund sand

that can be applied, where κ = the slope of the isotropic expansion line in V : $\log_e p'$ space.

3.4 Test Results

3.4.1 Test series

The results of a total of 12 tests in Hokksund sand, 1 test in Leighton Buzzard sand, 33 tests in Dogs Bay carbonate sand and 12 field tests in Bothkennar soft clay are presented in this thesis - a total of 58 tests. This chapter concentrates on the tests in Hokksund sand, which were intended to supplement the main test series in carbonate sand reported in Chapter 4, however, a brief explanation of the system applied to naming all tests is presented here so that future reference to particular tests can be made easily.

The name of a test commences with two letters which specify the soil type tested. HS refers to Hokksund sand, LB refers to Leighton Buzzard sand, DB refers to Dogs Bay sand and BK refers to the field tests in clay at Bothkennar. This is followed by a test number which is

usually (but not always) an indication of the chronological order in which the test was performed. On occasion it was necessary to duplicate a test and this is indicated by exchanging the second letter of a test with the letter X, or the letter Y if the test was duplicated a second time. For example, Test HX07 is a different test from Test HS07, although the samples were tested at the same density and stresses.

The results of the tests in Hokksund sand are presented in Table 3.3 which lists the stress conditions, sample density and the cone resistance and limit pressure. Corrections for stresses at mid-height of the chamber have already been made.

Table 3.3 Results of tests in Hokksund sand

Test No.	Stress path	σ_v' (kPa)	σ_h' (kPa)	p' (kPa)	K	D_r (%)	ψ_l (kPa)	q_c (MPa)	$\frac{q_c-\sigma_h}{\sigma_h'}$	$\frac{q_c-\sigma_h}{\psi_l-\sigma_h}$
HS01	OA	57.4	31.6	40.2	0.55	33.0	280	1.29	39.8	5.1
HS02	OB	147.7	75.7	99.7	0.51	35.8	628	3.04	39.2	5.4
HS03	OC	38.2	40.4	39.7	1.06	32.6	341	1.74	42.1	5.7
HS04	OD	101.4	101.9	101.7	1.00	37.5	782	4.01	38.4	5.7
HS05	OBA	59.8	30.3	40.1	0.51	30.8	306	1.63	52.8	5.8
HS06	OA	60.9	31.2	41.1	0.51	-	444	-	-	-
HX06	OA	59.7	29.3	39.4	0.49	87.4	540	5.90	200.4	11.5
HS07	OB	149.9	75.0	100.0	0.50	-	910	-	-	-
HX07	OB	149.8	73.8	99.1	0.49	74.3	1047	10.66	143.4	10.9
HS08	OC	40.5	40.9	40.8	1.01	92.5	1005	12.35	301.0	12.8
HS09	OD	100.6	100.2	100.3	1.00	86.6	1529	21.43	212.9	14.9
HS10	OBA	59.9	39.1	46.0	0.65	88.5	892	12.25	312.3	14.3

The results for tests HS06 and HS07 have been included although no estimates of D_r or q_c are given. This is because the cone profile obtained in these two tests was too uneven to make a sensible interpretation of q_c at mid-height of the chamber. This implied large variations in density throughout the sample due, most likely, to problems involved in sample preparation. The test results will only be used to provide data on shear modulus from unload-reload loops of the pressuremeter.

3.4.2 Cone results

The cone profiles of Figures 3.10 and 3.11 illustrate that the samples were prepared uniformly. The rate of increase of the penetration resistance with depth in the top 200mm of the sample is probably affected by the proximity of the rigid top plate of the chamber. There is a trend in most of the tests to show a very slight drop in cone resistance at the centre of the sample. This is due, most likely, to a sensitivity of the sample density to the preparation procedure, as discussed in Chapter 2. Such variations must be tolerated and are, in fact, no greater than those reported by Parkin and Lunne (1982) or Last *et al.* (1987), both in calibration chambers using Hokksund sand.

The Hokksund sand tests were carried out using combinations of two stress levels, two stress ratios, at two densities as indicated in Table 3.3. The influence of these parameters on cone resistance measured in calibration chambers is well reported by Schmertmann (1975), Villet and Mitchell (1981), Baldi *et al.* (1982) and more recently by Houlsby and Hitchman (1988) and Schnaid (1991). The Hokksund results, not surprisingly, follow the same trends, as shown in Figures 3.10 and 3.11, where the cone results at a constant stress ratio are presented for the two densities and stress levels tested. Increasing q_c with increasing p' and increasing D_r is evident, and from a comparison between the figures, q_c is also shown to increase with increasing stress ratio, K.

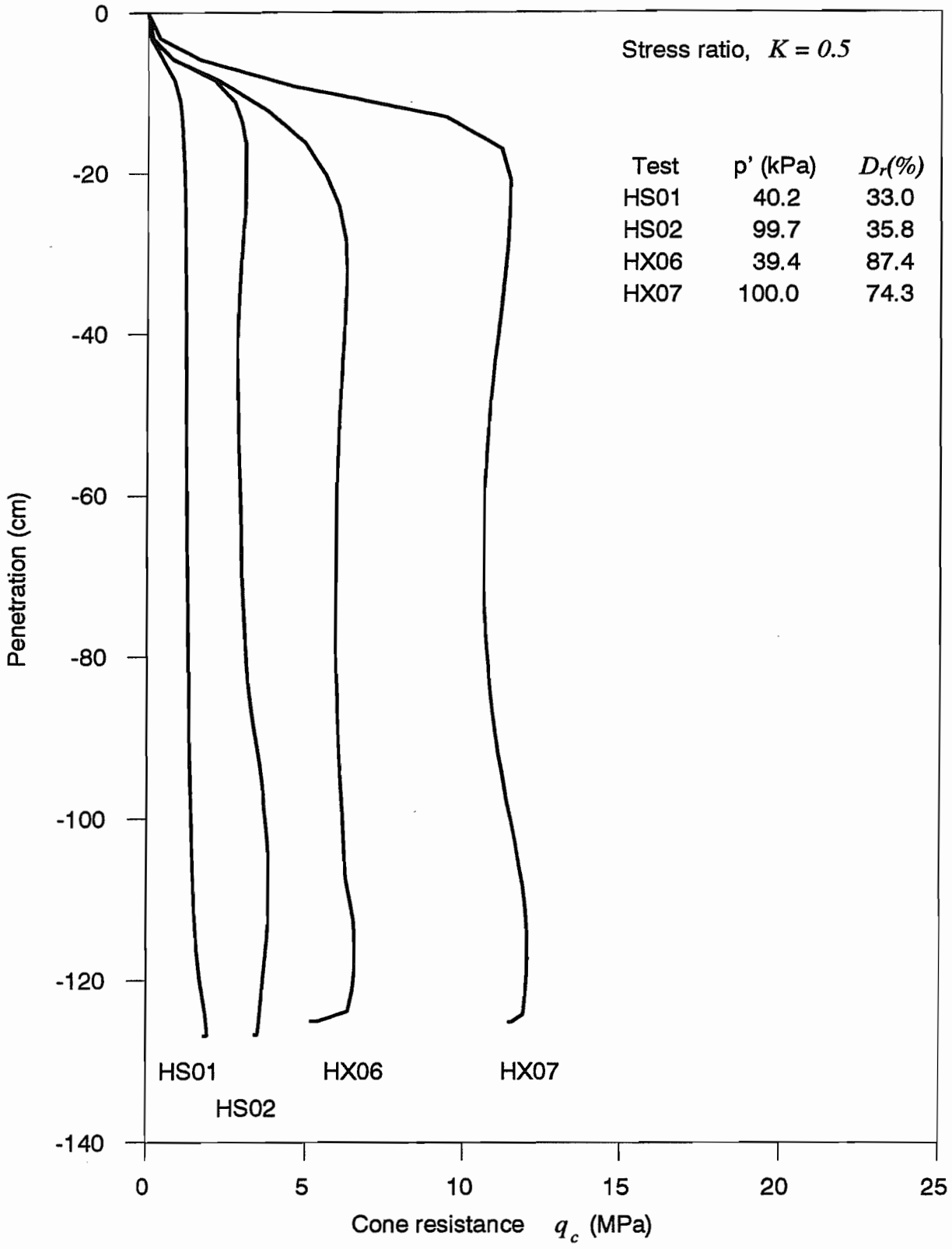


Figure 3.10 Cone resistance profiles for CPM tests in Hokksund sand at a stress ratio K = 0.5

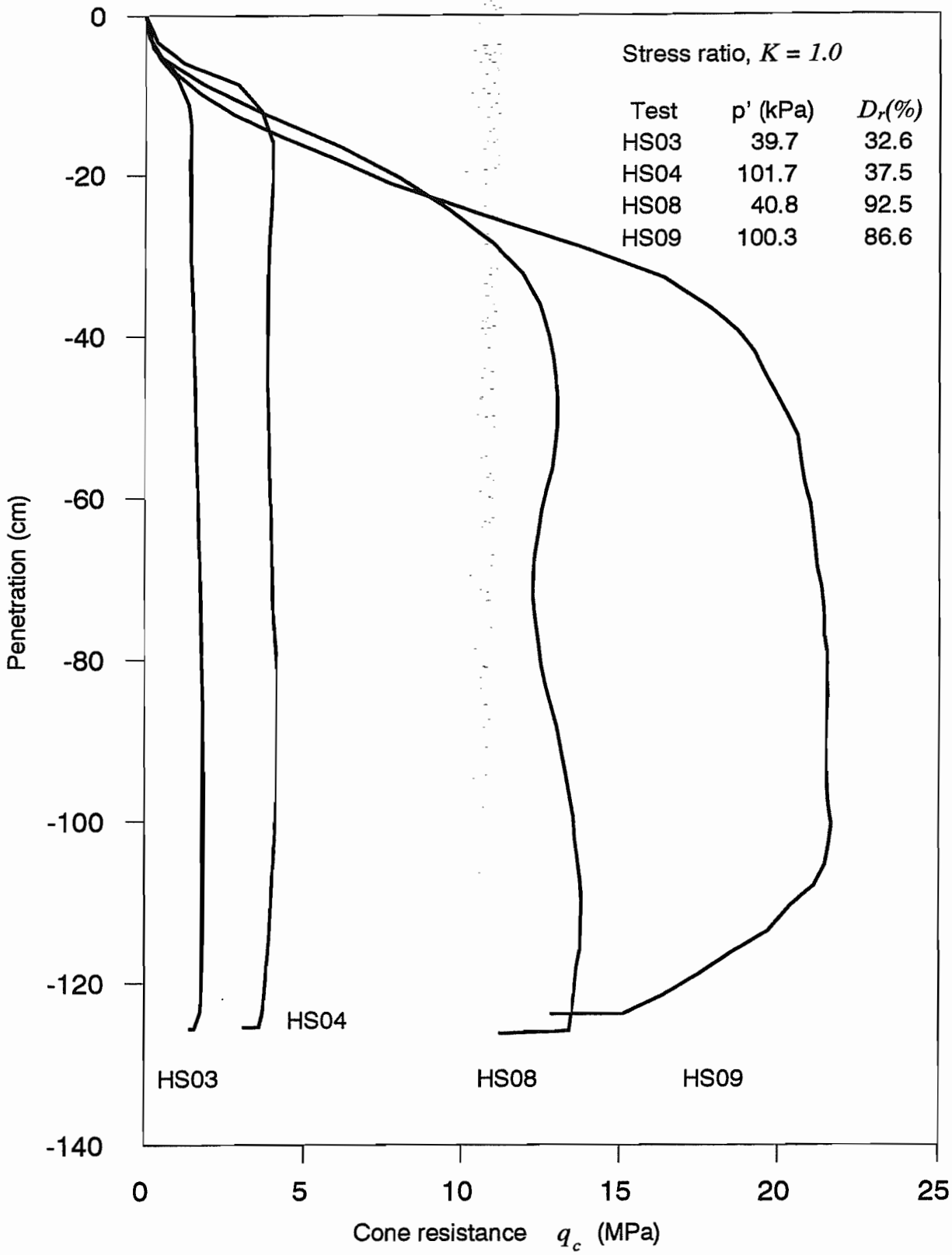


Figure 3.11 Cone resistance profiles for CPM tests in Hokksund sand with a stress ratio K = 1.0

3.4.3 Pressuremeter results

The influence of the controlling parameters of density and effective stress are also evident in the Hokksund sand pressuremeter tests. It is clear from Figures 3.12 and 3.13 that increasing p' and D_r both result in increasing limit pressure. At the same p' and D_r, an increase in stress ratio results in higher limit pressure values.

3.4.4 Verification of cone and pressuremeter results

Confidence in the results of the testing programme was extended through running three levels of check on repeatability of tests carried out:

(i) in the same sand, in different calibration chambers across the world, by different operators

(ii) in the same sand, in the same calibration chamber but by different operators

(iii) in an identical environment by the author

(i) Under a variety of testing conditions and prepared densities, a database of results from other calibration chambers was referred to in order to verify the trends of the cone penetration tests (Last *et al.*, 1987). No such data is available from an equivalent database of cone pressuremeter tests.The database drew on results reported from tests at Southampton University (SU), the Norwegian Geotechnical Institute (NGI) and Enel Cris in Italy (ENEL). In Figure 3.14, the results of this database in a plot of normalised cone resistance against relative density are presented. Obviously a degree of scatter is evident; tests with K_0 values ranging between 0.3 and 1.3 are shown, together with OCR values between 1 and 14.5 and varying boundary conditions. But this has been done intentionally to show that the Hokksund sand cone tests reported here can also be superimposed and yield the same trends.

(ii) A comparison was made between the procedure reported in this thesis and that reported by Schnaid (1990) of CPM tests in Leighton Buzzard sand. Table 3.4 presents the results of

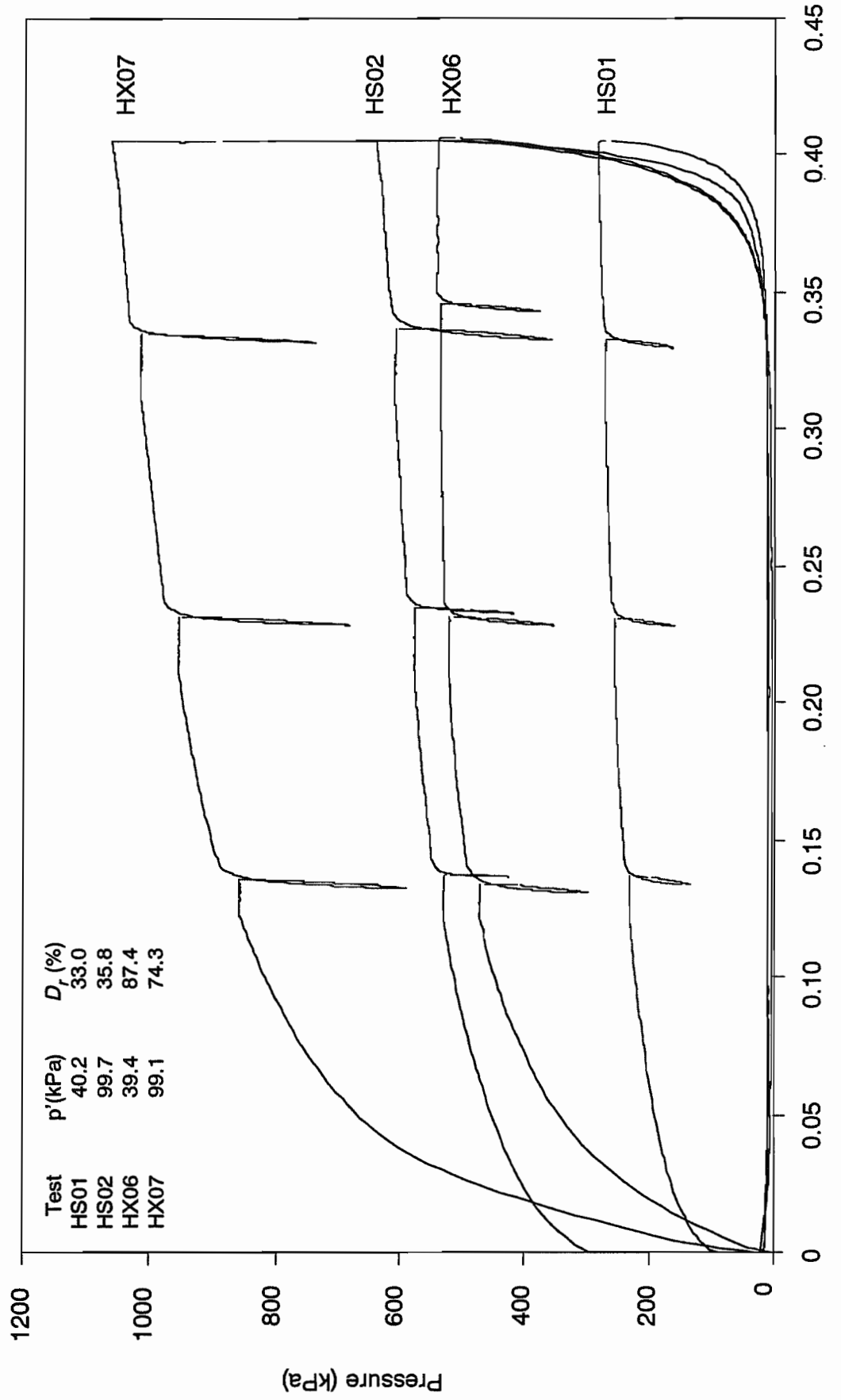


Figure 3.12 Pressure-strain curves for CPM tests in Hokksund sand at a stress ratio $K = 0.5$

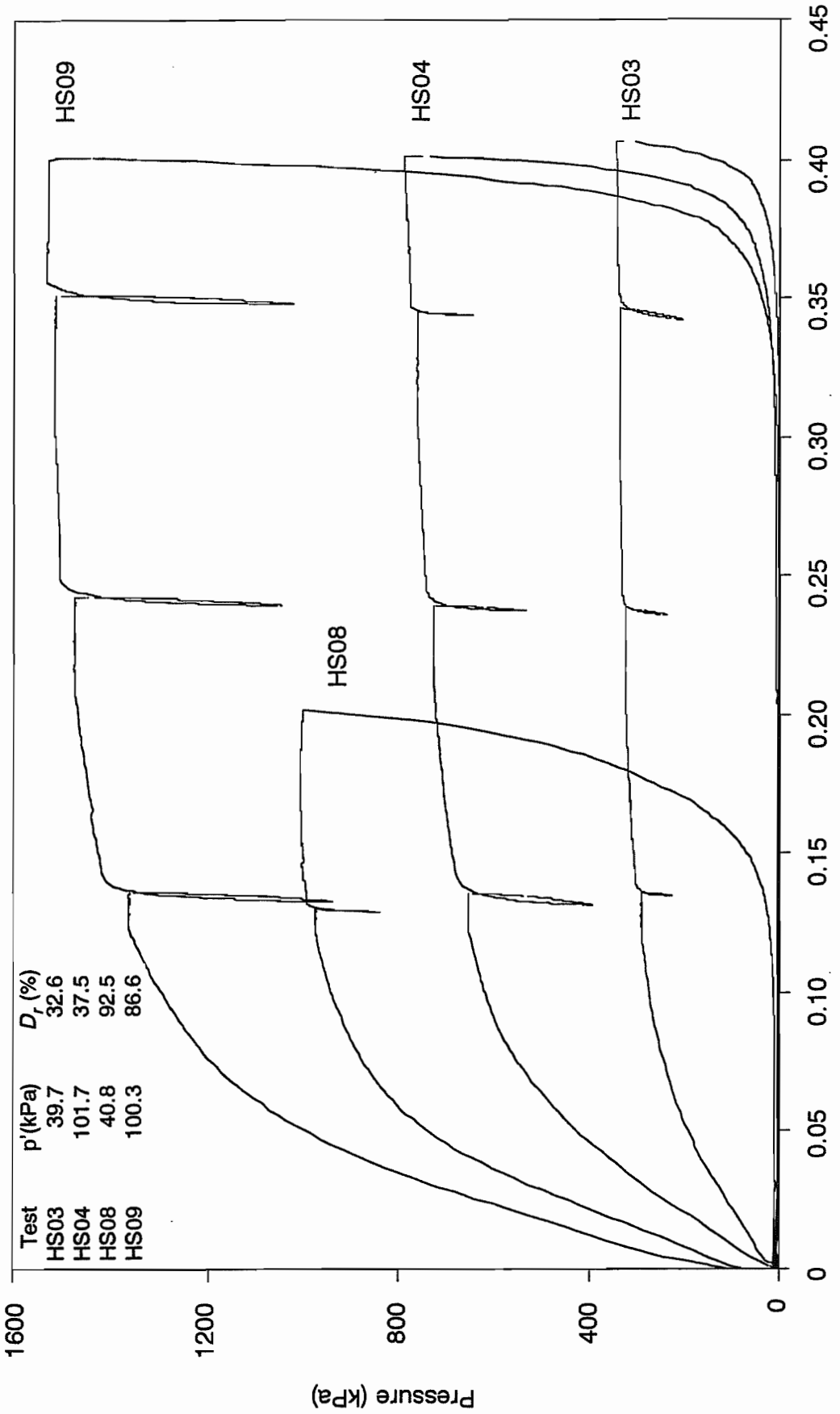


Figure 3.13 Pressure-strain curves for CPM tests in Hokksund sand at a stress ratio $K = 1.0$

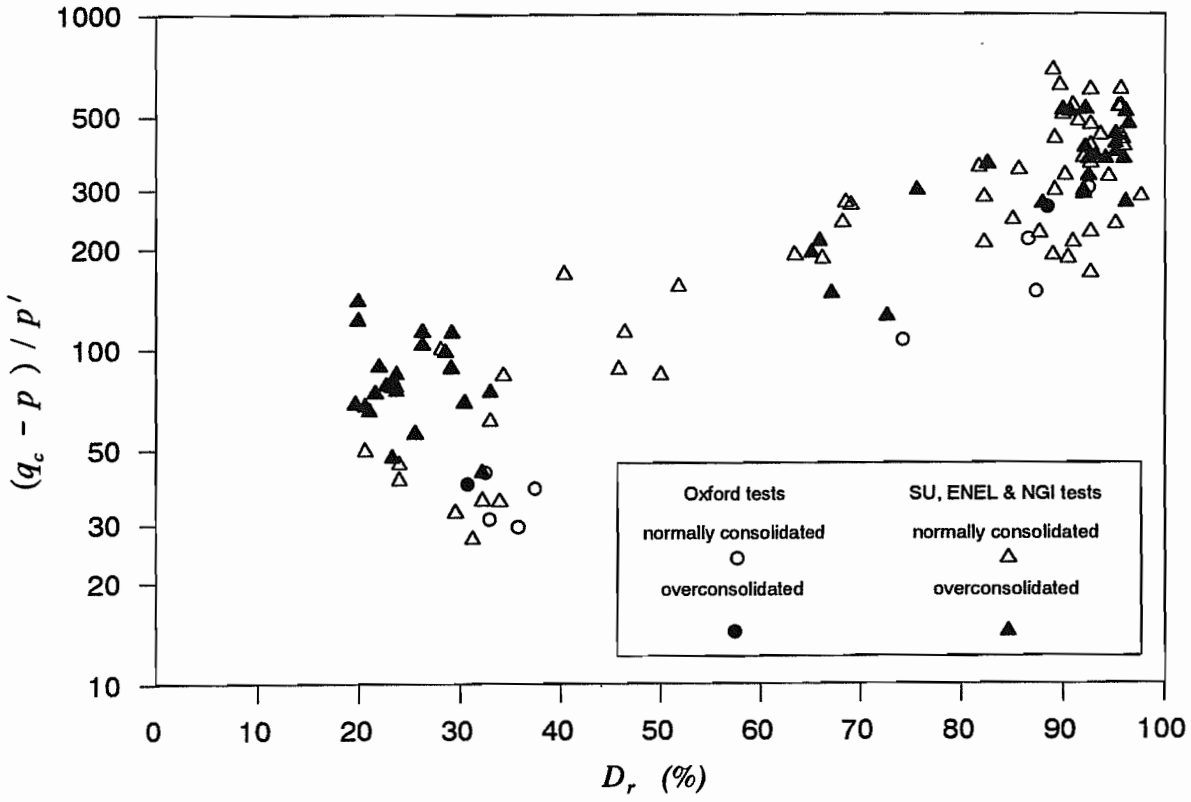


Figure 3.14 A comparison of cone tests in Hokksund sand carried out in different calibration chambers

test LB01 carried out by the author, and test 10CPMT04, carried out by Schnaid. From a comparison between the tests in Table 3.4, it is evident that test LB01 gave higher results than test 10CPMT04. This may be due to the slightly higher density measured. Otherwise it suggests a small operator influence; something that is very difficult to correct,

Table 3.4 A comparison of tests LB01 and 10CPMT04

Operator	Test	D_r (%)	σ_v' (kPa)	σ_h' (kPa)	p' (kPa)	K	ψ_l (kPa)	q_c (MPa)
Nutt	LB01	22	94.1	97.6	96.4	1.04	818	4.4
Schnaid	10CPMT04	17	89.8	96.6	94.3	1.08	750	3.8

(iii) To check the repeatability within a test programme, two identical tests were carried out in the Dogs Bay sand and the pressuremeter curves are plotted in Figure 3.15, with the results

of the tests given in Table 3.5.

Table 3.5 A comparison of tests DB10 and DB18

Operator	Test	D_r (%)	σ_v' (kPa)	σ_h' (kPa)	p' (kPa)	K	ψ_l (kPa)	q_c (MPa)
Nutt	DB10	54	100.5	98.9	99.4	0.98	1054	7.3
Nutt	DB18	55	99.2	99.2	99.2	1.00	1014	6.9

Here it can be seen that good confidence can be placed in the test procedure adopted as the difference in limit pressure is only 3.8% and the difference in cone resistance 5.5%.

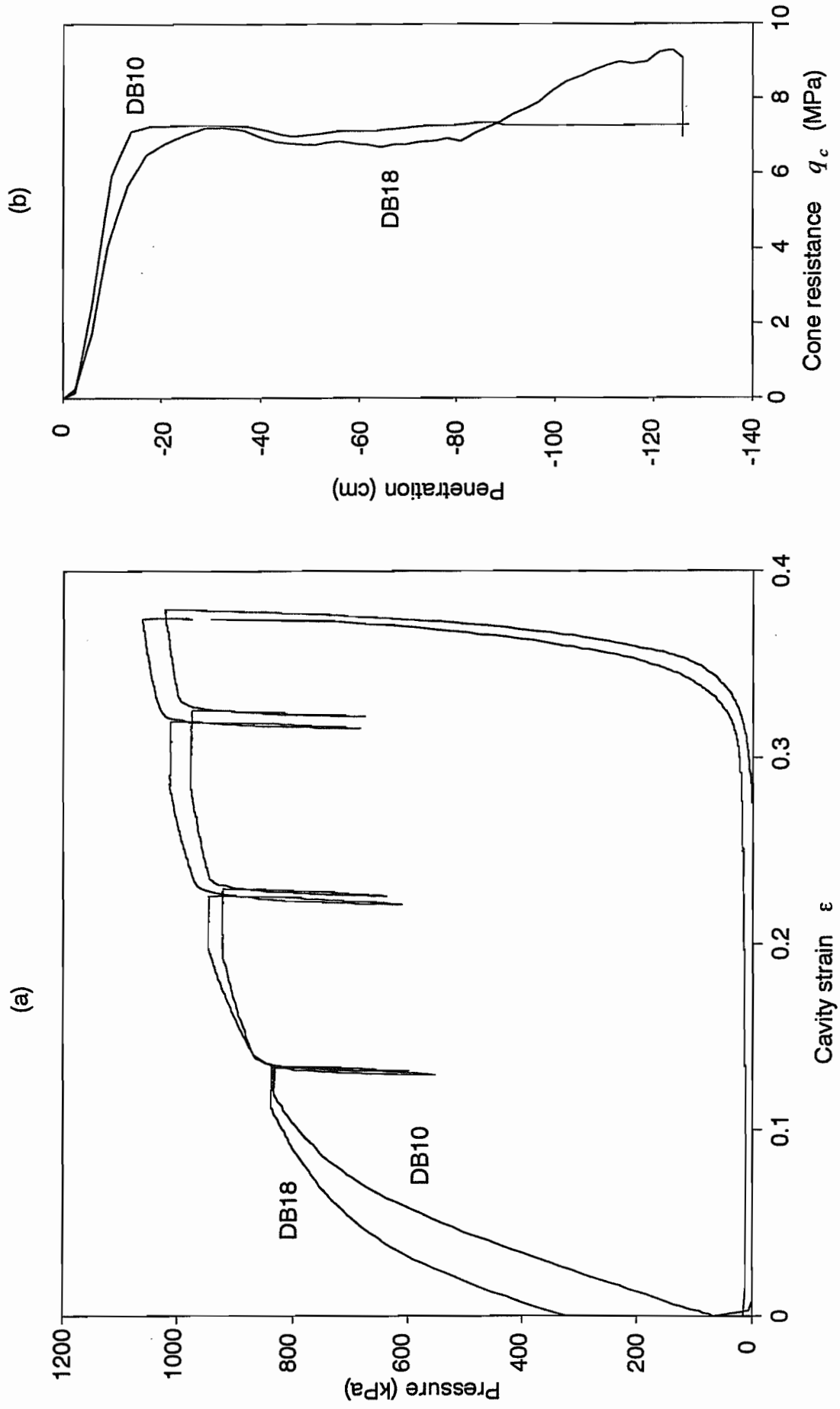


Figure 3.15 Comparison between similar tests in Dogs Bay sand: (a) pressuremeter tests (b) cone penetration tests

CHAPTER 4

TESTS IN DOGS BAY SAND

4.1 Introduction

In the last 25 years, carbonate sands have come into prominence in foundation design due to increased activity in offshore oil and gas production. Most design in these sands has been based on large scale testing in piled foundations, and the rôle of conventional methods of site investigation has remained limited (Murff, 1987). Laboratory testing is a complicated procedure because current methods of sampling (particularly offshore percussion methods) result in significant crushing of the brittle soil grains. Interpretation of *in situ* tests is primarily based on empirical correlations. Penetration tests, including the SPT (Angemeer *et al.*, 1973) and the CPT (Beringen *et al.*, 1982; Dutt *et al.*, 1985) have been correlated either with *in situ* properties, such as cementation, or directly with pile capacity (Hagenaar, 1982), but in both cases with only limited success.

Very little use of pressuremeters in carbonate sands is reported in the literature. Fahey (1988) presents the results of self-boring pressuremeter tests in a carbonate soil at an onshore site in South Australia. Most self-boring pressuremeter systems in current use, however, are not suitable for use offshore. A series of ten push-in pressuremeter (PIP) tests were reported at the North Rankin site by Renfry *et al.* (1988), and were used in assessing lateral pile response. However, this represents the total extent of pressuremeter testing for the North Rankin site investigation.

It is clear that only limited experience exists of *in situ* testing in carbonate soils. In this

chapter, by extending the database of cone pressuremeter tests in a carbonate sand from the west coast of Ireland, it is intended to improve existing knowledge of both cone and pressuremeter response in such types of sand. Firstly, a brief review of the constituents and mechanical properties of carbonate sands is presented, because it is important to highlight the differences between these sands and the more commonly reported silica sands. Classification tests, strength tests and compressibility tests have been carried out and the results from these tests are given.

A programme of cone pressuremeter testing in Dogs Bay sand comprised a total of 33 tests. In the main test series, the influence of stress level, stress ratio and relative density on cone pressuremeter measurements has been investigated. Additional tests were carried out to determine the effects of overconsolidation and time-dependent behaviour in carbonate sand.

4.2 Mechanical properties of carbonate sand

4.2.1 Constituents

More than one-third of the present day deep sea floor is covered by sediments containing over 30% calcium carbonate (Lees and Buller, 1972). Environmental conditions between the latitudes of 30°S and 30°N appear to be particularly favourable for the deposition of carbonate sediments, although areas do exist outside these limits, notably the Bass Strait, Australia (Angemeer *et al.*, 1973), and the western regions of the British Isles (Keary, 1967; Scoffin, 1988).

The majority of these sediments are biogenic, composed primarily of the skeletons of marine organisms living in the upper waters of the ocean. In the inshore environments and relatively shallow waters of the continental shelves, these sediments consist of molluscs, barnacles, foraminifera, algae, corals, sponges, echinoids and others. After death, these organisms sink slowly to the sea floor. Their solubility depends on water temperature, amount of light penetration, salinity and the presence of dissolved CO_2, which is dependent on the water

depth. Hence the sediments of the continental shelves exist as sands and silts; solubility of $CaCO_3$ is low and organic activity is high. At greater depths up to 5000 metres, carbonate sediments exist in the form of oozes, and in deeper waters, sediments are primarily siliceous, in the form of brown or red clays (Poulos, 1980).

The sands and silts of the continental shelves are of most engineering interest. They are comprised of platy and curved discs, hollow globules and tubes. These features are evident in Figure 4.1. The fine sand/silt shown in the figure is from the Goodwin field on the north west shelf of Australia.

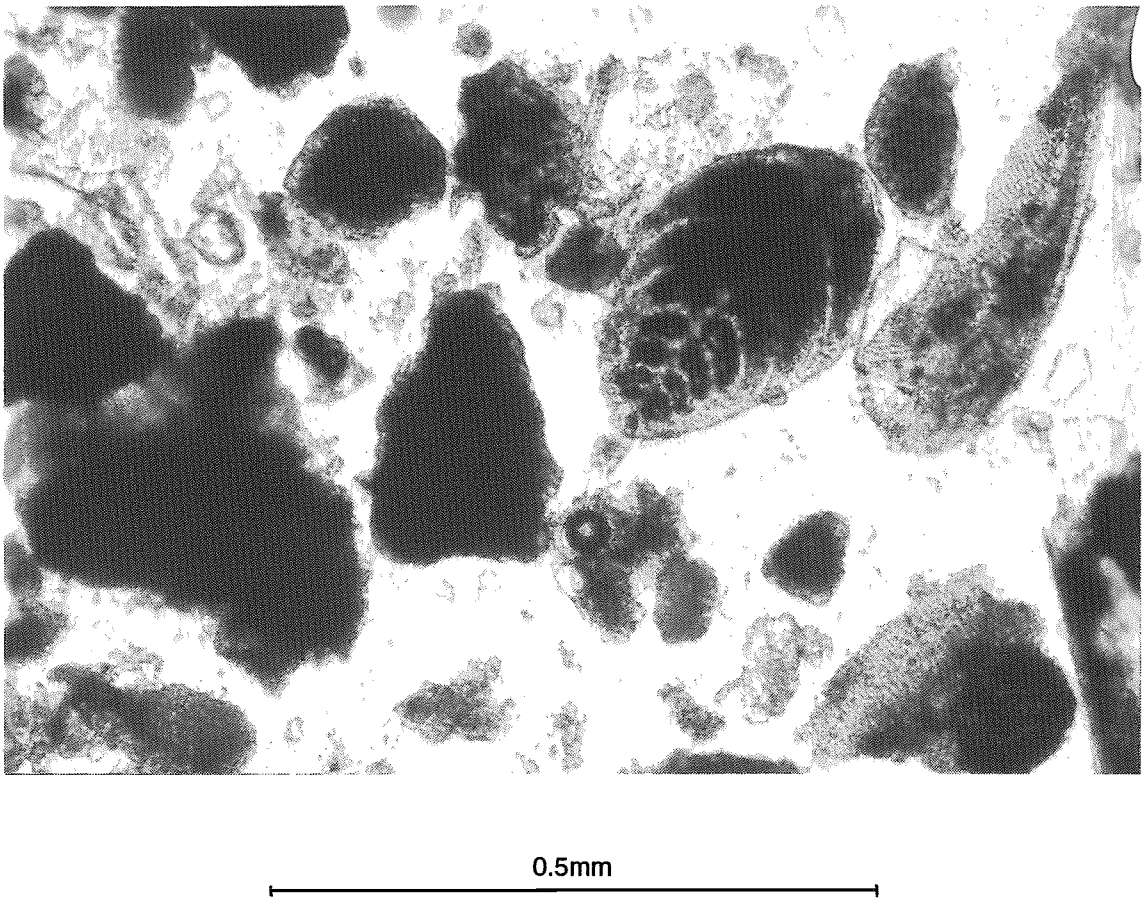


Figure 4.1 Carbonate sand/silt from the Goodwin field, north west shelf of Australia

4.2.2 Classification

Classification of carbonate sediments in a form applicable to engineers was attempted by Fookes and Higginbottom (1975) based upon grain size and post depositional induration, and

accounting for mineral composition, origin and strength. The system was extended by Clark and Walker (1977) to include non-carbonates. A more extensive system of classification is that proposed by King (1980) as shown in Figure 4.2. Full classification includes: grainsize; name of the base material; degree of induration (fine grained deposits); degree of cementation (medium to coarse grained deposits); bedding and lamination; origin of carbonate; colour; minor fractions.

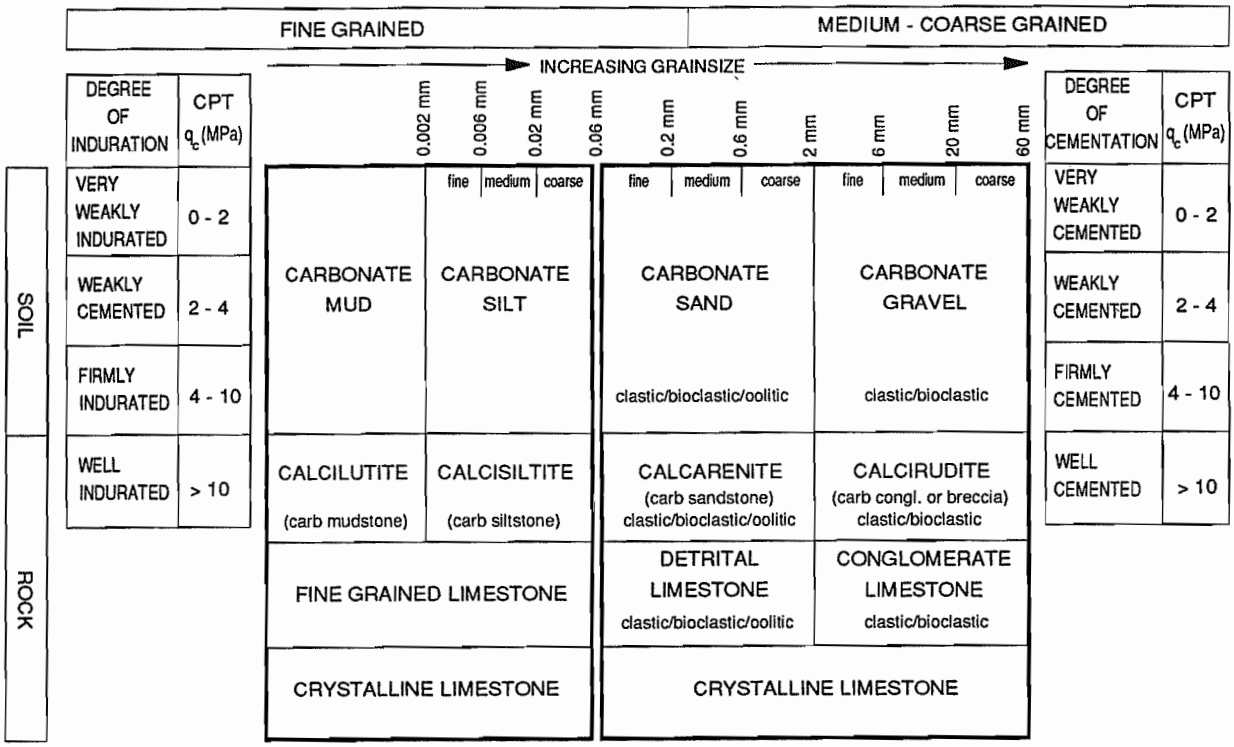


Figure 4.2 Classification system for carbonate soils (after King *et al.*, 1980)

4.2.3 Voids ratio

Almost all carbonate sands exhibit high void ratios in their natural state, and values in excess of unity are common for sub-seafloor depths up to 100m (Mostyn, 1988). Because angular grains will only touch each other at relatively few contact points, the voids between them will be high and the interparticle stresses will be concentrated. Semple (1988) argues that it is the high voids ratio of carbonate sand which dictates its behaviour under most loading conditions. When subjected to stresses sufficient to reduce the voids ratio to a value equivalent to that of a silica sand, the two types of soil will behave in a similar fashion, as shown in Figure 4.3

for the case of isotropic compression. In the figure, the compression behaviour of a weak calcarenite is shown to be comparable with silica sand, which exhibits somewhat higher yield values but similar post-yield compressibility. However, the initial voids ratio is not the sole contributing factor to assessing the behaviour of carbonate sands. In a series of triaxial tests on Dogs Bay sand at high stresses, Coop (1990) concluded that the locations of the normal compression line and critical state lines, in addition to the initial voids ratio, will control the compressibility of the soil.

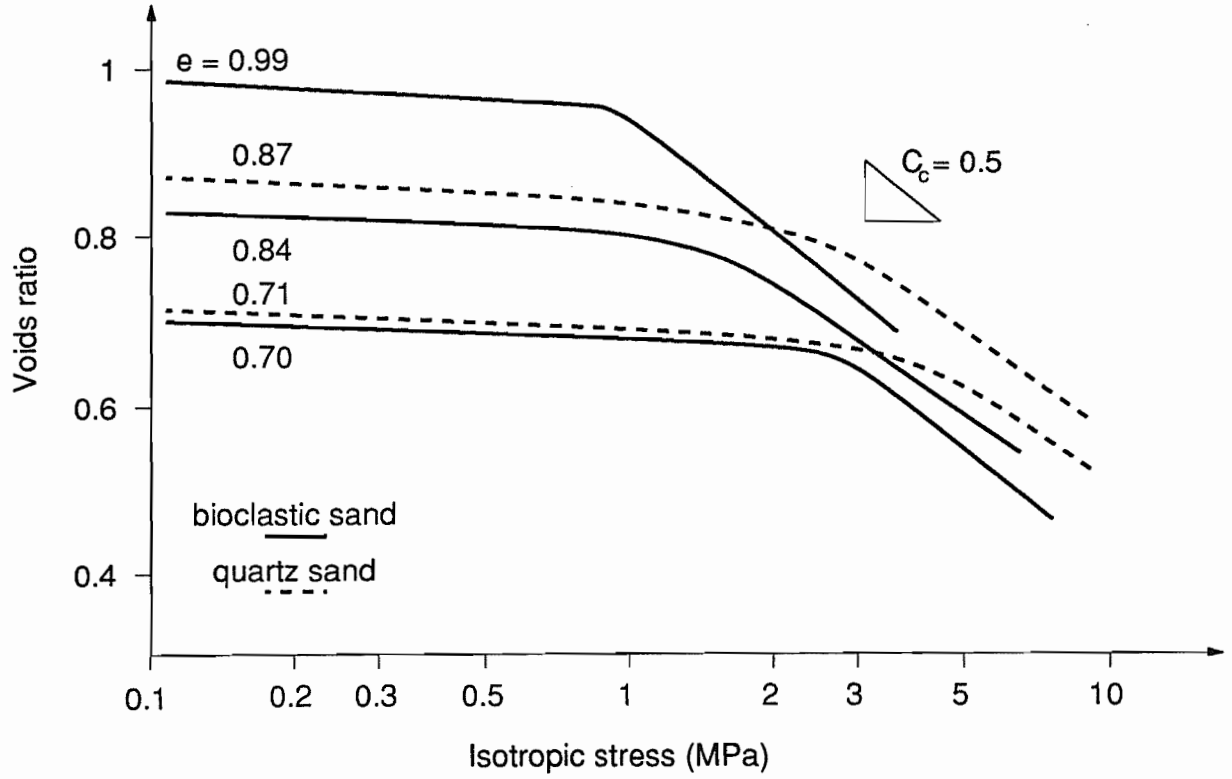


Figure 4.3 Behaviour of bioclastic sands in isotropic compression, after Semple (1988)

4.2.4 Grain crushing

The interparticle contacts between grains are readily damaged by stress concentrations, resulting in soil yield by grain crushing. It is not only the high angularity of carbonate grains that is responsible for this. Intraparticle voids, which exist because of the presence of hollow and tubular grains are also strongly linked to crushability (Datta *et al.*, 1979; Chaney *et al.*, 1982; Nauroy and le Tirant, 1983). Additionally, calcite has a hardness of 3 on Möh's scale, compared with 7 for quartz, and this leads to low strength of individual grains. It should be

noted, however, that grain crushing as part of the yield mechanism is primarily associated with relatively clean sands (Semple, 1988). Fine particles act to infill around contact points, effectively distributing interparticle forces to the extent that, in silty sands with sufficient fines, almost no grain crushing occurs (Demars, 1982; Morrison *et al.*, 1988).

4.2.5 Calcium carbonate content

$CaCO_3$ content is generally determined by the method of Chaney *et al.* (1982). Murff (1987) concludes that no explicit relationship between carbonate content and engineering properties exists, and simply labels the problem soils as those with $CaCO_3$ content greater than 50%, and frequently greater than 80%. Work by Demars *et al.* (1976), however, showed that with increasing carbonate content, friction angle increased while the pore pressure parameter at failure decreased.

4.2.6 Friction angle

The angle of friction that is mobilised in a soil subjected to shear is due to a combination of phenomena within the soil structure. As suggested by Rowe (1962), a base value of mineral sliding friction exists which is substantially higher in calcium carbonate (31° to 34°) than in quartz (23°). There is also a component due to particle rearrangement and crushing, and a component due to dilatancy. At low stress levels, carbonate sands exhibit significantly higher friction angles than quartz sands, by up to 10°, but with the onset of grain crushing, dilatancy effects tend to be suppressed (Golightly and Hyde, 1988).

Early work in silica sands at high stresses by Vesic and Clough (1968) showed that peak friction angle decreases with mean effective stress, implying a curved Mohr-Coulomb failure envelope. This is confirmed from triaxial tests in two carbonate sands from Bass Strait, Australia reported by Poulos *et al.* (1982), where friction angle was found to decrease with the logarithm of confining stress. Bolton (1986) has quantified this behaviour with his relationship for peak friction angle

$$\phi_p = \phi_{cv} + 3[D_r(Q - \log_e p') - 1] \quad ...(4.1)$$

where ϕ_{cv} is the constant volume triaxial friction angle, D_r is the relative density, p' is the mean effective stress expressed in kPa, and Q is a material parameter. This relationship was shown to fit well the behaviour of a large number of silica sands. Airey *et al.* (1988) suggest that the relationship holds for two carbonate sands from Bass Strait, Australia with Bolton's parameter, Q of 7.9 to 8.8 best fitting the data. Lower values of Q imply that ϕ_p reduces to ϕ_{cv} for lower confining pressures at a given relative density, and this is consistent with the observation of grain crushing in carbonate sand at relatively low stress levels.

4.2.7 Deformation

The stress-strain behaviour of carbonate soils is highly non-linear from small strains, and this is an indication that the stiffness varies considerably with confining stress. This is confirmed from drained triaxial tests reported by Poulos *et al.* (1982). Airey *et al.* (1988) found from drained triaxial tests that Young's moduli, determined from unload-reload loops, were generally 10 to 40 times greater than secant moduli determined at 50% of the maximum deviator stress.

With such a highly inelastic response, it is difficult to make a comparison between the stiffness of carbonate sands and silica sands without reference to a stress or strain level. Golightly (1988) measured secant shear moduli at a strain level of 0.25%. Moduli values in a silica sand were found to be significantly higher than in carbonate sand, and this feature was exacerbated with increasing confining pressure.

Poisson's ratio for carbonate sand is also a function of the stress level. Hull *et al.* (1988) showed that Poisson's ratio decreases with increasing confining stress, typically from initial values of 0.3 to 0.1 at stresses of 400 kPa.

K_0 values are given by many reporters for the particular sands tested. Most range between 0.16 and 0.46 as reported by Poulos *et al.* (1982), Airey *et al.* (1988) and Golightly (1988). These authors compared their observations with predictions of K_0 made from Jaky's (1944) empirical relationship

$$K_0 = 1 - \sin\phi \qquad ...(4.2)$$

with very different degrees of success. K_0 was, however, shown to increase with OCR in a very consistent manner.

In summary, some general statements can be made about the behaviour of carbonate sands:

(1) they exist at higher voids ratios than silica sands

(2) their particles are angular, structurally weak and contain intraparticle voids

(3) they develop significantly higher peak strengths than silica sands

(4) dilation response is supressed at relatively low stress levels on shearing after which there is an increasing tendency for volume reduction in the form of compression and crushing of grains

(5) friction angles reduce with increasing stress level

(6) stress-strain behaviour is non-linear from very small strain levels

4.3 Properties of Dogs Bay sand

4.3.1 Origins

With the permission of relevant authorities, approximately six tonnes of sand was obtained from the beach at Dogs Bay for use in the test programme reported in this thesis. Dogs Bay is on the extreme west coast of the Republic of Ireland in the region of Connemara. The beach faces in a westerly direction and is protected by a protruding peninsula on its southern edge. Prevailing winds and seas generally approach this portion of the coastline from the south west.

There are two factors which dictate the nature of the sediments in carbonate producing areas.

Firstly, the degree of shelter provided by the coastline is reflected by the grainsize and biogenic composition. In highly protected bays and inlets, the sediments are primarily composed of muds, and in the exposed portions of the coastline and headland, coarse patch sands and gravels predominate. The conditions at Dogs Bay lie between these two extremes.

Secondly, the amount of dilution by terregenous clastic materials is of importance. Clastic deposition is influenced by topographic relief, particularly the presence of streams or rivers, and local geology. Geological surveys indicate that Dogs Bay is underlain by intrusive igneous rocks, primarily granites and diorites. Relief is low and there are no major rivers in the region. Some Pleistocene glacial boulder clays outcrop along areas of the coast, but their clastic contribution to sediments at Dogs Bay is negligible.

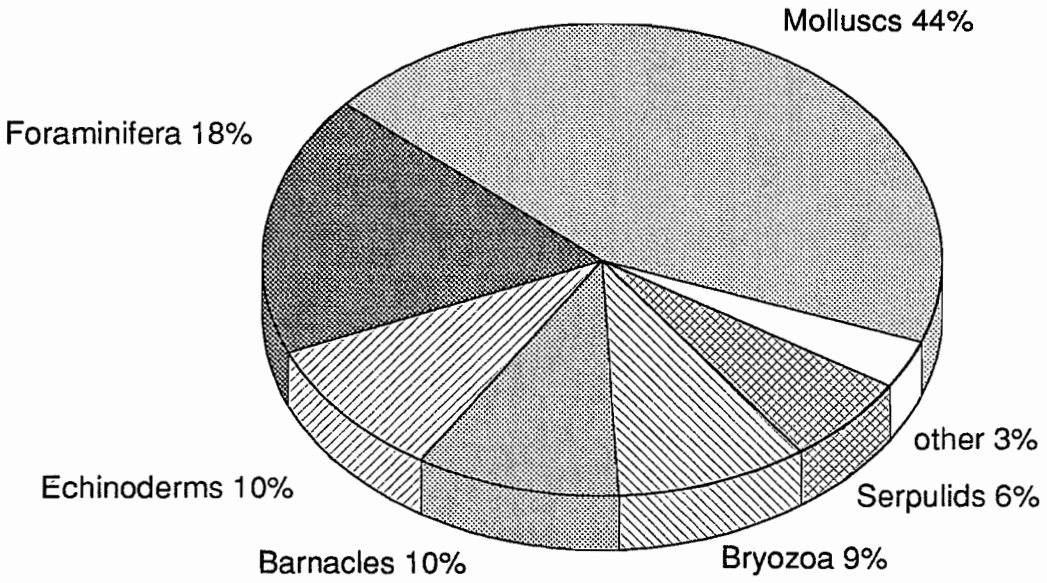


Figure 4.4 Microscopic constituents of Dogs Bay sand

Dogs Bay sand is a temperate water, continental shelf foramol carbonate sand. The term foramol refers to its primary contributors being foraminiferans and molluscs (Reading, 1978). An estimate of the relative proportions of these animals in Dogs Bay sand is shown in Figure 4.4, broadly based on the micro-environments described by Scoffin (1988). Molluscs are invertebrate animals of which the two main types in Dogs Bay sand are gastropods (coiled

or whorled cones ranging in size from 1mm to 100mm) and bivalves (with shell sizes ranging from 5mm to 100mm). Much smaller in size are the foraminiferans. Benthonic foraminifera (seafloor dwellers) have circular to sub-circular bodies comprising multiple chambers, and are usually less than 1mm across.

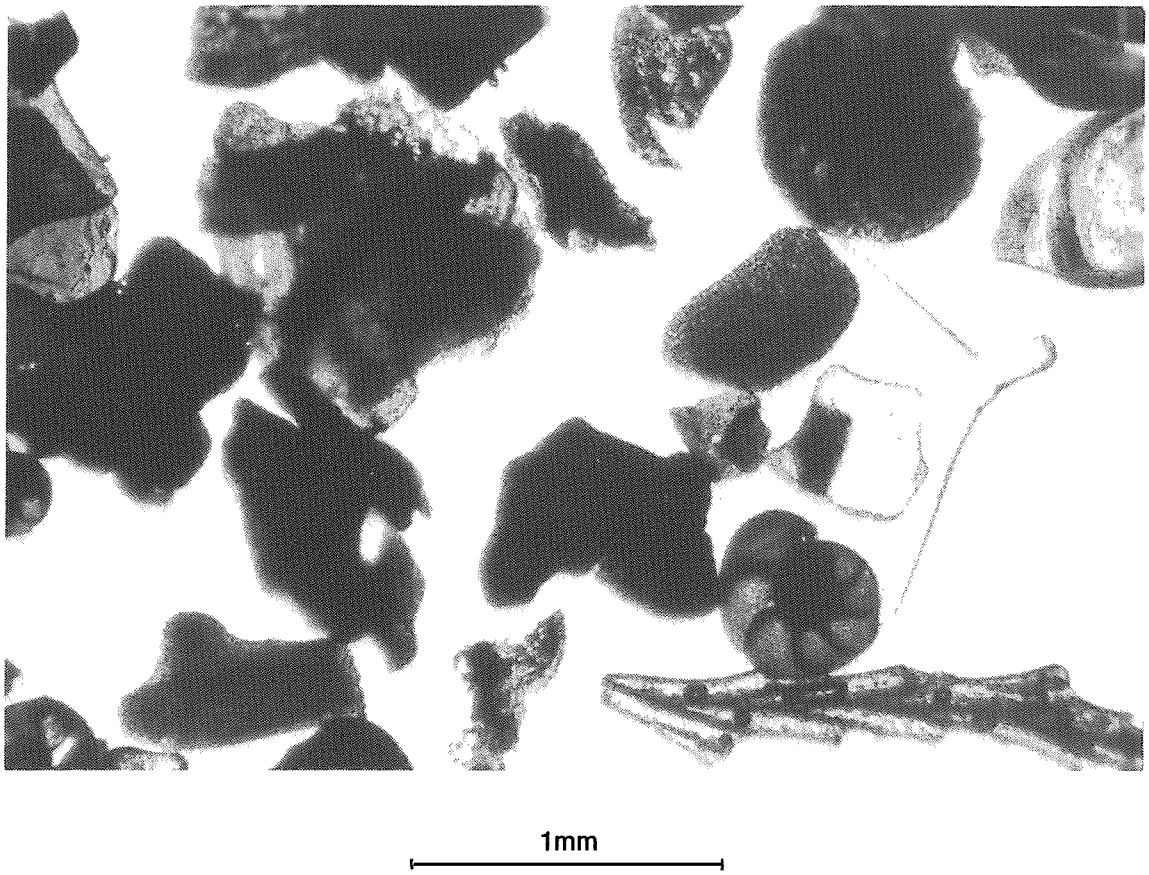


Figure 4.5 Micrograph of Dogs Bay sand

4.3.2 Classification

The mineralogy of Dogs Bay sand was determined by Golightly (1988) using X-Ray diffraction. The sand contains both low magnesium calcite (2% to 3% mol $MgCO_3$) and high magnesium calcite (12% to 17% mol $MgCO_3$) with some aragonite, and traces of quartz and feldspar. The age of the sand is reflected by the $MgCO_3$ content; high $MgCO_3$ contents are characteristic of relatively young sands, as this percentage tends to deteriorate with time.

A micrograph of Dogs Bay sand is shown in Figure 4.5. Several of the particle types can be

identified from the descriptions given above, and it is clear that the grains are angular, comprising plates, tubes and hollow globules. The sand is uniformly graded, medium grained containing a small proportion of fines as shown in the grading curve of Figure 4.6. D_{50} was found to be 0.25mm, and the Coefficient of Uniformity, U defined as D_{60}/D_{10} was 0.29/0.11 = 2.66.

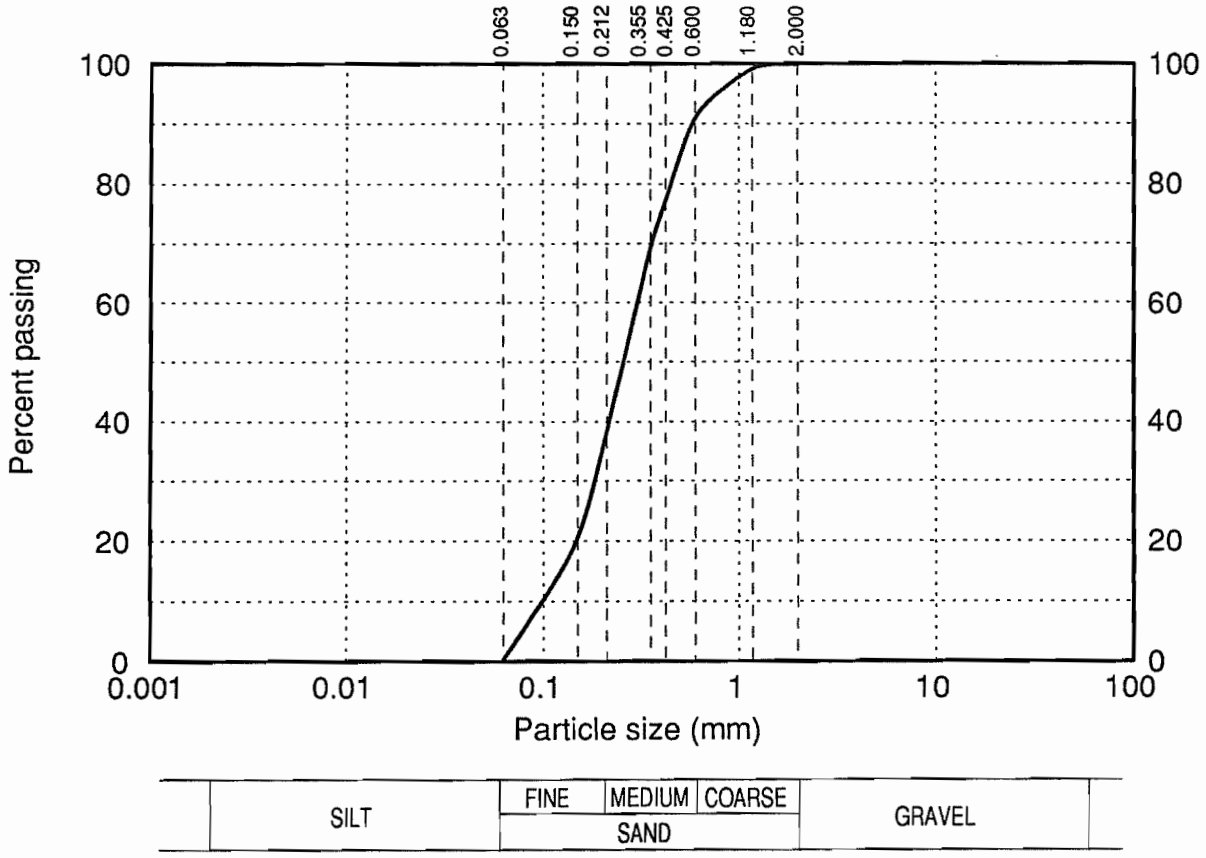


Figure 4.6 Grading curve for Dogs Bay sand

Minimum unit weight, γ_{dmin} was measured both by the inverted cylinder method of Kolbuszewski (1948) and by rapid pouring of the sand through a funnel, and minimum values of 9.64kN/m^3 and 9.52kN/m^3 respectively were obtained, hence the lower value of 9.52kN/m^3 has been adopted for the Dogs Bay sand. Difficulties arise when attempting to use standard procedures for the determination of maximum unit weight, γ_{dmax} and specific gravity, SG. Both the presence of intraparticle voids and the susceptibility of the grains to crushing when

subjected to excessive tamping or vibrations introduce significant errors. The method of BS1377 to determine γ_{dmax} requires compaction of the sand in layers with a hammer; an approach clearly not suitable to carbonates. Golightly (1988) used a vibrating, rotating mould to obtain γ_{dmax} of Dogs Bay sand of 13.6kN/m^3. To incorporate the presence of intraparticle voids in the measurement of specific gravity, Golightly saturated the sand in carbon dioxide prior to immersion in deaired water. A vacuum was then applied for around 30 seconds while the sand mixture was agitated. *SG* of 2.75 was determined in this manner, and these two measurements have been adopted in this thesis.

4.3.3 Strength tests

The results of a series of 10 direct shear tests in a 60mm x 60mm Casagrande shearbox are presented in Figure 4.7, and tabulated in Table 4.1. Loose samples were prepared by rapidly pouring sand through a funnel and dense samples were prepared by vibrating the shearbox during slow pouring of the sand.

In the loose tests, there is an obvious difference between the behaviour at an applied normal stress of 40kPa with tests at higher stresses. The test at lower stress exhibits some dilatancy. When the stress level is increased, the dilatancy is suppressed and similar amounts of volumetric contraction are evident. At the higher densities, however, confining stresses are not large enough to suppress dilatancy and volumetric expansion is evident in all the tests up to 200kPa normal stress. The constant volume friction angle, ϕ_{cv} has been determined after a correction according to Taylor (1948). Averaging all the tests, a ϕ_{cv} of 40.3° results. Coop (1990) found ϕ_{cv} for Dogs Bay sand to be 40.3° based on triaxial isotropic compression tests. Triaxial tests do not allow rotation of the principal axes during shear, while in the direct shear test, principal axes are free to rotate. Hence ϕ_{cv} values based on direct shear tests should be marginally higher.

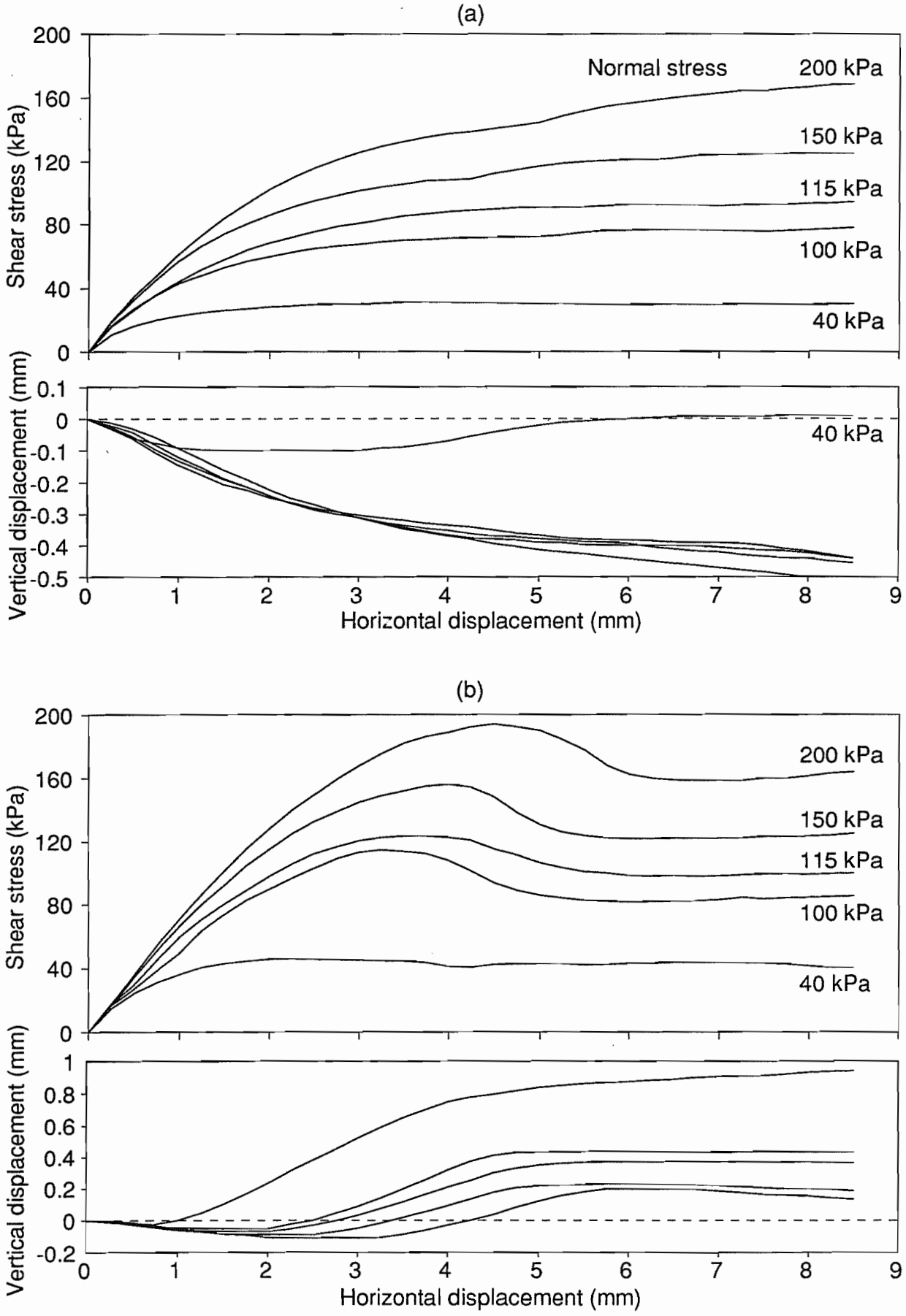


Figure 4.7 Results of shearbox tests on Dogs Bay sand (a) loose, (b) dense

Table 4.1 Direct shear tests on Dogs Bay sand

	Test	σ_v (kPa)	$\sigma_{h\text{-}peak}$ (kPa)	D_r (%)	ϕ_{peak} (degrees)	ϕ_{resid} (degrees)	ν (degrees)
Loose	1	40.0	31.4	1.8	37.1	36.7	3.0
	2	100.0	77.9	0.3	39.4	38.3	-
	3	115.0	94.5	4.6	40.4	39.6	-
	4	150.0	125.1	6.6	40.9	40.4	-
	5	200.0	168.8	8.6	41.6	40.9	-
Dense	6	40.0	45.8	46.0	47.2	46.1	16.5
	7	100.0	114.5	28.4	43.0	40.0	13.3
	8	115.0	123.6	43.6	42.2	40.7	10.4
	9	150.0	156.2	47.6	41.5	40.2	9.7
	10	200.0	194.2	38.9	41.0	40.3	9.2

4.3.4 Compressibility and crushing characteristics

Oedometer tests were carried out on loose and dense specimens of Dogs Bay sand, and an example of each is plotted in Figure 4.8. Based on these results, the compression and expansion indices were found to be for loose sand C_c = 0.73, C_s = 0.0284 and for dense sand, C_c = 0.476, C_s = 0.0236.

The compressibility of the sand continues to increase as shown in Figure 4.9, where C_c is calculated as the mean slope of the $V : \log_e p'$ curve for each increment of load. C_c is high compared to 0.185 for Hokksund sand determined in Chapter 3. This is the result of the breakage of soil particles, confirmed by the stiff swelling lines which indicate that a very large proportion of permanent, plastic deformation has occurred.

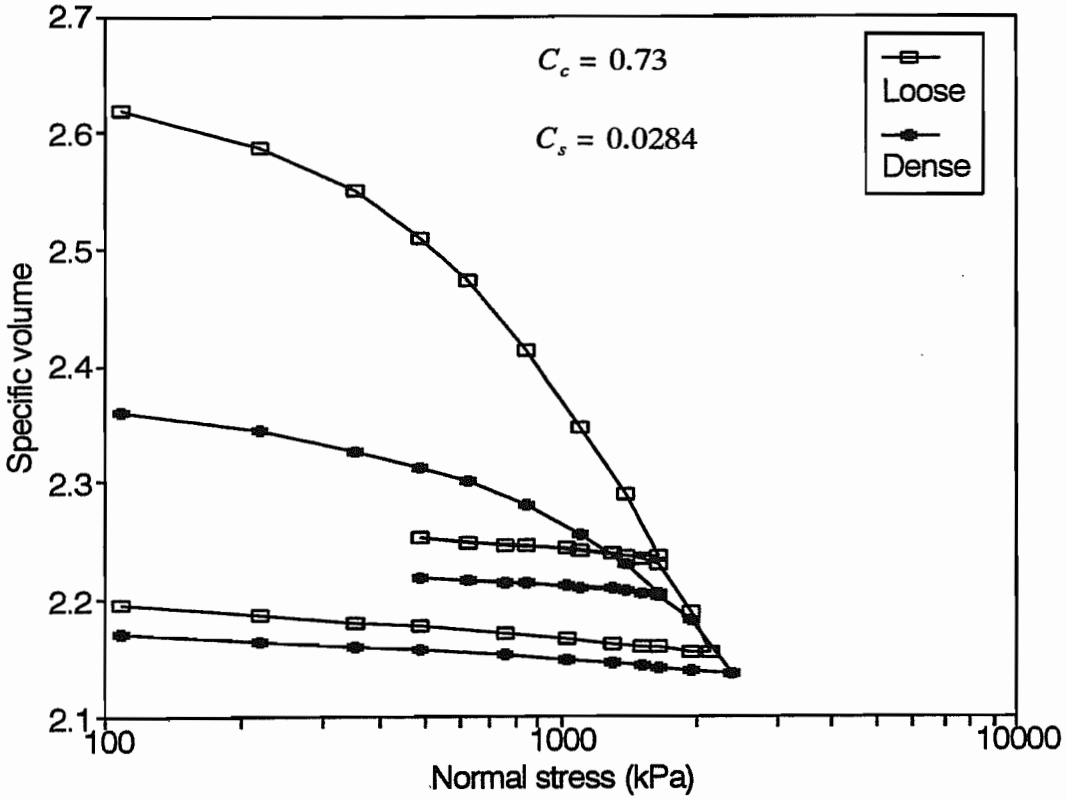


Figure 4.8 Oedometer tests on Dogs Bay sand

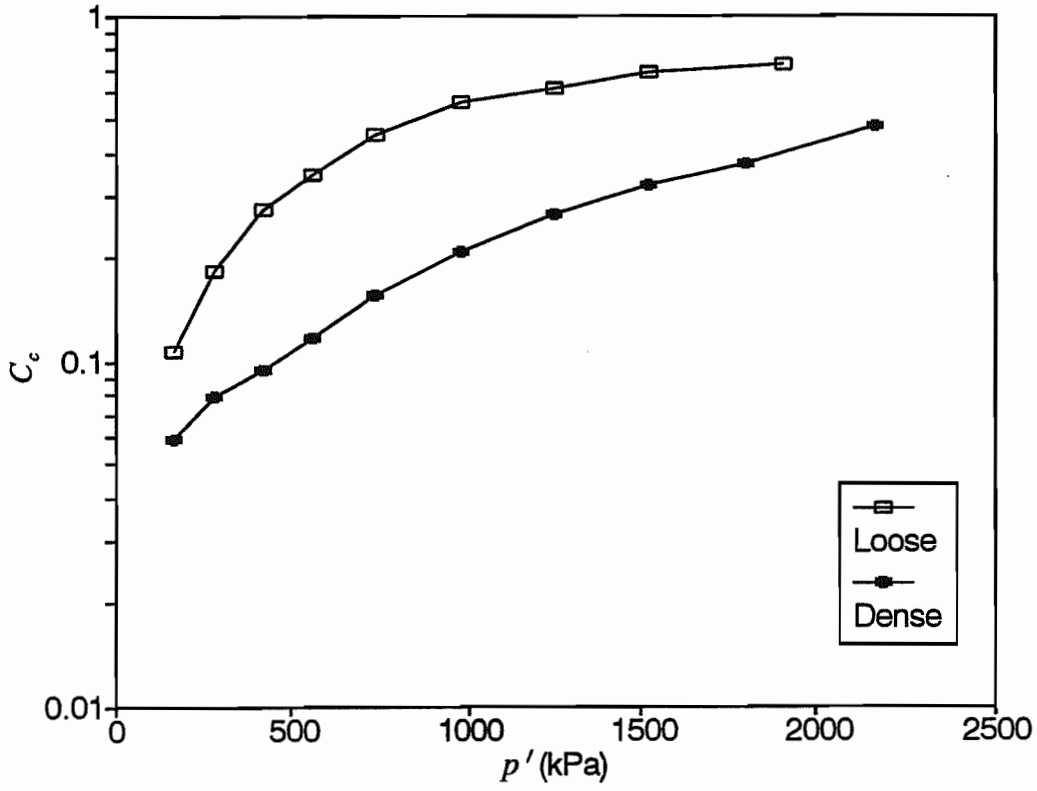


Figure 4.9 Variation of C_c with stress level from oedometer tests on Dogs Bay sand

A total of 33 test specimens of Dogs Bay sand were prepared in the calibration chamber. Because the sand was of limited availability, it was necessary to reuse it for subsequent tests. Testing on a fresh batch of sand commenced halfway through the test programme. Although the samples were stressed to relatively low levels, particle degradation was monitored closely throughout the test programme, and over 50 grading analyses have been performed from various test samples. The results appear in Figure 4.10 where D_{10}, D_{50}, and D_{60} have been plotted against the chronological number of the grading analysis. The degradation of D_{50} was found to be 0.06 mm. This is a very small change; of the same magnitude as the degree of uniformity in different grading tests taken from the same sample. Noorany (1985) investigated the effects of crushing on friction angle of two carbonate sands. He found that there was no difference between the friction angles measured in the sand in a natural state and when crushed and when fully ground. The influence of particle degradation on the results obtained in the Dogs Bay sand due to reusage, therefore, was considered to be negligible.

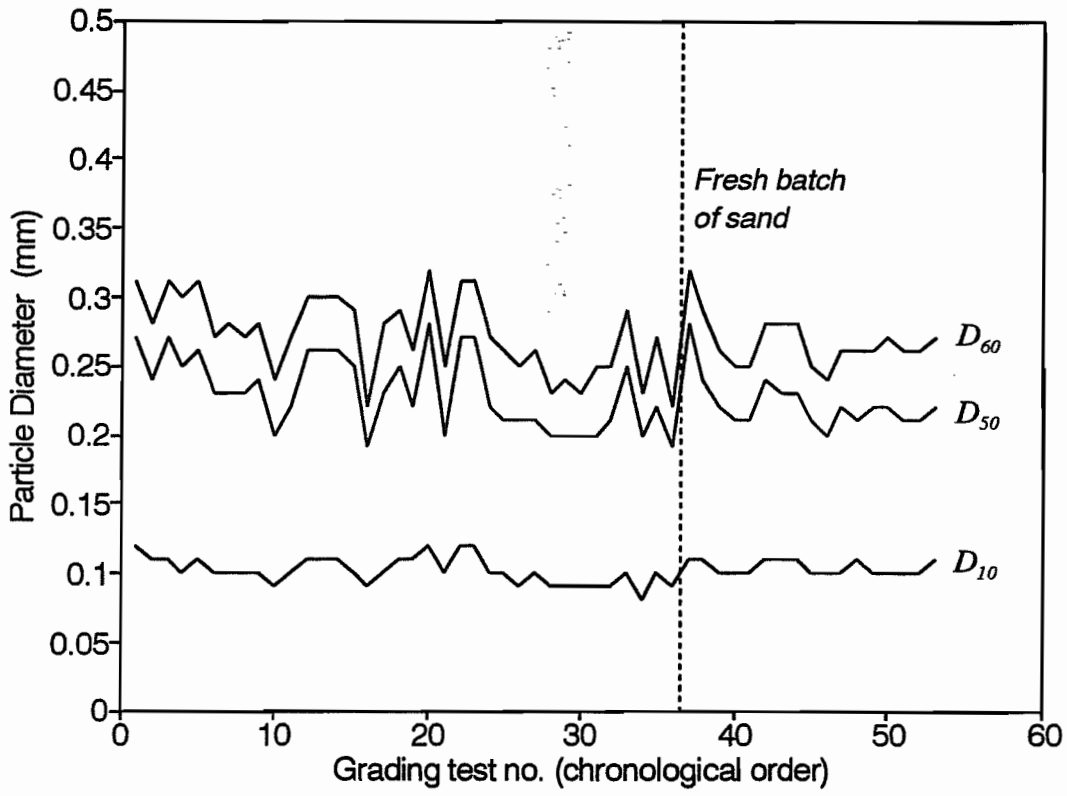


Figure 4.10 Particle degradation monitored during the test programme

4.4 Cone pressuremeter tests

4.4.1 Summary of results

The results of 33 cone pressuremeter tests in Dogs Bay sand are presented in Table 4.2. The tests are numbered in the same manner as outlined in section 3.4.1 and the stress states at which testing was performed are shown in Figure 3.1 and quantified in Table 3.1. In this series, several tests were carried out on samples that had been unloaded from a previous maximum effective stress, and this is indicated by a third letter in the stress path description of Table 4.2. Most of the loose samples had relative densities in the range 21% to 34% (tests DB0 and DB2 which lie outside this range were two of the first tests carried out in the entire programme). The dense samples lay in the range 47% to 57% relative density, and one test, DB15 at a D_r of 38.9% has been labelled as a sample of medium density.

4.4.2 Cone results

Typical cone resistance profiles are presented in Figures 4.11 to 4.13 for loose and dense sand. The profiles are uniform, confirming that the sample preparation techniques for Dogs Bay sand were satisfactory. In some of the tests, an early peak in the cone resistance was evident at the start of penetration. This is probably due to the manual process of flattening the surface of the sand by hand after placement, prior to fixing the top plate. The slightly less uniform nature of test DB17 in Figure 4.12 is typical of several of the tests in dense sand. It reflects a small influence of layering which was a feature of the preparation technique for dense samples. The influence of the controlling parameters of relative density, stress level and stress ratio is evident from cone resistance profiles. Mean effective stress, p' was varied from around 40kPa to 50kPa, 100kPa 150kPa and 250kPa for tests DB13, DB0, DB6, DX9 and DB32 respectively, and its influence on the measured cone resistance is shown in Figure 4.11 for loose samples at a stress ratio, K of 1. The same effect was found in dense samples as shown in Figure 4.12 for tests DB17 and DB18.

Table 4.2 Results of tests in Dogs Bay sand

Test No.	Stress path	σ_v' (kPa)	σ_h' (kPa)	p' (kPa)	K	D_r (%)	ψ_l (kPa)	q_c (MPa)	$\frac{q_c - \sigma_h}{\sigma_h'}$	$\frac{q_c - \sigma_h}{\psi_l - \sigma_h}$
Loose										
DX1	OA	59.2	28.7	38.9	0.48	22.4	247	0.74	24.8	3.3
DB11	OA	58.2	27.9	38.0	0.48	27.5	235	1.49	52.4	7.1
DB30	OA	59.4	29.3	39.3	0.49	26.0	237	1.52	50.9	7.2
DB3	OBA	58.2	27.1	37.5	0.47	28.4	388	2.92	106.7	8.0
DB2	OB	148.8	72.7	98.1	0.49	16.5	573	3.48	46.9	6.8
DB12	OB	149.6	74.6	99.6	0.50	28.4	619	3.58	47.0	6.4
DB14	OB	148.9	74.8	99.5	0.50	29.0	584	3.81	49.9	7.3
DB5	OC	38.6	37.8	38.1	0.98	23.9	297	1.29	33.1	4.8
DB13	OC	39.4	38.2	38.6	0.97	32.7	320	2.07	53.2	7.2
DB21	ODC	40.2	37.9	38.7	0.94	21.2	397	2.61	67.9	7.2
DB22	OGC	40.1	35.8	37.2	0.89	24.2	419	3.00	82.8	7.7
DB0	OJ	48.6	48.3	48.4	0.99	6.7	348	2.23	45.2	7.3
DB6	OD	98.6	97.8	98.1	0.99	22.1	686	3.99	39.8	6.6
DX9	OG	148.9	147.8	148.2	0.99	31.0	934	5.16	33.9	6.4
DB32	OH	249.9	253.3	252.2	1.01	34.1	1467	7.08	27.0	5.6
DB7	OE	23.2	47.2	39.2	2.03	25.7	352	2.24	46.5	7.2
DB20	OFE	25.0	43.8	37.5	1.75	25.7	528	3.47	78.2	7.1
DB4	OBE	23.0	46.2	38.5	2.01	23.0	384	2.43	51.6	7.1
DB8	OF	60.8	118.9	99.5	1.96	28.1	836	4.78	39.2	6.5
Medium										
DB15	OA	62.1	30.3	40.9	0.49	38.9	288	1.95	63.4	7.4
Dense										
DB23	OA	59.4	29.3	39.3	0.49	47.1	414	3.11	105.1	8.0
DB26	OBA	59.5	30.9	40.4	0.52	53.9	470	4.40	141.4	10.0
DB16	OB	147.3	74.9	99.0	0.51	56.6	920	6.90	91.1	8.1
DB17	OC	40.0	41.2	40.8	1.03	52.1	485	3.94	94.6	8.8
DB31	OC	39.1	40.3	39.9	1.03	52.6	526	4.21	103.5	8.6
DB27	ODC	39.4	40.2	39.9	1.02	55.7	599	5.74	141.8	10.2
DB24	OGC	40.1	40.9	40.6	1.02	52.1	660	6.53	158.7	10.5
DB18	OD	100.5	98.9	99.4	0.98	55.1	1054	7.27	72.5	7.5
DB10	OD	99.2	99.2	99.2	1.00	53.8	1014	6.87	68.3	7.4
DB25	OG	150.4	149.1	149.5	0.99	57.0	1332	-	-	-
DB19	OE	24.6	47.6	39.9	1.93	54.9	657	5.33	111.0	8.7
DB28	OFE	24.3	49.0	40.8	2.02	53.7	812	6.56	132.9	8.5
DY29	OBE	23.7	48.0	39.9	2.03	56.8	683	5.49	113.4	8.6

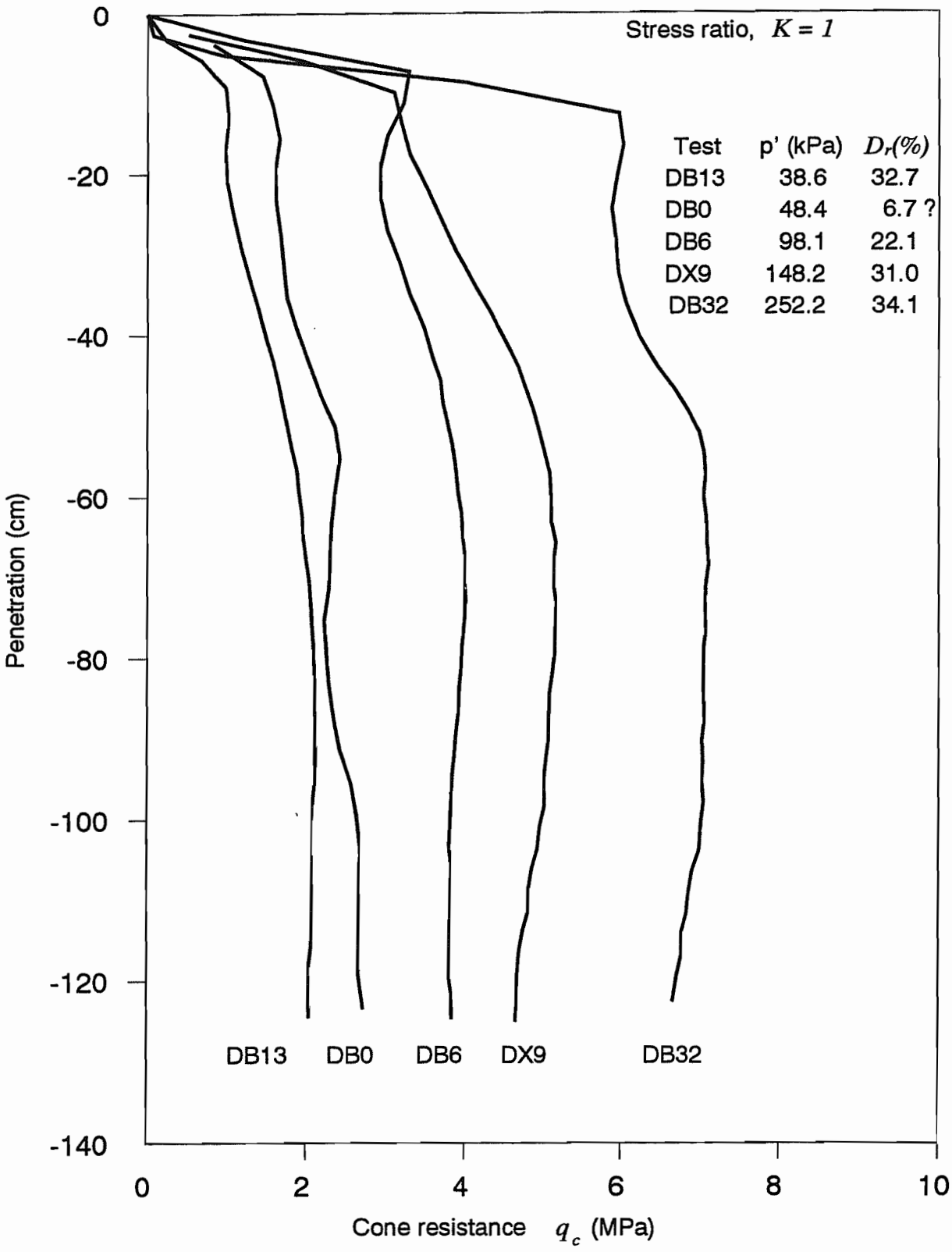


Figure 4.11 Cone resistance profiles for CPM tests in loose Dogs Bay sand at a stress ratio, K = 1.0

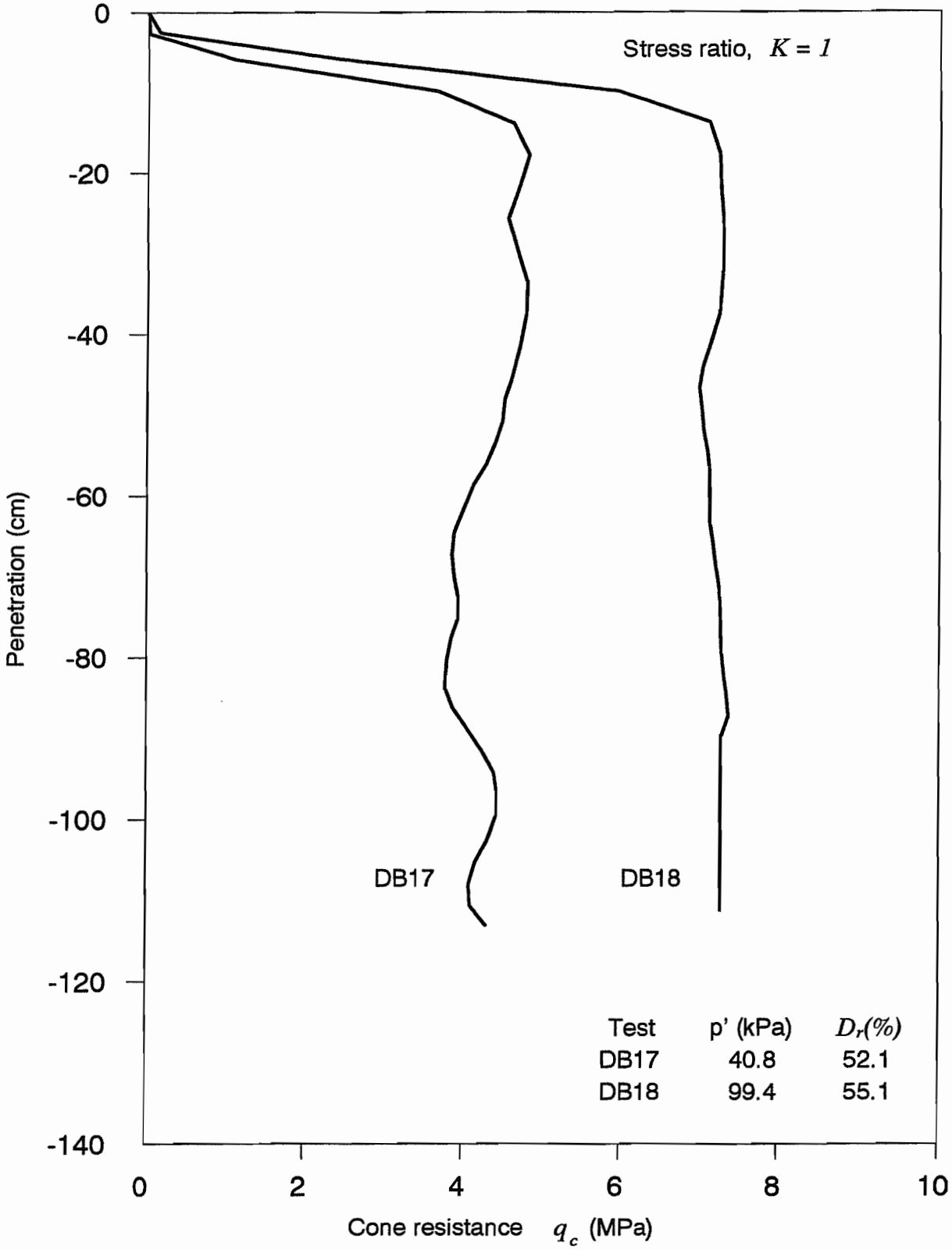


Figure 4.12 Cone resistance profiles for CPM tests in dense Dogs Bay sand at a stress ratio, K = 1.0

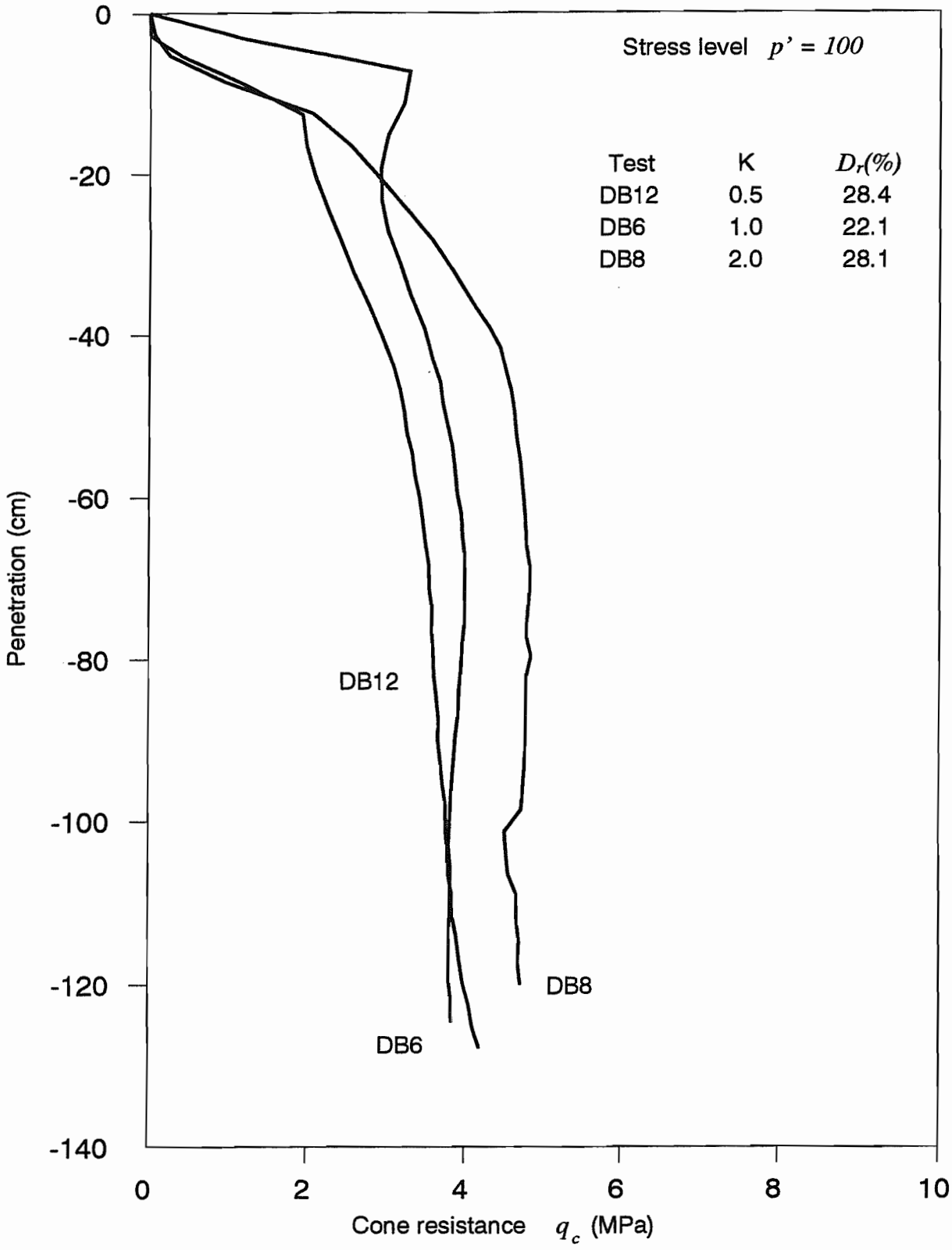


Figure 4.13 Cone resistance profiles for CPM tests in loose Dogs Bay sand at a mean effective stress of 100kPa

It is clear that an increase in p' results in an increase in cone resistance, q_c. Further, the stress ratio influences q_c as shown in Figure 4.13 for tests DB12, DB6 and DB8 in loose sand at a p' of 100kPa and K of 0.5, 1.0 and 2.0 respectively. Results from calibration chamber tests reported by Houlsby and Hitchman (1988) revealed that it is the horizontal stress which dominates the measured q_c as opposed to the vertical stress, and this is supported by the results in Dogs Bay sand which are plotted in Figure 4.14. No relationship exists between q_c and σ'_v for either the loose or dense sands.

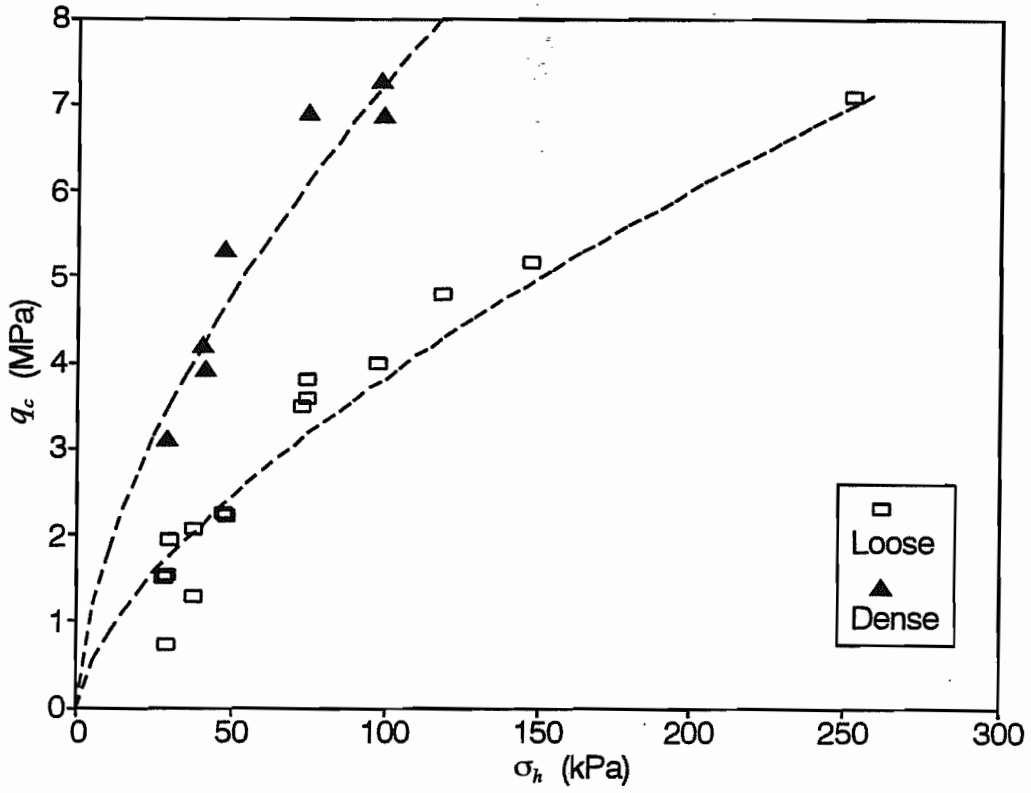


Figure 4.14 Influence of σ_h on q_c determined from CPM tests in Dogs Bay sand

It has been argued by Been *et al.* (1986) that p' should be the normalising parameter for the interpretation of cone data, because such an approach accounts for any influence of σ'_v. Fioravante *et al.* (1991) suggest that σ'_v does indeed influence q_c. There is, however, no reason why the independent effects of σ'_h and σ'_v should be combined in the ratio 2 to 1 (as implied by the definition of $p' = (2\sigma'_h+\sigma'_v)/3$) to normalise cone behaviour other than

convenience of use of p'. From the tests in Dogs Bay sand, more confidence is placed in the relationship between q_c and σ'_h than that of q_c and p' because of the dependency of q_c on the stress ratio, K. This has led to the use of the normalised cone resistance, $(q_c-\sigma_h)/\sigma'_h$ as shown in Table 4.2. Wroth (1988) advocates the subtraction of the total normalising stress from q_c. This is an allowance made for the ambient level of total ground pressure at the outer boundary of the test. Its inclusion in the normalised cone resistance is for consistency and does not greatly influence the result.

4.4.3 Pressuremeter results

Typical pressuremeter curves are presented in Figures 4.15 to 4.17 where inflation pressure has been plotted against cavity strain for loose and dense sand. The shape of the curves is extremely repeatable, with the exception of the initial stage of pressuremeter inflation (up to around 0.02 strain), where differences in the individual readings of the strain arms were more pronounced. Relative density, stress level and stress ratio affect the pressuremeter results in a similar manner to that described in the previous section. In Figure 4.15, the pressure-strain curves of tests DB11, DB15 and DB23 are shown at a p' of 40kPa and K of 0.5. Increasing limit pressure with D_r is evident. An increase in p' also results in an increase in limit pressure, and this is shown in Figure 4.16 for tests DB17, DB18 and DB25. Following the discussion in the previous section on a suitable normalising parameter for q_c, the influence of stress ratio on the pressuremeter tests is shown in Figure 4.17 for tests DB12, DB6 and DB8 with K = 0.5, 1.0 and 2.0 respectively. Because the limit pressure, ψ_l also increases with increasing K, it is suggested that p' is not the most suitable parameter with which to normalise ψ_l. A strong relationship between ψ_l and σ'_h is shown in Figure 4.18, which is dependent upon density but independent of stress ratio. No relationship exists for ψ_l and σ'_v.

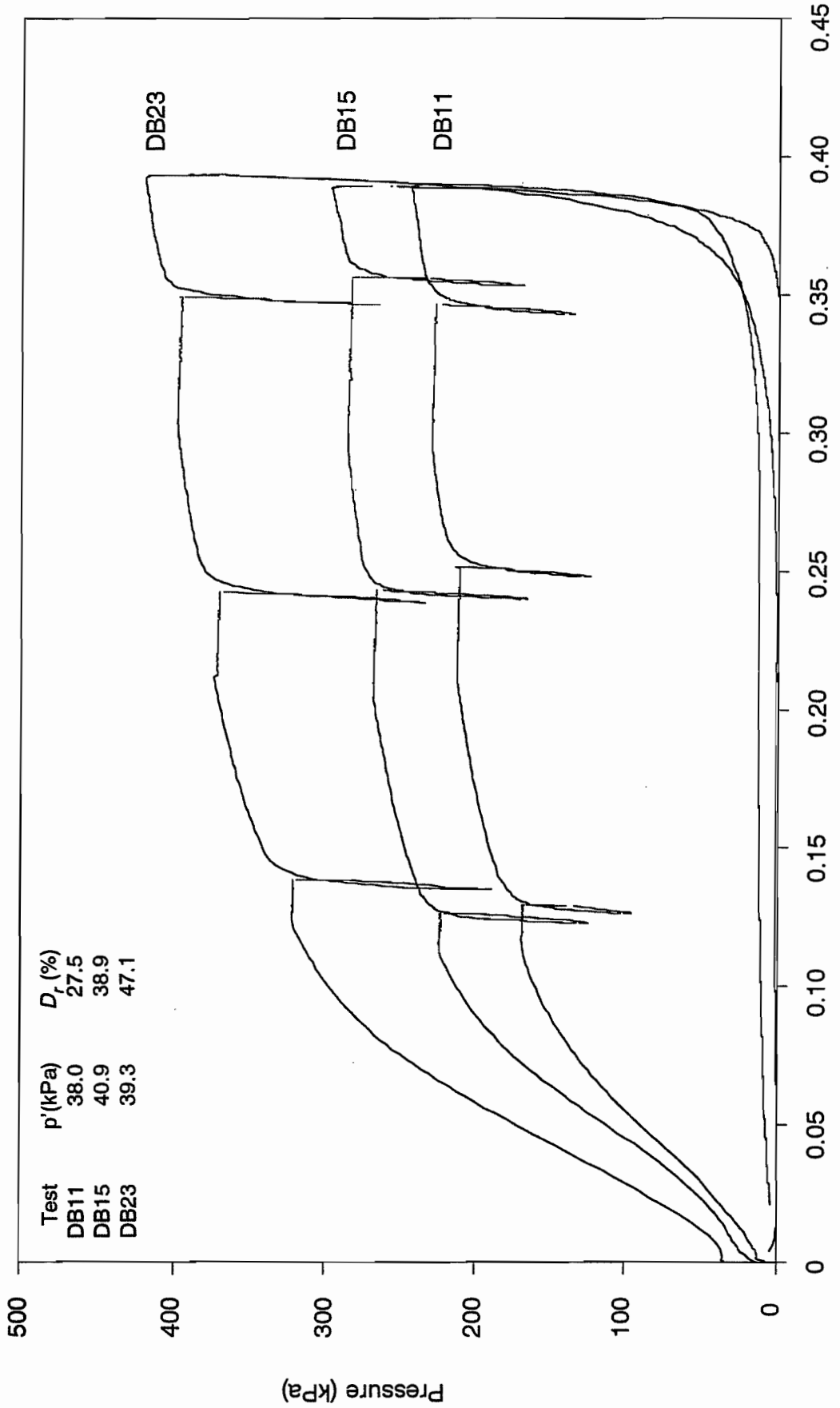


Figure 4.15 Pressure-strain curves for CPM tests in Dogs Bay sand at a stress ratio $K = 0.5$

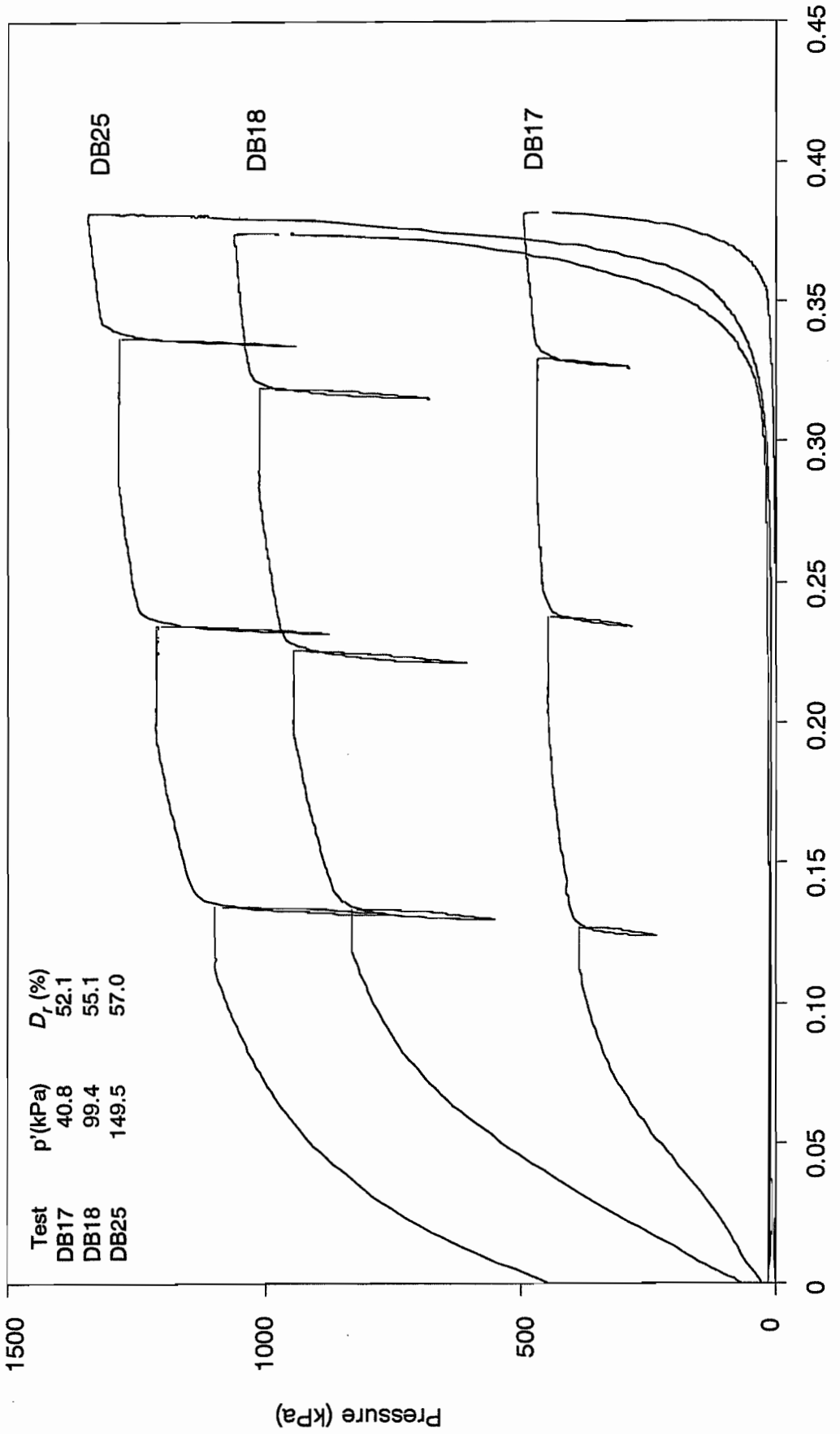


Figure 4.16 Pressure-strain curves for CPM tests in dense Dogs Bay sand at a stress ratio $K = 1.0$

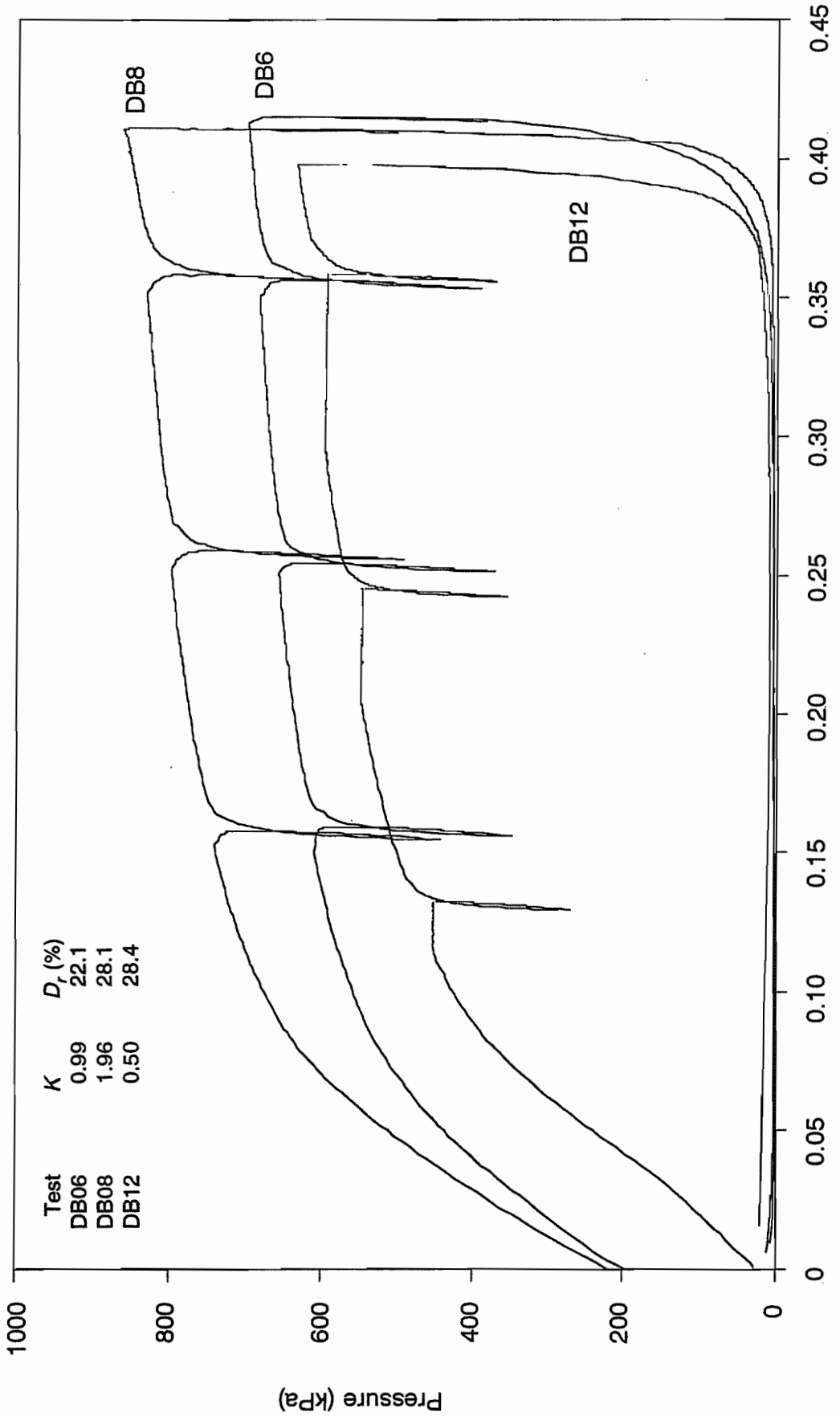


Figure 4.17 Pressure-strain curves for CPM tests in loose Dogs Bay sand at a mean effective stress p' = 100kPa

Since both q_c and ψ_l are primarily controlled by σ'_h, the combination of these parameters in the form $(q_c - \sigma_h)/(\psi_l - \sigma_h)$ should also be influenced only by D_r. This ratio is referred to as the CPM factor and is shown in Table 4.2 for each of the tests. The application of this

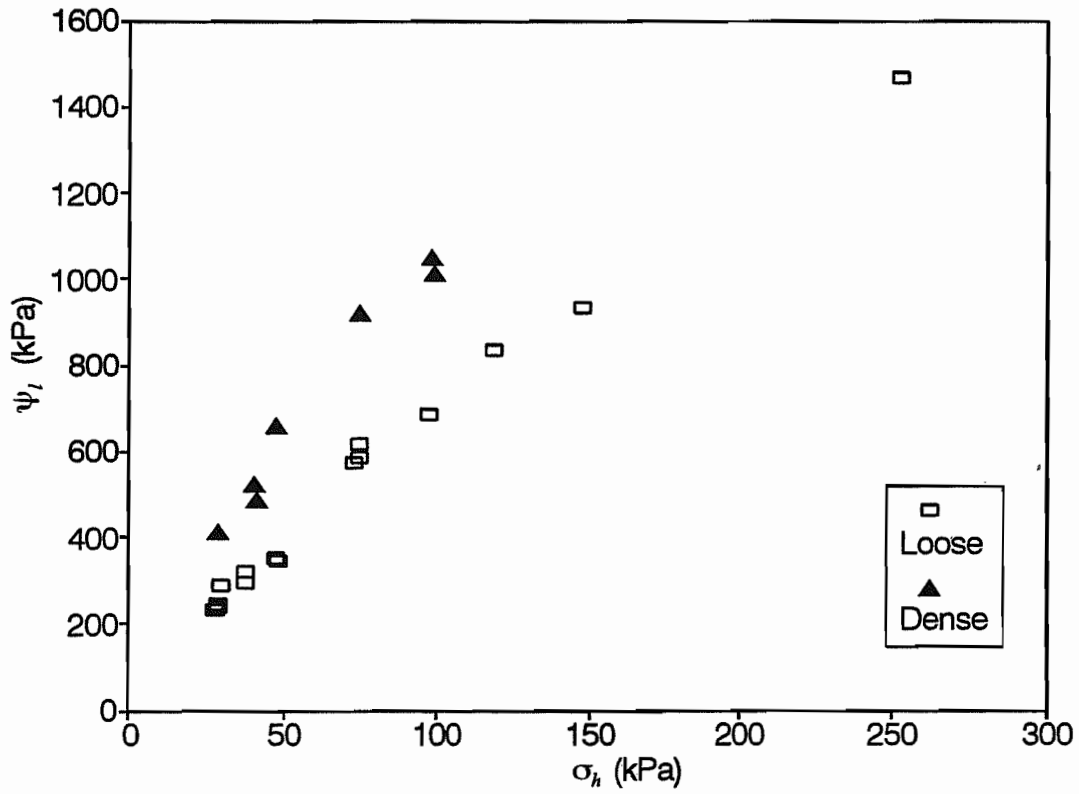


Figure 4.18 Influence of σ_h on limit pressure determined from CPM tests in Dogs Bay sand

4.5 Tests in overconsolidated sand

Ten of the tests in Dogs Bay sand were performed in overconsolidated samples. The objective was to use cone pressuremeter measurements to assess the response of carbonate sand which had been subjected to a past maximum effective stress, higher than the current stress.

In a natural state, sands are frequently deposited in approximately horizontal layers and then subjected to one-dimensional loading, resulting in anisotropic stresses since the coefficient of earth pressure at rest, $K_0 = \sigma'_{h0}/\sigma'_{v0}$ is less than unity during virgin compression. Removal of these stresses in one direction results in a change of the principal stress ratio, and if the

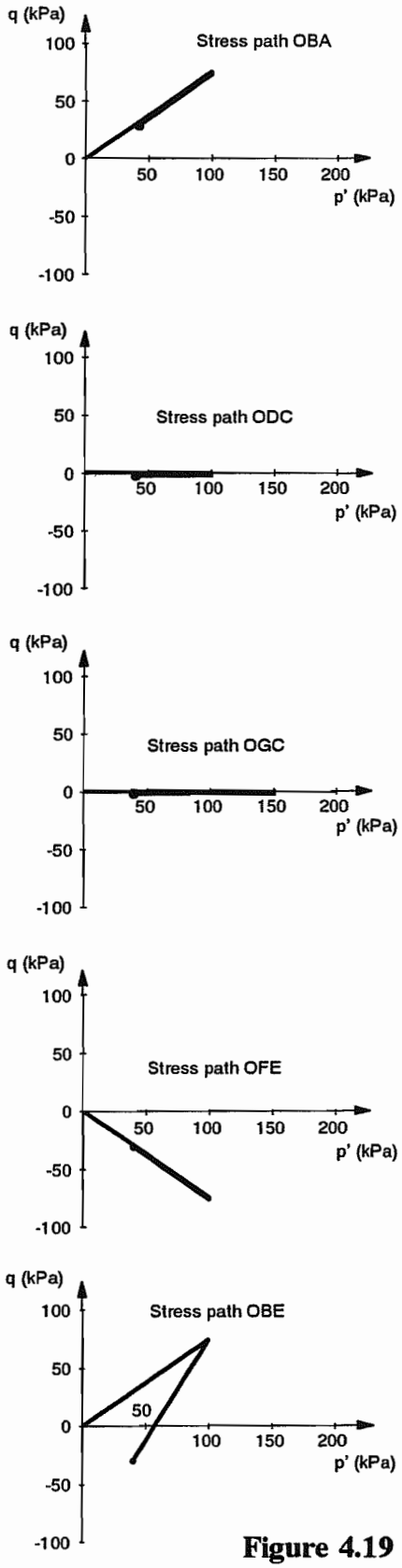
unloading is in the direction of the major principal stress (usually the vertical stress, σ_v'), K_0 will increase.

Stresses have been applied to samples in the calibration chamber at predetermined stress ratios of K = 0.5, 1.0 and 2.0, which, in the case of Dogs Bay sand, are greater than K_0 (Golightly, 1988 reports K_0 of Dogs Bay sand to range from 0.24 to 0.38 up to a confining stress of 500kPa). This has been done to isolate the influences of σ_v' and σ_h' upon the cone and pressuremeter results. To simulate overconsolidation, samples were taken along a linear stress path to one of the states shown in Figure 3.1 and then brought back along a linear path to a state of lower mean effective stress.

The results of the overconsolidation tests are presented in Figure 4.19, where the various stress paths travelled to obtain an overconsolidated state are matched with the ratios of limit pressure, ψ_l^{oc}/ψ_l^{nc} and cone resistance, q_c^{oc}/q_c^{nc}. For both the loose and dense samples, overconsolidation is shown to result in an increase in limit pressure and cone resistance, and this increase, in most cases, is more apparent in the loose samples. This phenomenon is attributed to the high crushing characteristics of Dogs Bay sand.

The angular nature of the particles results in relatively few interparticle contacts after sample preparation. On the application of chamber stresses, local crushing occurs at these particle contacts. The amount of crushing is strongly affected by the maximum stress level experienced by the soil fabric. A greater amount of crushing occurs in overconsolidated samples than in normally consolidated samples because sand particles, obviously cannot become "uncrushed".

Particle crushing causes two changes to the soil fabric. Firstly, the voids ratio in the fabric is decreased. This influences the soil strength directly because of an increase in density.



$\frac{q_c^{oc}}{q_c^{nc}}$		$\frac{\psi_l^{oc}}{\psi_l^{nc}}$		Overconsolidation ratios		
				$\frac{\sigma_h^{max}}{\sigma_h}$	$\frac{\sigma_v^{max}}{\sigma_v}$	$\frac{p'_{max}}{p'}$
Loose	Dense	Loose	Dense			
1.92	1.41	1.64	1.14	2.5	2.5	2.5
1.26	1.36	1.24	1.14	2.5	2.5	2.5
1.45	1.55	1.30	1.25	3.75	3.75	3.75
1.55	1.23	1.50	1.24	2.5	2.5	2.5
1.08	1.03	1.09	1.04	1.56	6.25	2.5

Figure 4.19 Overconsolidated stress states and their influence on cone resistance and limit pressure

However, the relative densities of the overconsolidated samples shown in Table 4.2 are not noticeably greater than the corresponding densities of the normally consolidated samples, and so it is concluded that the influence of this change to the soil fabric on measured values of cone resistance and limit pressure is minor.

The second of these changes is an increase in the average contact area between individual particles. From Hertzian contact theory, this results in an increase in the stiffness of the soil fabric. On examination of the shear moduli measured from unload-reload loops and reported in Chapter 7, Table 7.1, it is evident that the shear moduli of overconsolidated samples are greater than the shear moduli of corresponding normally consolidated samples (taking into account the stress level at which stiffness was determined). This helps to explain the observed increases in cone resistance and limit pressure of tests in overconsolidated samples.

It is also evident from Figure 4.19 that for the stress path OBE, where the ratio of chamber stresses, K is increased from 0.5 to 2, the effect upon ψ_l and q_c is notably less pronounced. Despite the large ratio of vertical stresses $\sigma_v^{oc}/\sigma_v^{nc}$ = 6.25, the ratio of horizontal stresses was lower, $\sigma_h^{oc}/\sigma_h^{nc}$ = 1.56. Because of the platy and elongated nature of the Dogs Bay sand particles, after sample preparation there is a preferential particle orientation in the horizontal direction. On the application of chamber stresses, more particle contacts are therefore broken down in the horizontal direction than in the vertical direction and so the influence of horizontal overconsolidation is greater than vertical overconsolidation. This also reflects the fact that cone resistance and limit pressure depend more on σ_h' than σ_v'.

Not suprisingly, results reported by Fioravante *et al.* (1991) for CPT tests in a calibration chamber in Toyoura silica sand found that the influence of K_0 overconsolidation was negligible on the normalised cone resistance, and a similar observation was reported by

Houlsby and Hitchman (1988) for dilatometer tests in Leighton Buzzard silica sand, also in a large calibration chamber. K_0 overconsolidation resembles most the stress path OBE of Figure 4.19 which has been found to have the least effect on q_c and ψ_I.

4.6 Time-dependent behaviour

4.6.1 Pressure holding tests

Under conditions of constant stress, most soils exhibit continued accumulation of strain with time. This phenomenon, referred to as creep, has engineering significance in assessing the long term deformation of structures. Creep strains are easily determined in laboratory triaxial or oedometer tests, but little effort has been made to use *in situ* tests for time-dependent measurements.

In pressuremeter testing, the pressure required to expand a cavity in soil is controlled, and the strains are measured. Hence, it could be expected that under conditions of constant pressure, the strain-time behaviour of a soil could be observed with a pressuremeter. To date, most time-dependent observations made with pressuremeters have been used to examine the effects of test procedures on measured parameters. Anderson and Pyrah (1989) reported the results of self-boring pressuremeter tests in clay carried out in a calibration chamber. It was shown that derived strength and modulus values were affected by the rate of pressuremeter expansion, due to both consolidation and creep behaviour of the soil. In granular soils, pressure expansion is always slow enough that strains occur under drained conditions, and hence elastic and plastic strains are immediate. When the applied pressure is held constant, all further strains are attributed solely to creep. In a series of self-boring pressuremeter tests at an onshore carbonate sand site in Australia, Fahey (1988) used both pressure holding and strain holding tests to isolate the influence of soil creep. Holding tests were carried out at different stages of an SBPM expansion, in which the cavity pressure was held constant while the gradual increase of cavity strain with time was observed. Strain holding tests were more

difficult to control; pressure was reduced rapidly with the aim of "freezing" the cavity strain. Fahey's conclusions were entirely qualitative, revealing the tendency for creep to depend on the stress level. The gradient of the pressure-expansion curve, particularly at the higher stress levels, was therefore, dependent on the rate of pressure increase.

Pressure holding tests were also carried out by Withers *et al.* (1989) with the cone pressuremeter in two silica sands, in each case prior to an unload-reload loop. The primary aim of these tests was to minimise the influence of creep on the measurement of shear modulus, observed by the hysteresis in each unload-reload loop. In addition, it was postulated that an appropriate analysis could lead to a calculation of the creep properties of the soil.

A similar procedure was adopted for most of the CPM tests in Dogs Bay sand. At three cavity strain levels, inflation pressure was held constant and the increase of strain with time was recorded. An unload-reload loop was carried out when the strain rate was sufficiently low, as discussed in Chapter 3 and shown in Figure 3.2. Further to the observations of Withers *et al.* (1989), a soil model has been used to quantify creep behaviour as measured in the pressure holding tests (PHT), and is shown to reproduce the features of the creep mechanism in both Dogs Bay sand and Hokksund sand.

The occurrence of creep strains is shown in Figure 4.20 for test DB30. Three pressure holding tests are shown in the figure, PHT1, PHT2 and PHT3 where the zero time and strain are taken at the point where the pressure is first held constant. While the shape of the three curves is similar, it is clear that the current stress level ψ/ψ_l dictates the amount and rate of creep experienced by the soil, where ψ_l is the limit pressure.

Singh and Mitchell (1968) present creep data for many different soil types, ranging from clays to sands. Two fundamental observations from many of these data can be made. Firstly, the

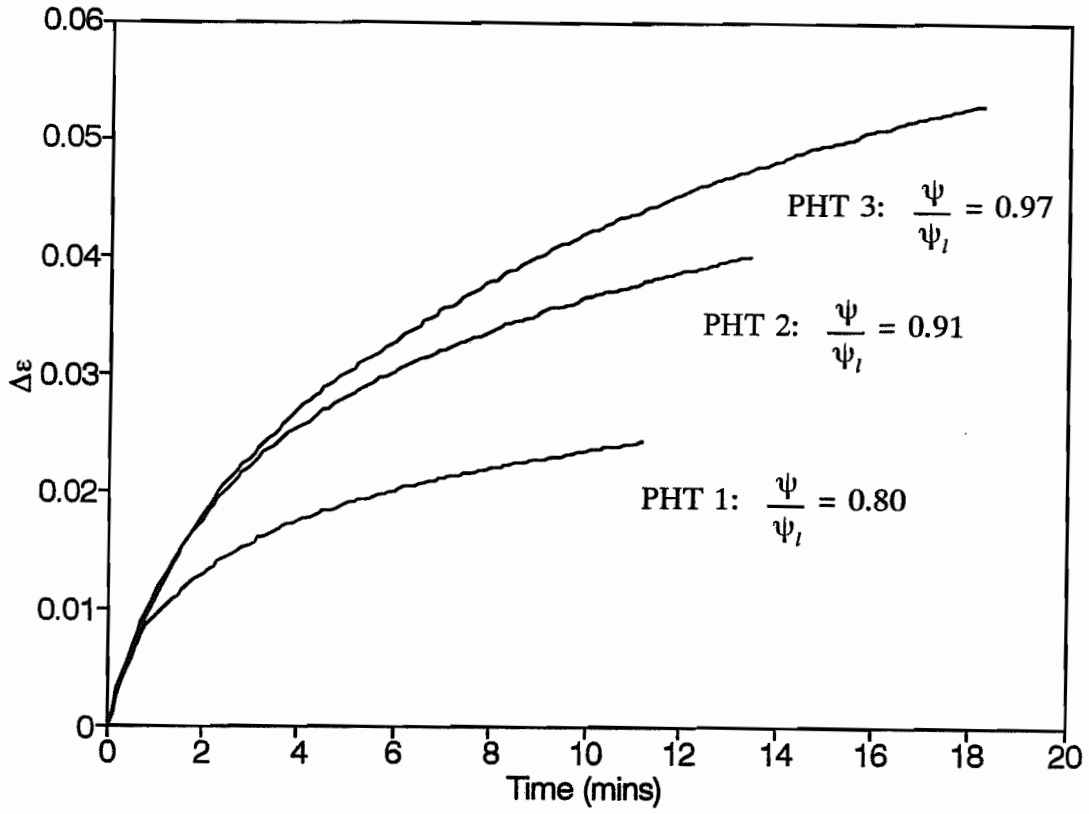


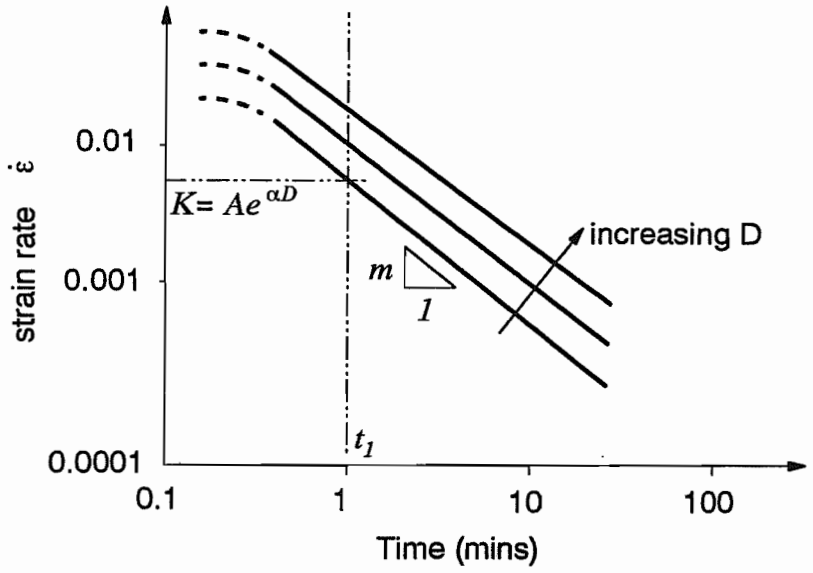
Figure 4.20 Creep strains obtained from pressure holding tests during test DB30

logarithm of strain rate is proportional to the logarithm of time, as presented schematically in Figure 4.21(a). This behaviour can be expressed in the form

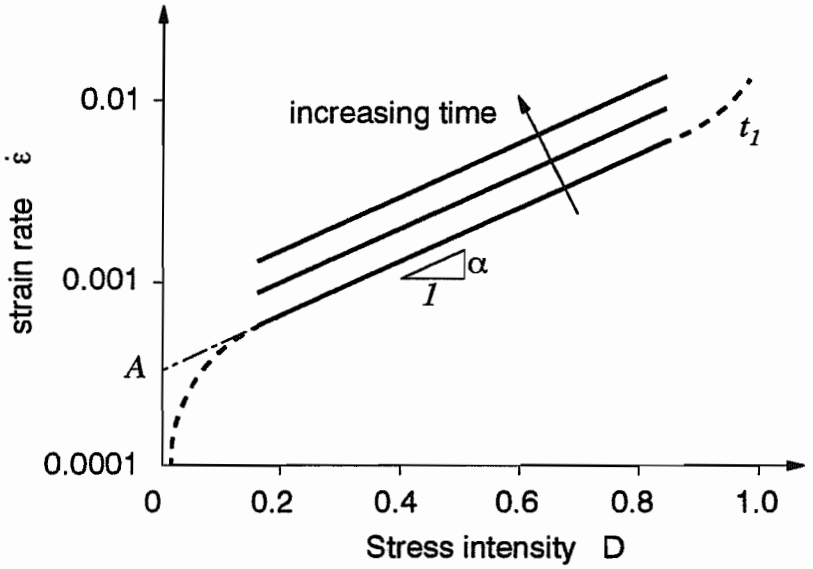
$$\log_e \dot{\varepsilon} = \log_e K - m\log_e\left(\frac{t}{t_1}\right) \qquad ...(4.3)$$

where m is the absolute value of the slope of the straight line portion of the $\log_e \dot{\varepsilon}$ versus $\log_e t$ plot, and K is a strain rate intercept at a reference time, t_1. Note that K is dependent upon a stress intensity, D.

The second observation is that creep rate after a given elapsed time is controlled by the stress intensity in a form shown in Figure 4.21(b). At low stress intensities, creep rates are small and generally not of engineering interest, and hence it is the linear portion of the curve shown in the figure that is used in the model, expressed by



(a) Decay of creep strain rate with time



(b) Variation of creep strain rate with stress intensity

Figure 4.21 Generalised creep behaviour of sands

$$\log_e \dot{\varepsilon} = \log_e A + \alpha D \qquad ...(4.4)$$

where A is the strain rate intercept for a reference time, t_1. Combining equations (4.3) and (4.4) and rearranging leads to the result

$$\dot{\varepsilon} = K\left(\frac{t}{t_1}\right)^{-m} \qquad ...(4.5)$$

where $K = Ae^{\alpha D}$, which is the Singh and Mitchell (1968) relationship for soil creep.

In terms of pressuremeter testing, the stress intensity, D can be represented by the ratio of the holding pressure to the limit pressure. The parameter m can be determined directly from each pressure holding test using the logarithmic plot of strain rate against time, and an example of this plot is shown in Figure 4.22 for test DB30. From the figure, an estimate of the strain rate intercept, K at a reference time of 1 minute is made. Since there are three pressure holding tests in a pressuremeter test, it is possible to obtain three estimates of the parameter K, and A and α can be determined locally from a regression analysis. Alternatively, K determined globally from 48 pressure holding tests has been plotted against the stress intensity, D in Figure 4.23. From a linear regression, A was found to be 5.85×10^{-5} and the gradient α was found to be 5.23. The data show scatter, but almost all fall within a range of $\alpha = 5.23 \pm 10\%$.

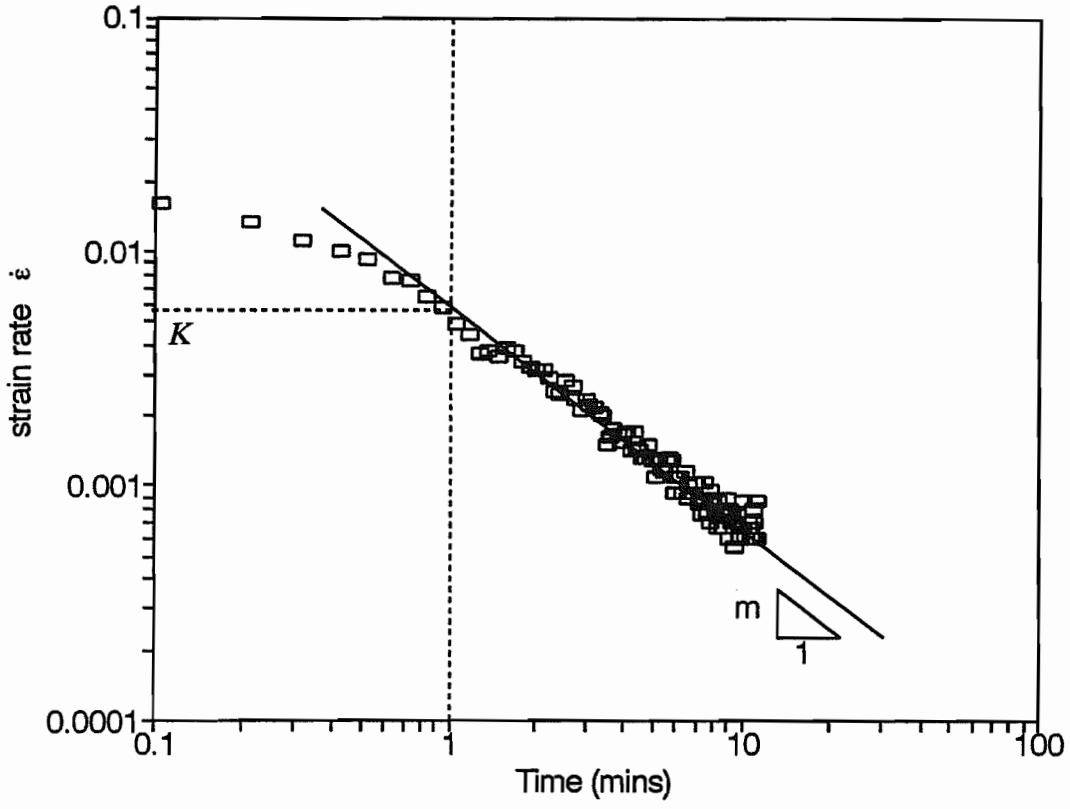


Figure 4.22 Logarithmic plot of PHT1 from test DB30

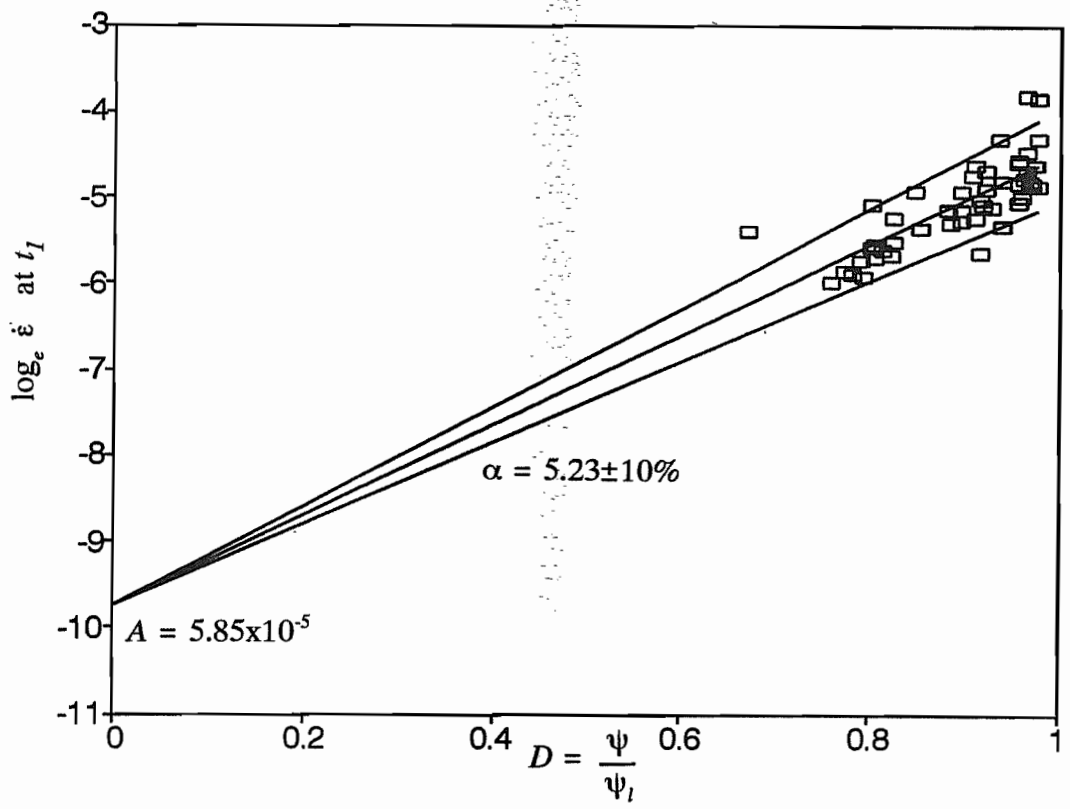


Figure 4.23 Plot to determine strain rate intercept, *A* and gradient α

The final strain-time relationship can be obtained by integration of equation (4.5) to yield

$$\varepsilon = \frac{t_1 A e^{\alpha D}}{1-m}\left(\frac{t}{t_1}\right)^{1-m} + constant \quad \text{for } m \neq 1 \qquad ...(4.6)$$

and

$$\varepsilon = A e^{\alpha D}\, t_1 \log_e t \quad \text{for } m = 1 \text{ and } t > 1 \qquad ...(4.7)$$

The success of the Singh and Mitchell (1968) model in predicting creep strain behaviour from the CPM test is shown in Figure 4.24 for test DB30, PHT1. When *A* and α are determined locally from three pressure holding tests, a remarkably close fit results. The upper and lower limits determined from most of the 48 pressure holding tests are also shown in the figure. The range between these limits is broad because a large extrapolation was required to determine *A* as shown in Figure 4.23. This extrapolation could be shortened by performing pressure holding tests at lower stress intensities, *i.e.* at an earlier stage of pressuremeter testing.

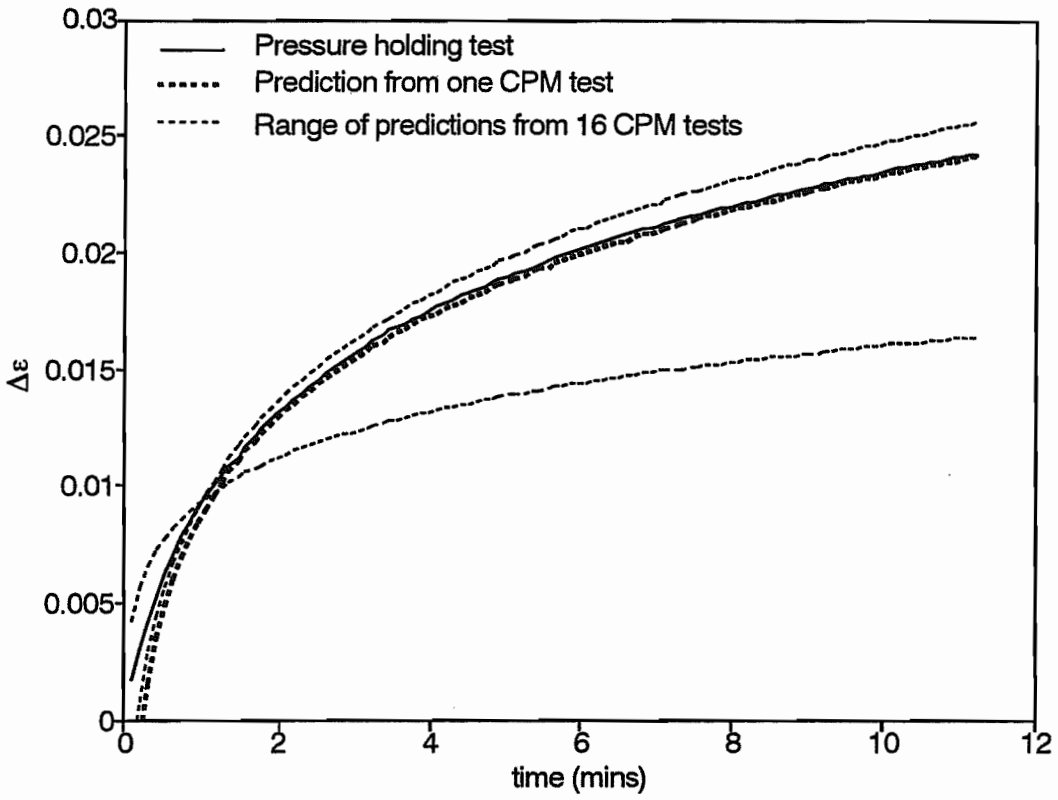


Figure 4.24 Creep behaviour from a pressure holding test as predicted by the Singh and Mitchell (1968) model

4.6.2 Strain holding tests

At the end of pressuremeter expansion, the driving motor was switched off for a period of about 3 to 4 minutes before deflation of the membrane, and the decay of pressure with time was recorded. Throughout this period, volumetric cavity strain remained constant, although there were some small fluctuations in the arm measurements of strain in the initial 30 seconds of the test. This procedure is referred to as a strain holding test, and an example is plotted in Figure 4.25. The current stress intensity, D expressed as a ratio of cavity pressure to limit pressure, is plotted against the logarithm of time. The relationship is very close to linear.

The Singh and Mitchell (1968) relationship given by equation (4.7) is applicable only to pressure holding tests, because it is assumed that the stress intensity, D is constant with time. To model the behaviour of a strain holding test, the strain must be expressed as a function of both time and stress intensity.

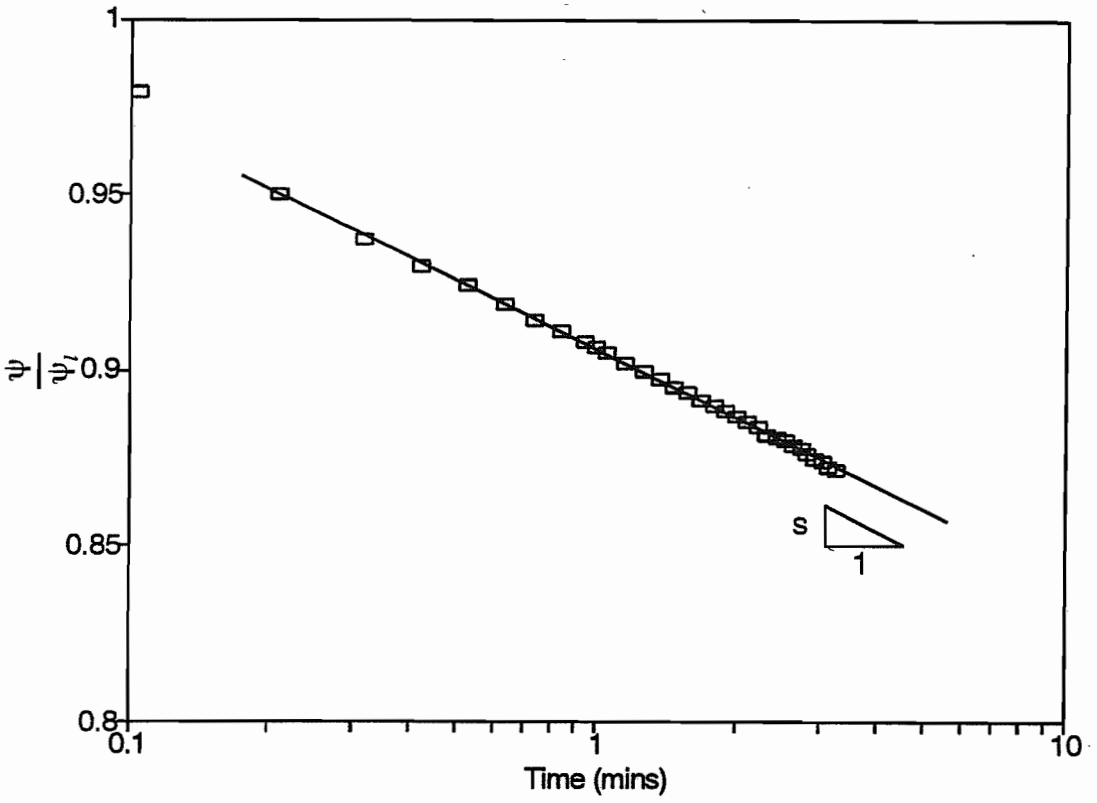


Figure 4.25 Decay of cavity pressure with time determined from a strain holding test during CPM test DB30

An expression which is consistent with the above takes the form

$$\varepsilon = \frac{t_1 A e^{\alpha D}}{1-m}\left(\frac{t}{t_1}\right)^{1-m} + constant \qquad ...(4.8)$$

At the start of unloading, $t = 0$ and $\varepsilon = f(D) = \varepsilon_0$ which is constant during the strain holding test. Differentiating equation (4.8) with respect to time for cases where D can vary gives

$$\dot{\varepsilon} = A e^{\alpha D}\left(\frac{t}{t_1}\right)^{-m} + \frac{\alpha t_1 A e^{\alpha D}}{1-m}\left(\frac{t}{t_1}\right)^{1-m}\frac{dD}{dt} \qquad ...(4.9)$$

In a pressure holding test, $dD/dt = 0$ and equation (4.9) reduces to equation (4.5). In a strain holding test, $\dot{\varepsilon} = d\varepsilon/dt = 0$ and equation (4.9) can be solved for dD/dt to give

$$\frac{dD}{dt} = \frac{m-1}{\alpha t} \qquad ...(4.10)$$

This result has been reported by Lacerda and Houston (1973) for $m < 1$. Integration of equation (4.10) gives

$$D = \frac{m-1}{\alpha} \log_e t + constant \qquad ...(4.13)$$

which is a linear relationship between D and $\log_e t$. This behaviour was indeed observed from the strain holding tests as shown for test DB30 in Figure 4.25. The gradient of the line of best fit to the data shown in the figure was found to be 0.0652. Using $\alpha = 5.23$ from the pressure holding tests, m was estimated to be 0.66. The average value of m from the three pressure holding tests was 0.87. There is a slight underprediction of m using the results of the strain holding test, but in general, the time-dependent behaviour is well modelled by equation (4.9).

4.6.3 Variation of strain rate

To understand the link between creep and strain rate, additional tests were carried out where the rate of pressuremeter strain was manually controlled. Two examples of this type of test are shown in Figure 4.26 for tests DB13 and DB31 in loose and dense sands respectively at a stress ratio of $K = 1$ and a stress level of $p' = 40$kPa. It is clear that the slower strain rates result in reduced pressure curves, which are seemingly parallel to the original curve. It is hypothesized that there exists a family of pressuremeter curves, each corresponding to a particular rate of strain or a particular rate of decay of pressure.

The model of time-dependent behaviour represented by equation (4.8) has been extended to incorporate this hypothesis. For a test of constant strain rate, $\dot{\varepsilon} = B$ and so

$$(\varepsilon - \varepsilon_0) = B(t - t_0) \qquad ...(4.12)$$

It is necessary to assume a set of initial conditions, and the relationship of equation (4.8) is simplified if these conditions are taken as the start of a cone pressuremeter test, *i.e.* $\varepsilon_0 = 0$ and $t_0 = 0$.

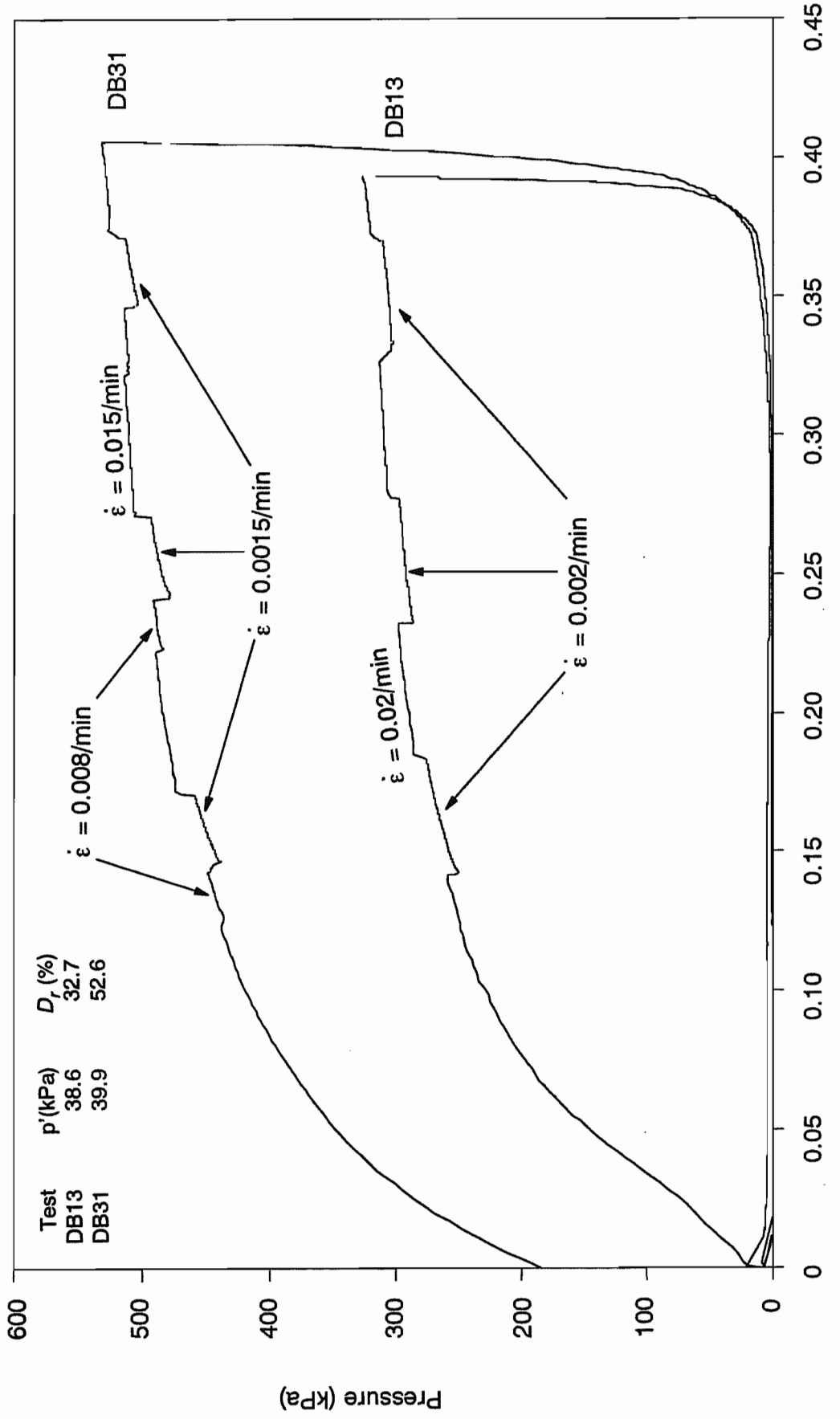


Figure 4.26 Pressure-strain curves for variable strain rate tests in Dogs Bay sand at a stress ratio K = 1.0

Equation (4.8) combined with equation (4.12) can be written as

$$\varepsilon = \frac{Ae^{\alpha D}t_1}{1-m}\left(\frac{\varepsilon}{Bt_1}\right)^{1-m} \qquad ...(4.13)$$

Equation (4.13) can be rearranged to give

$$\frac{\varepsilon}{t_1}\left(\frac{\varepsilon}{t_1}\right)^{m-1} = \frac{Ae^{\alpha D}}{1-m}B^{m-1} \qquad ...(4.14)$$

which can be rewritten as

$$\log_e\left(\frac{1-m}{A}\right) + m\log_e\left(\frac{\varepsilon}{t_1}\right) = \alpha D + (m-1)\log_e B \qquad ...(4.15)$$

and further rearrangement leads to

$$D = \frac{m}{\alpha}\log_e\varepsilon + \left(\frac{1-m}{\alpha}\right)\log_e B + \frac{1}{m}\log_e\left(\frac{1-m}{t_1 A}\right) \qquad ...(4.16)$$

for $m < 1$. For a given strain rate, B equation (4.16) is a unique relationship between D and ε and has been used to model test DB13. For $m = 0.9$, $\alpha = 5.23$, as determined from the pressure holding tests, and using strain rates of $B = 0.02$ and 0.002 ε/min, a comparison between equation (4.16) and test DB13 is shown in Figure 4.27. The parameter A has been taken as 0.032, which is somewhat larger than was obtained from the pressure holding tests, but its only influence on the result in the figure is to cause a vertical shift of all the curves. The influence of strain rate on cavity pressure clearly has been well predicted by the model of equation (4.16).

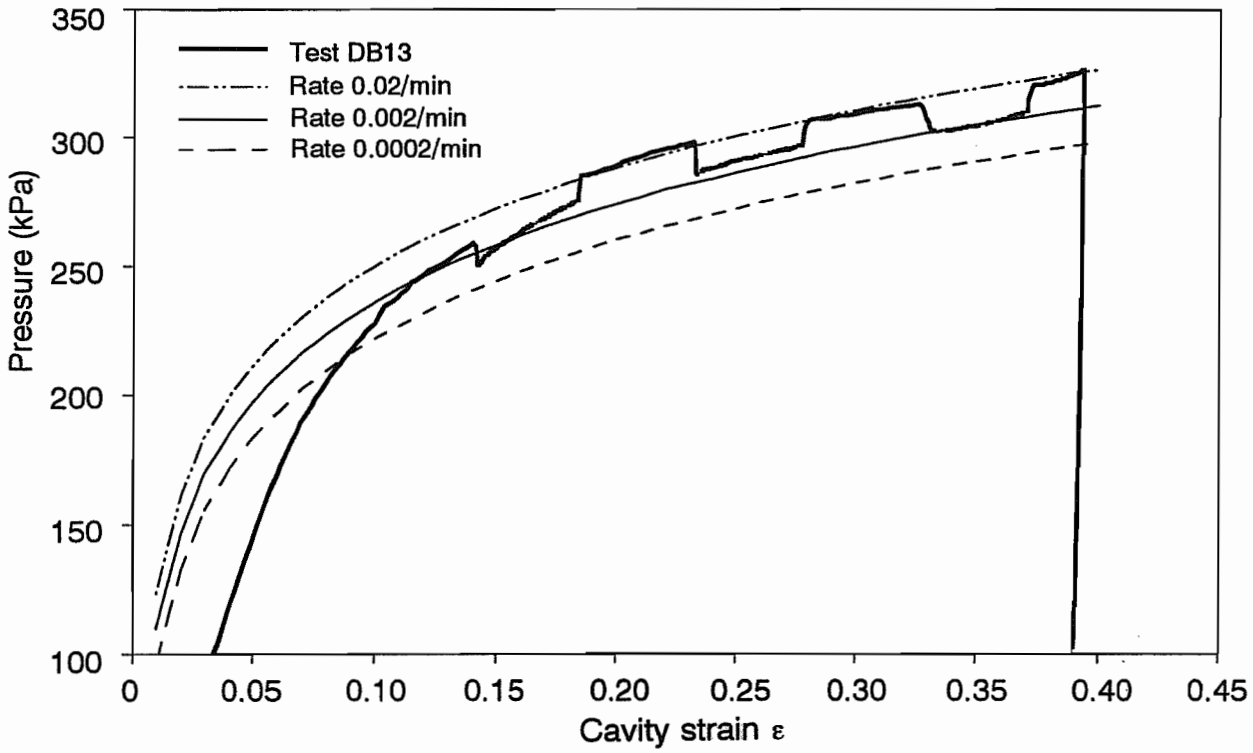


Figure 4.27 Comparison between constant strain rate curves and test DB13

4.7 Conclusions

From the tests in Dogs Bay sand, the following conclusions were drawn:

(1) Dogs Bay sand is typical of many carbonate sands in that it is characterised by angular, platy and tubular grains of biogenic origin. This results in high voids ratios in the natural state, and high compressibility and crushability.

(2) Both cone resistance and limit pressure as measured by the CPM are primarily controlled by relative density and horizontal stress.

(3) q_c and ψ_l of Dogs Bay sand are influenced by a cycle of overconsolidation. This is due to crushing at particle contacts resulting in an increased stiffness of the soil fabric. Cone resistance and limit pressure are more strongly influenced by overconsolidation in the horizontal direction than in the vertical direction.

(4) A soil model has been successfully applied to time-dependent tests carried out

with the CPM. The model incorporates observed features of both creep and stress relaxation in Dogs Bay sand.

(5) This model has been extended to assess the influence of variations in strain rate on limit pressure. There exists a family of pressure-strain curves each corresponding to a constant strain rate which affect the magnitude of limit pressures obtained with the CPM.